Università degli Studi di Padova

DIPARTIMENTO DI FISICA E ASTRONOMIA "GALILEO GALILEI"
DIPARTIMENTO DI INGEGNERIA DELL'INFORMAZIONE
Corso di Laurea Magistrale in Fisica

Quantum Mechanical Experiments using Optical Techniques in Space

Laureando:
Giacomo Pantaleoni

Relatore:
Chiar.mo Prof. Paolo Villoresi

Correlatore:
Chiar.mo Prof. Giuseppe Vallone

Anno Accademico 2015-2016

Contents

Summary

The focus of this work is discussing the realization of space based experiments testing quantum mechanics, specifically quantum optics. Firstly, the theoretical aspects of quantum optics relevant to the dissertation will be laid out, particularly the physics behind Mach-Zehnder interferometers with input states given by pulsed lasers. The state of the art of the experimental advancement on the topic of *delayed-choice* interferometric measurements with photons will be presented, along with the theoretical framework at play. The reasons why it is relevant to realize space based versions of such experiments will be discussed, and an example of an experiment measuring interference fringes of an interferometer composed by an earthbound and satellite part will be given. The presentation of said experiment will be mainly focused on a relativistic effect due to the relative speed between Earth and the satellite. The main experimental work which this thesis is based on is the experimental realization of the earthbound part of another possible interferometric experiment that can be realized with methods similar to the one previously discussed. The full Earth-satellite realization of this experimental scheme could set a new record on the distance to which delayed-choice schemes have been experimentally realized. The last chapter will be dedicated to the discussion of general relativistic effects on Earth-satellite experiments, in the case of two different setups. One of those is essentially the ground-space implementation of the interferometer realized in the laboratory, while the other represents a different possibility that could in principle measure gravitational redshift to single photons to greater extent.

Sommario

Il filo conduttore di questo lavoro è la discussione della realizzazione di esperimenti di meccanica quantistica, nello specifico ottica quantistica, basati su distanze fornite da satelliti. Inizialmente verranno presentati gli aspetti teorici dell'ottica quantistica, in particolare la fisica degli interferometri di tipo Mach-Zehnder nel caso in cui gli stati quantistici iniziali siano dati da laser impulsati. Lo stato dell'arte sperimentale per quello che riguarda misure interferometriche di tipo *delayed-choice* verrà presentato, insieme ai concetti teorici necessari per la discussione. Si discuterà poi la ragione per la quale realizzare esperimenti di questo tipo è rilevante dal punto di vista sperimentale, e verrà dato un esempio di una misura di tipo interferometrico realizzata tramite un interferometro composto da una parte a terra e una su satellite. La parte sperimentale principale di questo lavoro consiste nella realizzazione in laboratorio di un interferometro che potrebbe andare a costutuire la parte terrestre di un esperimento di tipo delayed-choice, possibilimente realizzabile tramite metodi simili a quelli dell'esperimento discusso precedentemente. La realizzazione Terra-satellite di tale esperimento costituirebbe un record di distanza per misure di tipo delayed-choice. L'ultimo capitolo è dedicato alla discussione di effetti gravitazionali che potrebbero influenzare misure interferometriche Terra-spazio, per due specifici schemi sperimentali. Il primo è essenzialmente la realizzazione Terra-spazio dell'interferometro realizzato in laboratorio in questo lavoro, mentre il secondo è uno schema che potrebbe in principio misurare ad un ordine di grandezza superiore il redshift gravitazionale su singolo fotone.

1 Basic review of quantum optics

1.1 Encoding information with photons

The most basic example of classical unit of information is the bit, which can take only two values. Bits can be represented by any double valued set, depending on the context: 1/0, true/false, on/off, etc. The most straightforward notation is arguably the set $\{0, 1\}$, since in this case it is particularly obvious what the outcome of simple binary operations between bits is (e.g. multiplication). Any 2-state physical system can be used as an implementation of a bit. Needless to say, persistent multi-bit systems, along with the possibility of performing automated operations on them, is what brought about modern computing.

The quantum analougous of the bit is the *qubit*, representing the simplest example of unit of quantum information. Physical implementations of qubits are *quantum* 2-degrees of freedom systems, which obey a set of rules very different from classical ones. The qubit is fundamentally different from the classical case because of the superposition principle of quantum states. qubits are typically represented in Dirac's notation, with the 2 orthonormal base vectors labeled as $|0\rangle$ and $|1\rangle$. Quantum states lie on complex Hilbert spaces modulo global phase and normalization; as a result, the smallest non-trivial Hilbert space that can be used to encode quantum information must be an *infinite* space of dimension 2, rather than just the discrete space with only two values for the classical bit. There is an infinity of states that are physically acceptable indeed, the states spanned by the base vectors. A two dimensional Hilbert space can be physically thought of –and physically realized– in many different ways, for example with two spin $\frac{1}{2}$ particles, or the polarization of two photons. A single qubit is given in general by the superposition of the two base states $|\psi\rangle = \alpha\,|0\rangle + \beta\,|1\rangle$, where the coefficients are complex numbers, and the state ψ is normalized so that $\|\alpha\|^2 + \|\beta\|^2 = 1$. Furthermore, multiplication by a global phase is irrelevant, so two qubits that differ by a global phase are physically equivalent because they give rise to the same probabilities. The probability that a measurement in the $\{|0\rangle, |1\rangle\}$ base reveals the system to be in either one of the base states is respectively $\left\|\alpha^2\right\|$ for $|0\rangle$ and $\left\|\beta^2\right\|$ for $|1\rangle$. Right after the measurement the state will be either $|0\rangle$ or $|1\rangle$, according to the the projection axiom of Quantum Mechanics.

A geometrical representation of the 1-qubit pure state space is the so-called Bloch sphere: because any two-level pure quantum state can be parametrized as

$$|\psi\rangle = \cos\theta/2\,|0\rangle + e^{i\phi}\sin\theta/2\,|1\rangle \tag{1}$$

with $\phi \in [0, 2\pi], \theta \in [0, \pi]$, it is natural to use the vector

$$\begin{pmatrix} \sin\theta\cos\phi \\ \sin\theta\sin\phi \\ \cos\theta \end{pmatrix} \tag{2}$$

to represent all the possibile states of a qubit. For example, we can label three orthonormal bases borriwing the notation from quantum optics, where it is customary to set

Table 1: the most common states represented with Jones notation

$\|0\rangle$	$\|H\rangle$	$\begin{pmatrix} 1 \\ 0 \end{pmatrix}$
$\|1\rangle$	$\|V\rangle$	$\begin{pmatrix} 0 \\ 1 \end{pmatrix}$
$\frac{1}{\sqrt{2}}(\|0\rangle + \|1\rangle)$	$\|+\rangle$	$\frac{1}{\sqrt{2}}\begin{pmatrix} 1 \\ 1 \end{pmatrix}$
$\frac{1}{\sqrt{2}}(\|0\rangle - \|1\rangle)$	$\|-\rangle$	$\frac{1}{\sqrt{2}}\begin{pmatrix} 1 \\ -1 \end{pmatrix}$
$\frac{1}{\sqrt{2}}(\|0\rangle + i\,\|1\rangle)$	$\|L\rangle$	$\frac{1}{\sqrt{2}}\begin{pmatrix} 1 \\ i \end{pmatrix}$
$\frac{1}{\sqrt{2}}(\|0\rangle - i\,\|1\rangle)$	$\|R\rangle$	$\frac{1}{\sqrt{2}}\begin{pmatrix} 1 \\ -i \end{pmatrix}$

$$|0\rangle \rightarrow |H\rangle \tag{3}$$
$$|1\rangle \rightarrow |V\rangle \tag{4}$$

the horizontal (H) and vertical (V) polarization states are the two orthogonal states that we previously labeled $|0\rangle$ and $|1\rangle$, and the qubit now has a clear physical meaning as the polarization of a photon. The Bloch vector spans a sphere in 3 dimensions with unit radius, where the orthonormal vectors belonging to the three standard bases representing linearly (horizontal/vertical, and diagonal) and circularly polarized base states $\{|H\rangle, |V\rangle\}$, $\{|+\rangle, |-\rangle\}$ and $\{|L\rangle, |R\rangle\}$ lie along the three different axes x, y, z. With this representation, antipodal points represent orthogonal vectors.

1.2 Jones representation for states and optical elements

Since the Hilbert state we are dealing with is 2-dimensional, instead of the braket notation one can use the standard vector notation defined in a two dimensional complex space. This is particularly useful because various manipulations on qubits can then be represented by 2 by 2 matrices, and many computations are completely analogous to the classical case of polarized light. This is called the Jones matrix representation [22]. In this section we will list some of the more useful optical elements and their description with this formalism, along with their action on some polarization states as an example. Later on we will discuss more implementations of the quantum bit on photons that are not based on polarization and see how some other optical elements act on these different degrees of freedom that can be used to encode a qubit. Since Jones representation is purely formal, the methods developed can be extended to the latter cases.

1.2.1 Linear Polarizer

A linear polarizer is used to prepare a state with specific linear polarization defined by the optical axis of the polarizer. Upon crossing the polarizer, the photons' polarization will be parallel to the optical axis. So, for example, when

the axis lies along the horizontal plane, then the matrix associated with the polarizer will be a matrix that always outputs linearly polarized states

$$M_{P_H} = \begin{pmatrix} 1 & 0 \\ 0 & 0 \end{pmatrix} \tag{5}$$

so that the output state after the application of the polarizer will be horizontally polarized regardless of the input state

$$M_{P_H} |\psi\rangle = |H\rangle \tag{6}$$

Similarly, a polarizer with optical axis along the vertical polarization axis is associated with the matrix

$$M_{P_V} = \begin{pmatrix} 0 & 0 \\ 0 & 1 \end{pmatrix} \tag{7}$$

thus

$$M_{P_V} |\psi\rangle = |V\rangle \tag{8}$$

Typically, a linear polarizer can be rotated at will, so that any linearly polarized state can be created. The matrix associated with a linear polarizer rotated by an arbitrary angle χ with respect to the horizontal axis is

$$M_{P_\chi} = \begin{pmatrix} \cos^2\chi & \cos\chi\sin\chi \\ \cos\chi\sin\chi & \sin^2\chi \end{pmatrix} \tag{9}$$

indeed, taking a generic linear polarization vector $\left(\begin{smallmatrix} x \\ y \end{smallmatrix}\right)$, and applying the polarizer matrix, we get

$$M_{P_\chi} \begin{pmatrix} x \\ y \end{pmatrix} = (x\cos\chi + y\sin\chi) \begin{pmatrix} \cos\chi \\ \sin\chi \end{pmatrix} \tag{10}$$

which is always parallel to the polarization axis of the polarizer.

1.2.2 Waveplates

Waveplates are slices of birifrangent material constructed in such a way that the amount of birifrangence allows to accomplish a certain manipulation on the relative phase of the photons' polarization state. Practical uses are mainly rotation of the polarization axis and linear/circular conversion. They have a fast and a slow axis, perpendicular to each other and to the surface of the plate. When light travels perpendicularly through the plate, the polarization component parallel to the slow axis travels at slower phase velocity than its perpendicular component (which in turn is parallel to the fast axis), inducing a relative phase between the polarization components. Two very useful waveplates are the half-wave plate and the quarter-wave plate. The former introduces a π phase, while the latter introduces a $\pi/2$ phase.

1.2.3 Half-wave plate (HWP)

The Jones matrix of a $\lambda/2$-wave plate with the fast axis oriented at angle θ with respect to the x axis is

$$M_{\lambda/2}(\theta) = \begin{pmatrix} \cos 2\theta & \sin 2\theta \\ \sin 2\theta & -\cos 2\theta \end{pmatrix} \tag{11}$$

Which is a rotation matrix of an angle 2θ. Suppose light has a linear polarization vector at an angle α with respect to the x-axis. After crossing the waveplate, the new vector will be at a the new angle $2\theta - \alpha$. The $\lambda/2$ waveplate flips linear polarizations to the other side of the optical axis. For example, a typical procedure is to keep the axis at a $\pi/4$ angle with respect to the incident polarization, resulting in a final polarization state which is orthogonal to the initial one.

1.2.4 Quarter-wave plate (QWP)

For a $\lambda/4$ wave plate with fast axis at an angle θ with respect to the x-axis we have the following matrix

$$M_{\lambda/4}(\theta) = \begin{pmatrix} \cos^2\theta + i\sin^2\theta & (1-i)\sin\theta\cos\theta \\ (1-i)\sin\theta\cos\theta & \sin^2\theta + i\cos^2\theta \end{pmatrix} \tag{12}$$

Quarter-wave plates are usually employed to turn linear polarization into circular, and vice-versa. This is accomplished by placing the fast axis at a $\pi/4$ angle with respect to the polarization axis of impinging linearly polarized light. For example, if the incident light is diagonally polarized in the $|+\rangle$ state, and the plate is parallel to the x-axis, the explicit computation yields

$$\begin{pmatrix} 1 & 0 \\ 0 & i \end{pmatrix} \frac{1}{\sqrt{2}} \begin{pmatrix} 1 \\ 1 \end{pmatrix} = \frac{1}{\sqrt{2}} \begin{pmatrix} 1 \\ i \end{pmatrix} \tag{13}$$

which is the circularly polarized state $|L\rangle$.

1.3 Path-encoding

Another way to realize a qubit with photons is the so called path-qubit. Instead of using polarization to encode information, one can use the photon's path inside a quantum system. For example, when a photon can only travel through two different routes inside a system –path a and path b–, the qubit can be still represented as a state in a 2-dimensional Hilbert space

$$\psi = \alpha\,|a\rangle + \beta\,|b\rangle \tag{14}$$

This is obviously just a relabeling of the orthonormal base $\{|0\rangle, |1\rangle\}$, in order make it clear which physical implementation we are considering. The simplest optical elements that physically manipulate the spatial modes of a photon are phase shifters and beam splitters.

1.3.1 Beam splitter (BS)

A beam splitter can be thought of as an element with two input ports and two output ports (figure 1). The ideal BS is lossless, i.e. no photons are absorbed inside it. A very simple beam splitter is a half-silvered mirror placed at a 45 degrees angle with incident photons, so that they can be either transmitted (photons keeps travelling in the same direction), or reflected at a 90 degrees angle (the photons' path is changed).

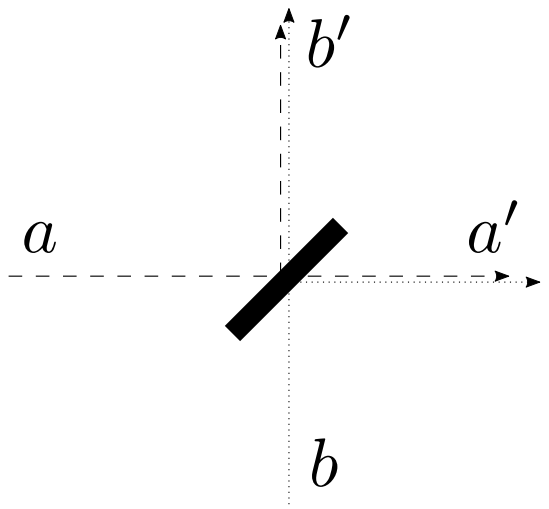

Figure 1: Schematic representation of the action of a beam splitter. Input modes are labeled by a and b, while output modes are labeled by a' and b'.

Regardless of the specific implementation, as long as there are 2 input and 2 output ports, the input photons can be associated to the paths a and b, and similarly a' and b' will label the output spatial modes. Using the column vector representation, the action of the beam splitter on an input state is a matrix $\mathbf{M}$ that maps input vectors into output vectors. We associate $\binom{1}{0}$ to a and a', and $\binom{0}{1}$ to b and b'. Naming the matrix elements with the following scheme makes sense from a physical point of view (r stands for reflection and t for transmission):

$$\begin{pmatrix} t & r' \\ r & t' \end{pmatrix} \tag{15}$$

indeed when the input photon comes from a, the output is the vector representing a transmission and reflection rate $\binom{t}{r}$ and similarly for the photon crossing the BS from the other port we get $\binom{r'}{t'}$. Note that the rates are complex, because the space we are dealing with is complex and so must be any general operator defined on it. If the beam splitter behaves the same way regardless of the port (symmetric beam splitter), the trasmission and reflection rates have to be the same, hence the first simplification.

$$M = \begin{pmatrix} t & r \\ r & t \end{pmatrix} \tag{16}$$

In order to preserve probability this matrix must be unitary: $MM^\dagger = \mathbb{I}$. Solving the resulting set of equations yields

$$M = e^{i\Lambda} \begin{pmatrix} \cos\theta & i\sin\theta \\ i\sin\theta & \cos\theta \end{pmatrix} \tag{17}$$

We can drop the multiplying phase since it affect states by an overall phase, which is irrelevant. In the 50:50 special case $|r| = |t|$, the matrix associated with a 50:50 symmetric beam splitter is given by

$$\frac{1}{\sqrt{2}} \begin{pmatrix} 1 & i \\ i & 1 \end{pmatrix} \tag{18}$$

1.4 Mach-Zehnder interferometer

In this section an explicit example of quantum mechanical complementarity is analyzed: the Mach-Zehnder interferometers (MZI). MZIs can be used to observe the wave and particle like behavior of photons, as a convenient alternative to the famous double slit experiment. The following calculation shows how a single photon interacts with itself, allowing for interference fringes to appear. A MZI is represented in figure 2.

The initial state is given by a single photon that enters the interferometer through either one of the 2 ports of the first BS, hence the initial state will be either $|a\rangle$ or $|b\rangle$ – and not a general superposition. Here we will choose port a. After the first BS, the bottom arm is labeled with a, and the top one is labeled with b. A phase shifter is placed on the top path, introducing a relative phase φ between the two states, and the two paths are recombined by a last BS. The unitary operator associated with the interferometer must be obtained with a combination of the two matrices describing the BS (B) and the phase shifter (P)

$$B = \frac{1}{\sqrt{2}} \begin{pmatrix} 1 & i \\ i & 1 \end{pmatrix} \tag{19}$$

$$P = \begin{pmatrix} 1 & 0 \\ 0 & e^{i\varphi} \end{pmatrix} \tag{20}$$

The quantum mechanical realization of the whole interferometer is then the operator BPB. Applying this operator to the initial state $|a\rangle = \left(\begin{smallmatrix} 1 \\ 0 \end{smallmatrix}\right)$ we get the final state

$$\frac{1}{2} \begin{pmatrix} 1 & i \\ i & 1 \end{pmatrix} \begin{pmatrix} 1 & 0 \\ 0 & e^{i\varphi} \end{pmatrix} \begin{pmatrix} 1 & i \\ i & 1 \end{pmatrix} \begin{pmatrix} 1 \\ 0 \end{pmatrix} = i e^{i\frac{\varphi}{2}} \begin{pmatrix} \cos\frac{\varphi}{2} \\ sin\frac{\varphi}{2} \end{pmatrix} \tag{21}$$

The detectors placed after the interferometer observe photons with the probabilities

$$\| \langle \psi | a \rangle \|^2 = \cos^2 \frac{\varphi}{2} \tag{22}$$

$$\| \langle \psi | b \rangle \|^2 = \sin^2 \frac{\varphi}{2} \tag{23}$$

i.e. interference fringes are observed by varying continuously the phase φ. The MZI (specifically the parameter φ) can be adjusted so that the measured

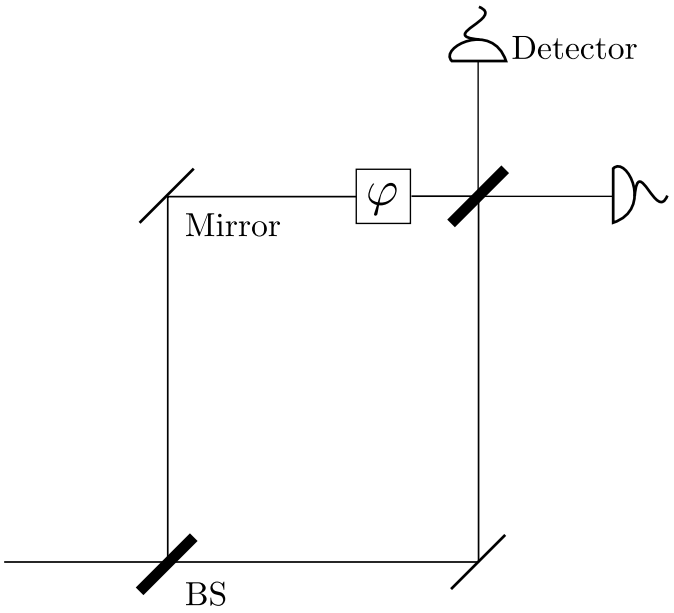

Figure 2: A Mach-Zehnder interferometer with a phase shifter on one of the two arms.

probabilities are

$$\|\langle\psi|a\rangle\|^2 = 0 \tag{24}$$

$$\|\langle\psi|b\rangle\|^2 = 1 \tag{25}$$

Which corresponds to the idealized case where the length difference between the two arms is identical (or that the phase introduced is an integer multiple of 2π). Interference of light is usually thought of as arising from the wave-like behavior of photons.

Particle behavior can e recovered with a simple modification to the setup, that is, the second beam splitter is removed. In this case the probabilities must be computed using the operator BP, yielding

$$\frac{1}{\sqrt{2}}\begin{pmatrix}1 & i\\ i & 1\end{pmatrix}\begin{pmatrix}1 & 0\\ 0 & e^{i\varphi}\end{pmatrix}\begin{pmatrix}1\\ 0\end{pmatrix} = \frac{1}{\sqrt{2}}\begin{pmatrix}1\\ i\end{pmatrix} \tag{26}$$

with probabilities $\frac{1}{2}$ and $\frac{1}{2}$. In this instance a somewhat naive reasoning applies: whenever the top detector clicks, it must mean that the photon, as a particle, has been transmitted by the BS, while a click on the other detector corresponds to a reflection at the BS. By placing or removing the second beam splitter one can choose whether to observe interference (wave-like behavior) or to know which path the photon has taken (particle-like behavior).

1.5 Time-bin encoding

The last physical implementation of the qubit that will be listed here is time-bin encoding. If Mach-Zehnder type of interferometer has two arms with different length, the photon will not take the same time to travel through the arms. The photons exit the interferometer on a superposition of states with either early of late travelling time. Measuring the time of arrival at the detector one understands which path the photon has covered. Once again we adapt the notation according to the physical implementation of the system, writing S for short and L for long

$$\psi = \alpha |S\rangle + \beta |L\rangle \tag{27}$$

where the usual rules apply to this qubit. The problem of how to practically implement operators on this type of states will be a physical one, much like the case where the matrix for the beam splitter was derived. Later on a more detailed, less idealized description of time-bin qubits will be presented, because they play a crucial role in this work.

1.6 Multiple degrees of freedom

Some optical elements can act on more that one degree of freedom. For example, a polarizing beam splitter (PBS) is a prism that separates a light beam in two different spatial modes, typically two perpendicular rays exiting the PBS, with defined polarizations. Such a device transmits the horizontal component of the polarization towards the spatial mode labeled a', and reflects the vertical one towards the perpendicular direction b'. As a result, a normalized input state coming from port a $|\psi\rangle = \alpha |a\rangle |H\rangle + \beta |a\rangle |V\rangle$ will be transformed by the PBS as

$$M_{PBS} |\psi\rangle = \alpha M_{BS,T} |a\rangle |H\rangle + \beta M_{BS,R} |a\rangle |V\rangle = \alpha |a'\rangle |H\rangle + i\beta |b'\rangle |V\rangle \tag{28}$$

where $M_{BS,T}$ is the operator associated to a beam splitter with $r = 0$ and $t = 1$, that is, a beam splitter that only transmits, whereas $M_{BS,R}$ is the operator representing an all-reflecting beam splitter. This is an example of manipulation of both the polarization and the spatial modes of light at the same time.

1.7 Basic principles of lasers

Lasers are used as a standard photon source for any of the experiments that are going to be discussed during this work, and are of fundamental importance for quantum optics. A LASER (acronym: light amplification by stimulated light emission) is a coherent and focused photon beam. The first laser was built in 1960 by Theodore H. Maiman at Hughes Laboratories, borrowing the theoretical framework from Charles Hard Townes and Arthur Leonard Schawlow. In this chapter we briefly sketch the base mechanism at play in laser theory.

The primary elements of a laser are the *gain medium*, which is where the light amplification occurs, and two mirrors called the *output coupler* and *high reflector*. The output coupler is partially reflective, and it is where the beam will come out of if certain conditions are satisfied. These two reflectors make sure

that light bounces back and forth between them, passing each time through the gain medium which amplifies the light every time. Amplification is quantified by the *gain coefficient* $\gamma(\omega)$ defined by (the following discussion is based on [12])

$$\frac{dI}{dz} = \gamma(\omega) I(z) \tag{29}$$

with z direction of propagation, ω angular frequency, and I optical intensity. A laser will work as long as amplification in the gain medium is sufficient to balance out the losses accumulated during the round a round trip. The gain medium is a population of atoms with different excitation states, so that absorption, spontaneous emission or stimulated emission occur. This kind of phoenomenology can be treated with the use of *Einstein coefficients*, which assigns different rates to different atomic transitions. For example, in a two-level population, if an atomic transition occurs between an excited level with energy E_2 and the ground state with energy E_1, a photon is emitted with angular frequency $\omega = \frac{E_2 - E_1}{\hbar}$. This process is called spontaneous emission, and the emission rate A_{21} (with obvious meaning of the subscript) will govern the rate of change over time of the number of atoms that populate the second level N_2 with the following relation

$$\frac{dN_2}{dt} = -A_{21} N_2 \tag{30}$$

While the number of the atoms at energy level 1 is not affected by spontaneous emission since they are at the ground state. The absorption process, on the other hand, is not spontaneous: if one wants to quantify absorption with a constant rate, as in B_{12}^{ω} for atoms that are excited from level 1 to level 2, an energy density $u(\omega)$ must be included in the treatment. The argument of the energy density is ω bacause atoms are excited only if the energy is exactly $\hbar\omega$. The rate of absorption of atoms populating the first excitation level, with this definitions, is

$$\frac{dN_1}{dt} = -B_{12}^{\omega} N_1 u(\omega) \tag{31}$$

There is a last process that occurs when considering this type of system: *stimulated emission*. In stimulated emission, an incoming photon triggers both downward emission and upwards absorption. This type of mechanism also must depend on the energy density. The corresponding coefficient is B_{21}^{ω} and the rate equation is

$$\frac{dN_2}{dt} = -B_{21}^{\omega} N_2 u(\omega) \tag{32}$$

A purely quantum computation shows that, for stimulated emission, the emitted photons are in phase with the incoming photons that triggered the transition in the first place. Note that Einstein's coefficients are not independent. Einstein found the relation between them by assuming thermal equilibrium, thus black body radiation is assumed for the energy density $u(\omega)$, and the rate of change of the population numbers is constant $\frac{dN_i}{dt} = 0$. The number ratio is given by the Boltzmann's law

$$\frac{N_2}{N_1} = \frac{g_2}{g_1} e^{-\frac{\hbar\omega}{k_B T}} \tag{33}$$

while the energy density at angular frequency ω is

$$u(\omega) = \frac{\hbar\omega^3}{\pi^2 c^3} \frac{1}{e^{\frac{\hbar\omega}{k_B T}} - 1} \tag{34}$$

where T is the temperature, k_B the Boltzmann's constant, and g_i is the degeneracy of level i. For 30, 31 and 32 to hold for all temperatures, the following relations between Einstein's coefficients must hold:

$$g_1 B_{12}^{\omega} = g_2 B_{21}^{\omega} \tag{35}$$

$$A_{21} = \frac{\hbar\omega^3}{\pi^2 c^3} B_{21}^{\omega} \tag{36}$$

Even though the last two equation were obtained with the assumption of thermal equilibrium, they are actually true in general, since it can be shown that the coefficients are intrinsic proprerties of the atom, rather than just global properties of an ensemble at thermal equilibrium. As far as lasers are concerned, in order for the gain medium to amplify we need that

$$B_{21}^{\omega} N_2 u(\omega) > B_{12}^{\omega} N_1 u(\omega) \tag{37}$$

meaning that the stimulated emission rate is greater than the absorption rate. The gain medium then increases the number of propagating photons at each passage, resulting in amplification of the beam. Substituting the relation between the coefficients,

$$N_2 > \frac{g_2}{g_1} N_1 \tag{38}$$

But at thermal equilibrium 33 must be satisfied, making it impossibile for this last relation to hold. A laser must therefore be operated at non-thermal equilibrium conditions, usually achieved by means of externally injecting energy into the system. These conditions are called *population inversion*. The population-inversion density is defined as

$$\Delta N = N_2 - \frac{g_2}{g_1} N_1 \tag{39}$$

It can be shown that under a population inversion ΔN, the gain is given by

$$\gamma = \frac{\lambda^2}{4n^2\tau} \Delta N F(\omega) \tag{40}$$

with λ vacuum wavelength, n refractive index of the gain medium, $\tau = A_{21}^{-1}$ is *radiative lifetime* of the upper level E_2, and $F(\omega)$ the spectral amplitude of the wavefunction. The spectral amplitude will be among the main conceptual points of the next section; for now we just point out that $F(\omega)$ is a normalized distribution describing the real shape of the wavepacket as opposed to the idealized version of a photon having perfectly defined energy $\hbar\omega$. A positive inversion represents a system where the number of excited atoms is greater than the number of atoms at the ground state. The last relation, coupled with 29, shows that for positive population inversions the beam is amplified, while negative ΔN results in attenuation. Positive ΔN cannot be obtained with a simple

two-level system, so lasers are always based off a gain medium with more than two energy levels. On a 4 level system, where $E_1 < E_2 < E_3 < E_4$ atoms are pumped from the ground state to level 4. These states quickly decay to level 3, so that a population inversion beween levels 2 and 3 is created. The spontaneous decay $E_2 \to E_1$ must be sufficiently fast so as to prevent atoms accumulating at level 2, which would destroy the population inversion. Atoms can be pumped either optically, (for example with a flash lamp or another laser), or electrically.

The population inversion is proportional to the pumping rate $\mathcal{R}$ which is in turn proportional to the power of the energy source used to pump the laser. For small $\mathcal{R}$, the gain increases linearly with it. When the pumping rate is high enough, the *laser threshold* is reached, that is, the gain is enough to actually output laser light out of the output reflector. This is also where population inversion does not increase anymore with the the pumping ratio. This *threshold gain* $\mathcal{R}_{th}$ is the minimum gain level required for the laser to operate, and is determined by factors such as length of the gain medium, reflection rates of the two mirrors, and losses due to scattering and absorption inside the cavity. Once $\mathcal{R} > \mathcal{R}_{th}$, all power is converted to intensity of the output laser light.

1.7.1 Laser modes

Laser beams are a great example of directional light. The divergence of a laser beam is quantified in terms of the *transverse mode* structure. Transverse modes are distinguished by the order of the Hermite polynomials which they depend on. The electromagnetic field associated with a cross section of a laser propagating on the z axis (the propagation direction is parallel to the cavity axis), is

$$\varepsilon_{mn} = \varepsilon_0 H_m(\sqrt{x/w}) H_n(\sqrt{y/w}) e^{-\frac{x^2+y^2}{w^2}} \tag{41}$$

where the integers m and n label different order Hermite polynomials. For $m, n = 0$ the multiplying factors H_0 are simply given by the constant 1, and the transverse shape of the beam ε_{00} is a 2-dimensional gaussian centered around $(x, y) = 0$. This is the familiar shape of "normal" lasers as commonly seen in the real world, and it is the mode with smallest divergence of all. The parameter w describes the width of beam, and is called beam spot size. In general, the beam is a superposition of an arbitrary number of such modes, which all contribute to the shape of the cross section of the ray of light.

The *longitudinal mode* structure of the beam is linked to the description of the cavity as a one-dimensional system: two mirrors placed in front of each other, with electromagnetic field oscillating strictly on the z axis. The electrical field is zero on the two reflectors, and the field inside the cavity is therefore a standing wave, where

$$\omega_{mode} = l \frac{\pi c}{n_{cav} L_{cav}} \tag{42}$$

represents the harmonics allowed inside the cavities, with l integer, n_{cav} refractive index of the cavity and L_{cav} length of the cavity. The separation between two modes is at least

$$\Delta\omega_{mode} = \frac{\pi c}{n_{cav} L_{cav}} \tag{43}$$

These separations as well as the spectral amplitude of the excitation energies of the atoms inside the cavity determine the spectrum of emission of the laser. If the width of the spectral amplitude of the cavity is smaller than the first harmonic, the laser will only output one mode. On the other hand, a broad frequency profile might allow it for some of the modes to be within the spectrum of the cavity, as often is the case. This does not necessarily mean that every resonating mode will actually add up to the output laser beam, because these oscillations still have to make it to the gain threshold: not every mode can trigger a gain value high enough to support lasing. When many modes compose the output light, we have a *multi-mode* laser, that needs to be supplied enough power to ensure that all the modes that fall within the spectral amplitude are above the laser threshold. A laser is *single mode* otherwise. Single mode can be obtained, for example, by introducing a frequency selective loss inside the cavity. In a multi mode laser, the relative optical phases between the modes are random. When different modes have a fixed phase difference, the laser is said to be *mode locked*. In a laser that is not phase locked, every longitudinal mode oscillates independently. Interference effects happen thanks to phase difference, but they are averaged out since these are random. As a result the cavity acts as many different lasers emitting light at slightly different frequencies. When all modes operate with a phase that has a definite relationship with every other mode, the output is rather different. This can be seen by analyzing the output from a temporal point of view via Fourier transform. In short, the fixed relationship between the modes allows for the light in the cavity to be modeled as a succession of single pulses that are emitted every time the output reflector is hit. Since the travel time in the cavity is $2n_{cav}L_{cav}/c$, laser light will be a regular train of pulses separated in time. Mode-locking is the only way to obtain very short pulse duration, in the order of picoseconds, or even femtoseconds.

1.8 Brief review of second quantization

The formalism adopted up until now is very useful for developing a basic understanding of idealized interferometers. However, the second quantization formalism is much more useful to deal with larger Hilbert spaces and non idealized models of photons, as in the case of laser pulses. Here we briefly introduce a more complete quantum description of the electromagnetic field and see how this is useful to better describe laser light and interferometers.

The potential vector of a polarized monochromatic wave is classically given by

$$A(\mathbf{r},t) = \boldsymbol{\varepsilon}^{\mu}_{\mathbf{k}} a^{\mu}_{\mathbf{k}}(t) e^{i\mathbf{k}\cdot\mathbf{r}} + \boldsymbol{\varepsilon}^{*\mu}_{\mathbf{k}} a^{*\mu}_{\mathbf{k}}(t) e^{-i\mathbf{k}\cdot\mathbf{r}} \tag{44}$$

Where a's time dependence from t is simply $a(t) = ae^{-i\omega t}$, a being a time independent complex coefficient, ω the angular frequency and $\mathbf{k}$ is the wave vector, and the dispersion relation for light in vacuum holds: $\omega = c|\mathbf{k}|$ (c is the speed of light). The indices of the polarization vectors are chosen $\mu = \pm 1$, labeling left and right handed polarization $\varepsilon^1 = -\frac{1}{\sqrt{2}}(e_x + ie_y)$ and $\varepsilon^{-1} = \frac{1}{\sqrt{2}}(e_x - ie_y)$, where x and y refer to the polarization vectors in cartesian coordinates.

The expression above represents the vector potential associated to a single mode of a monochromatic electromagnetic field. The whole field is retrieved either summing or integrating over the wave vectors $\mathbf{k}$, and on the two polar-

izations. When only considering a single mode, the following notation can be used

$$A(\mathbf{r},t) = a(t)e^{-i\mathbf{k}\cdot\mathbf{r}}\boldsymbol{\varepsilon} + c.c. \tag{45}$$

where c.c. is the complex conjugate. One can rescale the fourier coefficients a to get the classical Hamiltonian associated with this vector potential in more convenient units

$$H = \frac{1}{2}\hbar\omega(a^*a + aa^*) \tag{46}$$

This is a classical harmonic oscillator. We quantize it by promoting the classical amplitudes a to operators satisfying the following commutation relations

$$\left[a, a^\dagger\right] = 1 \tag{47}$$
$$[a, a] = 0 \tag{48}$$
$$\left[a^\dagger, a^\dagger\right] = 0 \tag{49}$$

The Hamiltionian for the quantum harmonic oscillator is

$$H = \hbar\omega(a^\dagger a + 1/2) \tag{50}$$

with orthonormal eigenstates $|n\rangle$ and eigenvalues $E_n = (\hbar\omega(n + 1/2))$. The normalized eigenstates are generated by means of operating with the $a^\dagger$ operator on the normalized vacuum state $|0\rangle$

$$|n\rangle = \frac{(a^\dagger)^n}{\sqrt{n!}}|0\rangle \tag{51}$$

This is because the eigenvectors satisfy

$$a|n\rangle = \sqrt{n}\,|n-1\rangle \tag{52}$$
$$a^\dagger|n\rangle = \sqrt{n+1}\,|n+1\rangle \tag{53}$$

hence their name *annihilation* and *creation* operators. Acting on a state with a creation operator "creates" a photon by changing the state from n to $n+1$ photons, as opposed to the *annihilation* operator (a) that "annihilates" a photon.

The usual way to label a mode is by polarization and wave vector. However, for the example of the beam splitter, one can label the different modes based on spatial information. Let us generalize the beam splitter case to a generic object that we will call "linear multiport" [36] that has N input modes and N output modes. A port is not necessarily a different physical path: as long as a mode can be distinguished from the others by any physical property (e.g. energy, polarization, entry/exit time etc.), we can associate a creation/annihilation type of operator. We use a_i for input modes, and b_i for output modes. States with multiple modes and number of photons are $|n_1 \dots n_j \dots n_N\rangle$, and define a space that is called Fock space. Linear optics deals with *linear* multiports, meaning that the outputs are a linear transformation of the inputs given by a matrix S_{ij}

$$b_i = \sum_{j=1}^{N} S_{ij} a_j \tag{54}$$

Or, using vector notation,

$$\mathbf{b} = S\mathbf{a} \tag{55}$$

If we want the total photon number to be conserved by the action of the multiport, S must be unitary; indeed

$$\mathbf{a}^\dagger \mathbf{a} = \mathbf{b}^\dagger \mathbf{b} = \mathbf{a}^\dagger S^\dagger S \mathbf{a} \tag{56}$$

implying

$$S^\dagger S = \mathbb{I} \tag{57}$$

Here we used the fact that the operator $\mathbf{a}^\dagger \mathbf{a}$ gives the total number of photons on a generic state. The commutation relations for a set of modes must reflect the fact that the modes are independent, so that a_i and b_i operators must satisfy

$$\left[a_i, a_j^\dagger\right] = \delta_{ij} \tag{58}$$

$$\tag{59}$$

all the other possibile independent commutators between these operators being equal to zero. One can verify with simple algebra that this set of equations, combined with 54 and the unitariety of S, implies

$$\left[b_i, b_j^\dagger\right] = \delta_{ij} \tag{60}$$

$$\tag{61}$$

and 0 for all other independent cases.

So far we have developed a description of the multiport in the so called *Heisenberg picture*. This framework is already useful to calculate the mean value of some observables, such as the number operator. Let us consider the example of the 50:50 symmetric beam splitter derived before with 2 input and 2 output ports. We already have the matrix operator associated with it. Suppose that we are interested in the mean value of the output photons on the second port when the state of one of the input ports, say, input port number 1, is $|n\rangle$, while at the other port the state is $|m\rangle$. The mean value we are looking for is

$$\langle nm| \, b_1^\dagger b_1 \, |nm\rangle \tag{62}$$

Using 54, and the commutation rules between the operators, we get

$$\langle nm| \left(S_{11}^* a_1^\dagger + S_{12}^* a_2^\dagger\right)(S_{11} a_1 + S_{12} a_2) |nm\rangle = \tag{63}$$

$$= \langle nm| S_{11} S_{11}^* a_1^\dagger a_1 + S_{12} S_{12}^* a_2^\dagger a_2 |nm\rangle = \tag{64}$$

$$\frac{1}{2} \langle nm| a_1^\dagger a_1 + i(-i) a_2^\dagger a_2 |nm\rangle = \tag{65}$$

$$\frac{1}{2} \langle nm| a_1^\dagger a_1 + a_2^\dagger a_2 |nm\rangle = \tag{66}$$

$$= \frac{n+m}{2} \tag{67}$$

$$\tag{68}$$

where products between orthogonal states have been omitted. A completely analogous computation yields the same result for $\langle nm| b_2^\dagger b_2 |nm\rangle$. Indeed total photon number is conserved by the multiport, as expected.

On the other hand, the Heisenberg picture does not provide a simple way to compute probabilities, for example the probability to measure a given number of photons in a given output mode. Indeed in this picture the states are fixed, and the operators evolve according to 54. We will need to translate this formalism to the Schroedinger picture, that is, operators are fixed and states evolve. As soon as we know how to compute the evolution of a state, then the transition probabilities are computed via

$$p_{a\to b} = |\langle \psi_{fin} | \psi_b \rangle|^2 \tag{69}$$

where $|\psi_{fin}\rangle$ and $|\psi_b\rangle$ are the two states we are interested in. This quantity represents the probability that the final state is found to be $|\psi_{fin}\rangle$, given that the initial state, before crossing the multiport, is $|\psi_a\rangle$. $|\psi_b\rangle$ is the state after crossing the multiport. In the Schroedinger picture states are not constant. Whenever a state undergoes an evolution (for example the photon passes through an optical element) we must compute the resulting state via the time evolution operator

$$|\psi_b\rangle = U |\psi_a\rangle \tag{70}$$

with U unitary operator that provides the evolution of states in the Schrodinger picture. In quantum mechanics, switching between different pictures is a symmetry (i.e. probabilities are conserved) since adopting a different formal description of a system cannot possibly affect physics. In the case we are dealing with, the states of the Heisenberg picture are exactly the initial states of the multiport $|\psi_a\rangle$. Mean values for a generic operators on a given state $|\psi_b\rangle$ are computed via

$$\langle A \rangle_{\psi_b} = \langle \psi_b | A |\psi_b\rangle = \langle \psi_a | U^\dagger A U |\psi_a\rangle \tag{71}$$

where the last equation is the mean value of the operator $U^\dagger A U$ on the Heisenberg states $|\psi_a\rangle$. This gives us the transformation law for states and operators when changing from the two pictures

$$A_H = U^\dagger A_S U \tag{72}$$

$$|\psi_H\rangle = U^\dagger |\psi_S\rangle \tag{73}$$

Because we can build up all states by means of creation and annihilation operators, it is natural to see how the transformation law 54 applies to these operators in the new picture.

$$a_i \to b_i = \sum_{i=1}^{N} S_{ij} a_j = U^\dagger a_i U \tag{74}$$

$$a_i^\dagger \to b_i^\dagger = \sum_{i=1}^{N} S_{ij}^* a_j^\dagger = U^\dagger a_i^\dagger U \tag{75}$$

Let us consider the simple case where we evolve a single mode state with an arbitrary number of photons n on the l-th mode, and zero elsewhere. Applying the evolution operator to 51,

$$|\psi_b\rangle = U|\psi_a\rangle = U|n_l\rangle = U\frac{(a_l^\dagger)^{n_l}}{\sqrt{n_l!}}|0\rangle \tag{76}$$

multiplying the identity $U^\dagger U$ before the ket

$$|\psi_b\rangle = U\frac{(a_l^\dagger)^{n_l}}{\sqrt{n_l!}}U^\dagger U|0\rangle \tag{77}$$

Since the multiport is lossles, the application of the evolution operator to the vacuum state cannot create photons. In general, $U|0\rangle = e^{i\alpha}|0\rangle$. This is a global phase that will not interfere with the probability calculations, so it can be omitted

$$|\psi_b\rangle = U\frac{(a_l^\dagger)^{n_l}}{\sqrt{n_l!}}U^\dagger|0\rangle = \frac{(Ua_l^\dagger U^\dagger)^{n_l}}{\sqrt{n_l!}}|0\rangle \tag{78}$$

to find out the inverse transformation law $Ua^\dagger U^\dagger$, we first multiply 75 by S_{il} and sum over i, use the fact that S is unitary and subsequently apply U from left and $U^\dagger$ from right.

$$U^\dagger a_i^\dagger U = \sum_j S_{ij}^* a_j^\dagger \tag{79}$$

$$\Rightarrow \sum_i S_{il} U^\dagger a_i^\dagger U = \sum_{ij} S_{ij}^* S_{il} a_j^\dagger = \sum_j \delta_{jl} a_j^\dagger = a_l^\dagger \tag{80}$$

$$\Rightarrow U a_l^\dagger U^\dagger = \sum_i S_{il} a_i^\dagger \tag{81}$$

using this into 78 we get

$$|\psi_b\rangle = \frac{(\sum_i S_{il} a_i^\dagger)^{n_l}}{\sqrt{n_l!}}|0\rangle \tag{82}$$

this result is easily generalized to states with different modes populated with different photon numbers, since a_i and a_j commute for $i \neq j$. For example, with 2 populated ports k and l

$$|\psi_b\rangle = \frac{(\sum_i S_{ik} a_i^\dagger)^{n_k}}{\sqrt{n_k!}} \frac{(\sum_i S_{il} a_i^\dagger)^{n_l}}{\sqrt{n_l!}} |0\rangle \tag{83}$$

Picking the scattering matrix associated with the beam splitter, with initial state $|10\rangle$, using the rules above,

$$|\psi_b\rangle = \frac{1}{\sqrt{2}}(a_1^\dagger + i a_2^\dagger)|0\rangle \tag{84}$$

The probability amplitudes of detecting a photon exiting respectively through port 1 and 2 is

$$p_1 = \langle 10|\psi_b\rangle = \frac{1}{\sqrt{2}} \langle 0| a_1 (a_1^\dagger + i a_2^\dagger)|0\rangle = \frac{1}{\sqrt{2}} \langle 0| a_1 a_1^\dagger |0\rangle = \frac{1}{\sqrt{2}} \tag{85}$$

$$p_2 = \langle 01|\psi_b\rangle = \frac{1}{\sqrt{2}} \langle 0| a_2 (a_1^\dagger + i a_2^\dagger)|0\rangle = \frac{i}{\sqrt{2}} \langle 0| a_2 a_2^\dagger |0\rangle = \frac{1}{\sqrt{2}} \tag{86}$$

the probabilities are found via square module, and are 1/2 and 1/2 as expected

1.9 Modeling real laser pulses

Second quantization gives rise to an arbitrary large (possibily infinite) number of modes for the electromagnetic field, but we restricted the discussion to a finite set of creation and annihilation operators associated to a finite subset of excitations where a photon is identified with a mode of the electromagnetic field. As a result we re-labeled the modes with a finite number of indices i, $i = 1, \ldots, N$ forgetting the fact that they were labeled by the wave vector in the first place. From now on we focus on photons propagating in one dimension, so that the modes will be defined by angular frequency and direction of propagation, instead of a three-dimensional vector.

The first noticeable deviation of the previous description, from more experiment oriented approaches, is the complete independence of the excitations from time and frequency. Forgetting all about the frequency, that is, assuming that a single mode will always consistently be associated to a specific known energy, is a simplification that does indeed suffice to describe the basic physics behind interferometers. However, in many experimental applications a less idealized description is needed; in fact, the typical light source never emits light consistently at the same energy. In these cases, the light emission process occurs over a limited time span, consequently giving rise to an energy uncertainty, meaning that light is emitted with an angular frequency distribution, rather than a single ω. The specific shape depends on the physical process employed for light creation. More often than not, the frequency profile of photons will be modeled as a pulse peaked around a certain value of ω. While many different distributions for wavepackets may exist, here we will focus on gaussian peaks because they are customarily associated with pulsed lasers.

This improved picture maintains the previous concept of optical mode labeled by a finite number of indices, while on the other hand adds a countinuous degree of freedom to every creation/annihilation operator that takes into account the energy distribution of a photon. The creation operator associated

with a photon centered around time t with a complex frequency distribution $F(\omega)$, in the optical mode i is [25]

$$a^\dagger_{i,F} = \int_0^\infty d\omega F(\omega) a^\dagger_i(\omega) \tag{87}$$

and similarly for the annihilation operator. $F(\omega)$ is the spectral amplitude of the wave packet, and $a^\dagger(\omega)$ is the continuous mode creation operator. Assuming that $F(\omega)$ is normalized, the continuous frequency annihilation and creation operators must satisfy the commutation relations

$$\left[a_i(\omega), a^\dagger_j(\omega')\right] = \delta(\omega - \omega')\delta_{ij} \tag{88}$$

Let us choose a Gaussian shaped pulse passing for the spatial origin at time t_0. The spectral amplitude is

$$F_{t_0}(\omega) = (2\pi\sigma^2)^{-1/4} e^{-i(\omega-\omega_0)t_0 - \frac{(\omega-\omega_0)^2}{4\sigma^2}} \tag{89}$$

and ω_0 is the central frequency ($c = 1$ from here on). We are interested in computing the commutator of two modes peaked around two different times. We can do so by extending the integration range to $[-\infty, +\infty]$. This is possible whenever $\sigma \ll \omega_0$ (small bandwidth approximation). Using 88, and integrating, the result is

$$\left[a_{i,t_1}, a^\dagger_{j,t_2}\right] = \delta_{ij} e^{-\frac{(t_2-t_1)^2}{2\tau_c^2}} \tag{90}$$

Where we dropped the F subscript from the operators because Gaussian distribution with fixed width and central frequency is implied, and we label the creation operator with the peak time instead. We define $\sigma^{-1} \equiv \tau_c$ as the coherence time. The separation between two wavepackets is controlled by two factors: the time separation of the pulses and the coherence time, that is, the width of the Gaussian. Specifically, if $t_2 - t_1 \gg \tau_c$, the pulses can be considered well separated and consequently their related operators commute. Therefore, the states $a^\dagger_{i,t_1}|0\rangle$ and $a^\dagger_{i,t_2}|0\rangle$ are orthogonal.

Because we extended the Hilbert space to an infinite space, operators must be generalized because they not only depend on the discrete indices i, but also on the ωs. All sums appearing in the section above must be replaced with a mixed sum and integration operator. In general,

$$U a_i(\omega) U^\dagger = \sum_j \int_0^\infty d\omega' S_{ji}(\omega', \omega) a_j(\omega') \tag{91}$$

For frequency independent operators the above becomes

$$U a^\dagger_i(\omega) U^\dagger = \sum_j S_{ji} a^\dagger_i(\omega) \tag{92}$$

and the transformation law for $a^\dagger_{j,F}$ is

$$U a^\dagger_{i,F} U^\dagger = \sum_j S_{ji} \int_0^\infty d\omega F(\omega) a^\dagger_j(\omega) = \sum_j S_{ji} a^\dagger_{j,F} \tag{93}$$

It is possibile to define operators that act on the time degree of freedom. We use a time label again since we once more fix the spectral amplitude to a Gaussian peaked around some time t_0. A time shift applied on a creation operator must give another creation operator peaked around a new value $t_0+\Delta t$, hence

$$a^\dagger_{i,t_0} \to a^\dagger_{i,t_0+\Delta t_0} \tag{94}$$

This is the case where every single discrete mode i is affected by the time shift. One can verify that this effect is obtained by applying to the continuous creation operator $a^\dagger_i(\omega)$ the unitary operator $S(\omega) = \delta_{ij} e^{i(\omega-\omega_0)\Delta t_0}$,

$$a^\dagger_{i,t_0} \to \int_0^\infty d\omega e^{-i(\omega-\omega_0)\Delta t_0} F(\omega)_{t_0} a^\dagger_i(\omega) = \int_0^\infty d\omega F(\omega)_{t_0+\Delta t_0} a^\dagger_i(\omega) = a^\dagger_{i,t_0+\Delta t_0} \tag{95}$$

If every mode is shifted by a different time, the operator will be $S_{ij} = \delta_{ij} e^{i(\omega-\omega_0)\Delta t_i}$, where Δt_i are the different delays associated to the different optical modes.

1.10 Mach-Zehnder interferometer with time degree of freedom

With this new formalism introduced, it is natural to go ahead and check how, for example, a simple system such as the Mach-Zehnder interferometer as seen from the previous sections is affected by taking into account this new model of a photon. As a first consideration, it is useful to emphasize that even though the formalism introduced so far is based on the frequency spectrum of the wavepackets, one can always switch to a time-based description of the photon via Fourier transform, since time is the conjugate variable to frequency. With this in mind, we can carry out the calculation in whatever variables we deem appropriate and Fourier transform (being careful to preserve normalization) to get a description that is easy to read from a temporal perspective.

Let us consider the *unbalanced Mach-Zehnder interferometer* represented in figure 3. Since light takes more time to travel through the longer arm, the effect is to introduce a delay $\Delta t = 2\Delta l/c$ to the photon taking the longer course, with Δl length of the unbalancement. There is an additional time delay Δt_0 affecting both routes to the same extent, due to the photon travel time across the horizontal portion of the arms, which is the same length for both routes. This delay will therefore contribute as a global phase according to 94. Let us write down the matrices associated to the beam splitters and to the time delays

$$B = \frac{1}{\sqrt{2}} \begin{pmatrix} 1 & i \\ i & 1 \end{pmatrix} \tag{96}$$

$$P_{\Delta t} = \begin{pmatrix} 1 & 0 \\ 0 & e^{-i(\omega-\omega_0)\Delta t} \end{pmatrix} \tag{97}$$

$$P_{\Delta t_0} = e^{-i(\omega-\omega_0)\Delta t_0} \begin{pmatrix} 1 & 0 \\ 0 & 1 \end{pmatrix} \tag{98}$$

The scattering matrix of this setup is

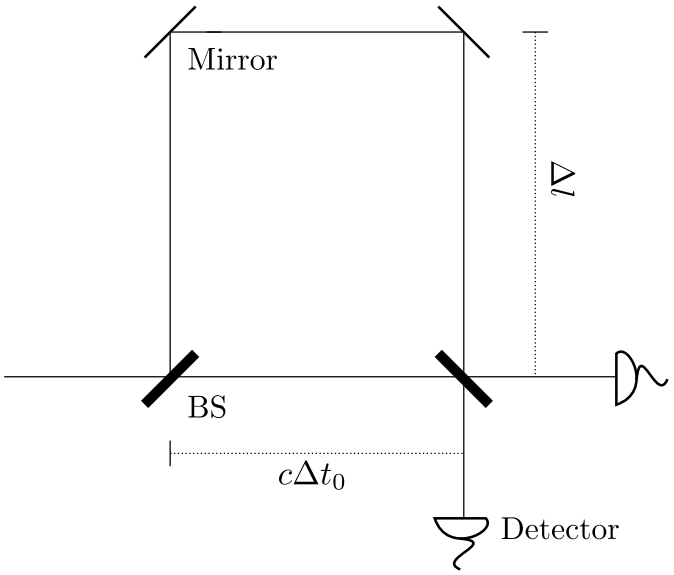

Figure 3: An unbalanced Mach-Zehnder interferometer

$$BP_{\Delta t_0}P_{\Delta t}B = \frac{1}{2}e^{-i(\omega-\omega_0)\Delta t_0}\begin{pmatrix} -e^{-i(\omega-\omega_0)\Delta t}+1 & i(e^{-i(\omega-\omega_0)\Delta t}+1) \\ i(e^{-i(\omega-\omega_0)\Delta t}+1) & +e^{-i(\omega-\omega_0)\Delta t}-1 \end{pmatrix} \tag{99}$$

If we want to compute the probability amplitudes, we should perform the calculation in the Schroedinger picture. As an initial state we will choose a distribution peaked at time t at the input 1 of the first beam splitter

$$|\psi_a\rangle = a^\dagger_{1,t}|0\rangle \tag{100}$$

and carry out the calculation in a similar fashion as the completely discrete case

$$\begin{aligned} |\psi_b\rangle = U|\psi_a\rangle = Ua_{1,t}|0\rangle = Ua_{1,t}U^\dagger|0\rangle \\ = \frac{1}{2}\int d\omega F(\omega)_{t_0}e^{-i(\omega-\omega_0)\Delta t_0}\Big[(-e^{-i(\omega-\omega_0)\Delta t}+1)a^\dagger_1(\omega)+ \\ +i(e^{-i(\omega-\omega_0)\Delta t}+1)a^\dagger_2(\omega))\Big]|0\rangle = \\ = \frac{1}{2}\int d\omega F(\omega)_{t_0+\Delta t_0}\Big[+a^\dagger_1(\omega)+ia^\dagger_2(\omega)\Big]|0\rangle + \\ +\frac{1}{2}\int d\omega F(\omega)_{t+\Delta t_0+\Delta t}\Big[-a^\dagger_1(\omega)+ia^\dagger_2(\omega))\Big]|0\rangle = \\ = \frac{1}{2}(a^\dagger_{1,t_0+\Delta t_0}-a^\dagger_{1,t+\Delta t_0+\Delta t}+ia^\dagger_{2,t+\Delta t_0}+ia^\dagger_{2,t+\Delta t_0+\Delta t})|0\rangle \end{aligned} \tag{101}$$

Suppose that we observe the output photons at the output port 1. The transition probability is obtained by choosing as the final state a photon with

exactly energy ω exiting port 1. Similar reasoning is applied when we shift the interest to the second port. For port one,

$$|\psi_{fin_1}\rangle = a(\omega)_1^\dagger |0\rangle \tag{102}$$

and the probability amplitude we get is

$$\begin{aligned}
\langle\psi_{fin_1}|\psi_b\rangle &= \frac{1}{2}\langle 0| a_1(\omega)\left(a^\dagger_{1,t+\Delta t_0+\Delta t} + ia^\dagger_{2,t+\Delta t_0+\Delta t} - a^\dagger_{1,t+\Delta t_0} + ia^\dagger_{2,t+\Delta t_0}\right)|0\rangle \\
&= \frac{1}{2}\langle 0| \int d\omega' a_1(\omega)\left(F(\omega')_{t_0+\Delta t_0} a_1^\dagger(\omega') - F(\omega')_{t_0+\Delta t_0+\Delta t} a_1^\dagger(\omega')\right)|0\rangle \\
= \frac{1}{2}\langle 0| \int d\omega' \left(F(\omega')_{t_0+\Delta t_0}\left[a_1(\omega), a_1^\dagger(\omega')\right] - F'(\omega)_{t_0+\Delta t_0+\Delta t}\left[a_1(\omega), a_1^\dagger(\omega')\right]\right)|0\rangle \\
&= \frac{1}{2}\int d\omega' \left(F(\omega')_{t_0+\Delta t_0}\delta(\omega'-\omega) - F(\omega')_{t_0+\Delta t_0+\Delta t}\delta(\omega'-\omega)\right) \\
&= \frac{1}{2}\left(F(\omega)_{t_0+\Delta t_0} - F(\omega)_{t_0+\Delta t_0+\Delta t}\right) \equiv \psi_1(\omega)
\end{aligned} \tag{103}$$

The annihilation operators on the left-hand side commutes with the creation operators associated to a different optical mode (2 in this case), so that after the commutation we can apply it to the vacuum and get zero. Such manipulations have been omitted in the calculation above. For the other output state $|\psi_{fin}\rangle = a_2^\dagger(\omega)|0\rangle$, the probability amplitude is computed bracketing the state with a photon in the second spatial mode. After an analogous computation, the end result is

$$\langle\psi_{fin_2}|\psi_b\rangle = \frac{i}{2}\left(F(\omega)_{t_0+\Delta t_0} + F(\omega)_{t_0+\Delta t_0+\Delta t}\right) \equiv \psi_2(\omega) \tag{104}$$

These are the probability amplitudes associated with the 2 exits of the interferometer. For future reference, we write down the action of the MZI on the spectral amplitudes as

$$\psi(\omega)_{t_{0,1}} \to \frac{1}{2}\left(\psi(\omega)_{t_0} - e^{i(\omega-\omega_0)\Delta t}\psi(\omega)_{t_0}\right) \tag{105}$$

$$\psi(\omega)_{t_0,2} \to \frac{i}{2}\left(\psi(\omega)_{t_0} + e^{i(\omega-\omega_0)\Delta t}\psi(\omega)_{t_0}\right) \tag{106}$$

Taking the Fourier transformation is much more insightful: because experimentally we measure the arrival time of the output photons, it makes sense to display the distribution as a function of the observation time. Here we use the convention for the Fourier transform $f(t) = \frac{1}{\sqrt{2\pi}}\int d\omega e^{i\omega t} f(\omega)$ to make sure that if the gaussian spectral amplitudes $F_{t_0}(\omega)$ are normalized, so are their Fourier transforms.

$$\psi_1(\omega) = \frac{1}{2}(2\pi\sigma^2)^{-1/4}\left(e^{-i(\omega-\omega_0)(t_0+\Delta t_0)} - e^{-i(\omega-\omega_0)(t_0+\Delta t_0+\Delta t)}\right)e^{-\frac{(\omega-\omega_0)^2}{4\sigma^2}}$$
$$\to \frac{1}{2}\left(\frac{2}{\pi\tau_c^2}\right)^{1/4}\left(e^{-(\frac{t-t_0-\Delta t_0}{\tau_c})^2} - e^{-i\omega_0\Delta t}e^{-(\frac{t-t_0-\Delta t_0-\Delta t}{\tau_c})^2}\right)e^{i\omega_0(t-t_0-\Delta t_0)} \equiv \psi_1(t) \tag{107}$$

$$\psi_2(\omega) = \frac{i}{2}(2\pi\sigma^2)^{-1/4}\left(e^{-i(\omega-\omega_0)(t_0+\Delta t_0)} + e^{-i(\omega-\omega_0)(t_0+\Delta t_0+\Delta t)}\right)e^{-\frac{(\omega-\omega_0)^2}{4\sigma^2}}$$
$$\to \frac{i}{2}\left(\frac{2}{\pi\tau_c^2}\right)^{1/4}\left(e^{-(\frac{t-t_0-\Delta t_0}{\tau_c})^2} + e^{-i\omega_0\Delta t}e^{-(\frac{t-t_0-\Delta t_0-\Delta t}{\tau_c})^2}\right)e^{i\omega_0(t-t_0-\Delta t_0)} \equiv \psi_2(t) \tag{108}$$

We have then derived the action of the interferometer on the Fourier transform of the initial spectral amplitude 89 before crossing the interferometer. Explicitly, the transform of the initial amplitude is

$$F(t) = \left(\frac{2}{\pi\tau_c^2}\right)^{1/4} e^{i\omega_0(t-t_0-\Delta t_0)}e^{-(\frac{t-t_0-\Delta t_0}{\tau_c})^2} \tag{109}$$

and the action of the interferometer as seen from the two ports is respectively

$$F(t) \to \frac{1}{2}F(t-\Delta t_0) - F(t-\Delta t_0-\Delta t) \tag{110}$$

$$F(t) \to \frac{i}{2}(F(t-\Delta t_0) + F(t-\Delta t_0-\Delta t)) \tag{111}$$

The probability amplitudes depending on time are the sums of two Gaussians peaked around the two "classical expected arrival times" $t_{short} = t + \Delta t_0$, and $t_{long} = t + \Delta t_0 + \Delta t$, representing the travel time of two classical particles moving at the speed of light travelling through the shorter and longer arm of the interferometer. Furthermore, a phase difference $\omega_0\Delta t$ between the two peaks is present, and it is explicitly linked to the path difference Δt. A more obvious feature of these amplitudes is that for sufficiently large t, they both vanish, since a single photon is created at a definite time t_0 before the interferometer, and we cannot expect it to take an arbitrarily long time to travel through it.

Let us adopt a more compact notation and define

$$\tau = t - t_0 - \Delta t_0 \tag{112}$$

The probabilities of detecting a photon at time τ are

$$|\psi_1(\tau)|^2 = \frac{1}{4}\left(\frac{2}{\pi\tau_c^2}\right)^{1/2}\left(e^{-2(\frac{\tau}{\tau_c})^2} + e^{-2(\frac{\tau-\Delta t}{\tau_c})^2} - 2e^{-(\frac{\tau-\Delta t}{\tau_c})^2}e^{-(\frac{\tau}{\tau_c})^2}\cos(\omega_0\Delta t)\right) \tag{113}$$

$$|\psi_2(\tau)|^2 = \frac{1}{4}\left(\frac{2}{\pi\tau_c^2}\right)^{1/2}\left(e^{-2(\frac{\tau}{\tau_c})^2} + e^{-2(\frac{\tau-\Delta t}{\tau_c})^2} + 2e^{-(\frac{\tau-\Delta t}{\tau_c})^2}e^{-(\frac{\tau}{\tau_c})^2}\cos(\omega_0\Delta t)\right) \tag{114}$$

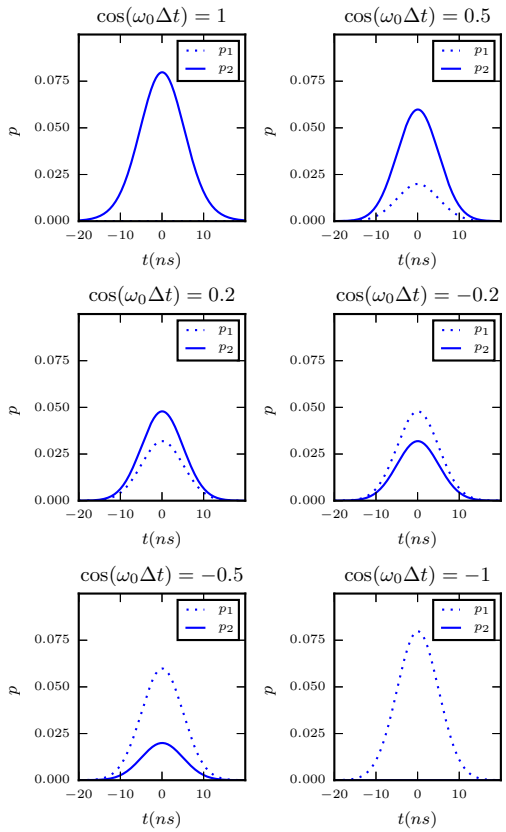

Figure 4: The probabilities at both ports are displayed when $\tau_c \gg \Delta t$.

The last term on both amplitudes gives rise to interference thanks to the cosine. Whether this interference is detectable or not depends on the ratio of the coherence time and the time shift Δt, as will become obvious in the following calculation. Integrating over time to get the total detection probabilities yields

$$p_1 = \int_{-\infty}^{\infty} d\tau |\psi_1(\tau)|^2 = \frac{1}{2}\left(1 - e^{-\frac{1}{2}\frac{\Delta t^2}{\tau_c^2}} \cos(\omega_0 \Delta t)\right) \tag{115}$$

$$p_2 = \int_{-\infty}^{\infty} d\tau |\psi_2(\tau)|^2 = \frac{1}{2}\left(1 + e^{-\frac{1}{2}\frac{\Delta t^2}{\tau_c^2}} \cos(\omega_0 \Delta t)\right) \tag{116}$$

Which is a common result in interferometry. Also, the probabilities add up to one, as expected. The term multiplying the cosine is customarily referred to as *visibility* ($\mathcal{V}$), while the argument of the cosine is the *phase* (φ). The visibility is a positive parameter always less than one, and is often given in terms of percentage.

If $\Delta t \gg \tau_c$, probability amplitudes become $\frac{1}{2}$ regardless of the phase and photons bear "which path" information. Indeed, much like in the classical analogous of this experiment, we know that if the photon took longer to travel

through the interferometer it must have taken the longer path, and similarly for the earlier time/shorter path.

Ultimately, adding the time degree of freedom, and using a "properly" set interferometer, we can destroy interference. When $\tau_c \gg \Delta t$ interference with maximum visibility is observed, and the phase is controlled by the path difference between the possibile routes of the interferometer. Time resolution is completely lost, and time can no longer be employed as a distinguishing factor for the photon state. Figure 4 represents the probabilities at the two ports in this limit.

$$p_1 = \sin^2\left(\frac{\omega_0 \Delta t}{2}\right) \tag{117}$$

$$p_2 = \cos^2\left(\frac{\omega_0 \Delta t}{2}\right) \tag{118}$$

the phase can be arranged, for example, to make only one of the detectors after the ports click. Note that if $\tau_c \ll \Delta t$, the states $a^\dagger_\tau |0\rangle$ and $a^\dagger_{\tau+\Delta t} |0\rangle$ are orthogonal:

$$\langle 0| a_\tau a^\dagger_{\tau+\Delta t} |0\rangle = \langle 0| \left[a_\tau, a^\dagger_{\tau+\Delta t}\right] |0\rangle = e^{-\frac{\Delta t^2}{\tau_c^2}} \approx 0 \tag{119}$$

where the commutator is computed via 90.

1.10.1 Measuring interference on time-bin encoded qubits

We already anticipated how the temporal degree of freedom can be used to encode qubits, and the treatment above is necessary to understand how an unbalanced Mach Zehnder interferometer can be employed as a simple tool to create such qubits. On a setup where this interferometer is used, one typically looks at either one of the two exits. Restricting the treatment to one of the ports means that mode indices can be omitted, and the state should be renormalized. Equation 101 tells us that from port 1 of the interferometer the state is

$$|\psi\rangle = \frac{1}{\sqrt{2}}(a^\dagger_{t_{0+\Delta t_0}} - a^\dagger_{t_0+\Delta_{t_0}+\Delta t}) |0\rangle = |S\rangle - |L\rangle \tag{120}$$

while, for port 2

$$|\psi\rangle = \frac{i}{\sqrt{2}}(a^\dagger_{t_{0+\Delta t_0}} + a^\dagger_{t_0+\Delta_{t_0}+\Delta t}) |0\rangle = |S\rangle + |L\rangle \tag{121}$$

Where S denotes the shorter path, and L the longer one. For this states to qualify as a genuine qubits, the ratio $\frac{\Delta t}{\tau_c}$ must be chosen sufficiently large to assume the two base states orthogonal upon exiting the interferometer, so that the photon does not interfere with itself, as seen in the previous section. This assumption will be implied throughout this whole work, unless otherwise stated. The qubits after respectively port 1 and 2 have a π and 0 phase. A general phase α is obtained by adding a phase shifter on one of the two arms of the interferometer (here we choose the long arm, hence the matrix is $\left(\begin{smallmatrix} 1 & 0 \\ 0 & e^{i\alpha} \end{smallmatrix}\right)$). The scattering matrix of the interferometer taking into account the additional phase becomes

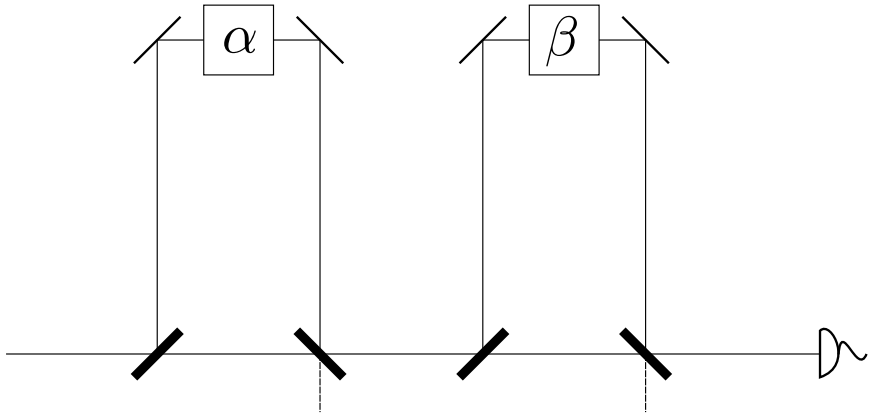

Figure 5: Two Mach Zehnder interferometers in series. Each one adds an adjustable phase α and β to the quantum state. The detector is placed at port I after the second interferometer. Dashed lines represent the part of signal that we discard in this treatment.

$$BP_{\Delta t_0}P_{\Delta t}P_{\alpha}B = \frac{1}{2}e^{-i(\omega-\omega_0)\Delta t_0}\begin{pmatrix} -e^{-i(\omega-\omega_0)\Delta t+i\alpha}+1 & i(e^{-i(\omega-\omega_0)\Delta t+i\alpha}+1) \\ i(e^{-i(\omega-\omega_0)\Delta t+i\alpha}+1) & +e^{-i(\omega-\omega_0)\Delta t+i\alpha}-1 \end{pmatrix} \tag{122}$$

thus, out of port 1

$$|\psi\rangle = \frac{1}{\sqrt{2}}(a^{\dagger}_{t_{0+\Delta t_0}} - e^{i\alpha}a^{\dagger}_{t_0+\Delta_{t_0}+\Delta t})\,|0\rangle = \frac{1}{\sqrt{2}}(|S\rangle - e^{i\alpha}\,|L\rangle) \tag{123}$$

while

$$|\psi\rangle = \frac{1}{\sqrt{2}}(a^{\dagger}_{t_{0+\Delta t_0}} + e^{i\alpha}a^{\dagger}_{t_0+\Delta_{t_0}+\Delta t})\,|0\rangle = \frac{1}{\sqrt{2}}(|S\rangle + e^{i\alpha}\,|L\rangle) \tag{124}$$

for port 2. These are *phase encoded* qubits. One way to observe quantum mechanical interference from this kind of qubits is, for example, to use the output states as an input to a second interferometer with the same properties of this first one, but with a different phase β. If the first pulse enters the second unbalanced interferometer at time t_1, the delayed pulse enters at $t_1 + \Delta t$. Reinstating the mode indices on the initial state to avoid confusion,

$$\begin{aligned} |\psi_b\rangle = U\,|\psi_a\rangle = U\frac{1}{\sqrt{2}}(a^{\dagger}_{1,t_1} - e^{i\alpha}a^{\dagger}_{1,t_1+\Delta_t})U^{\dagger}\,|0\rangle = \\ = \frac{1}{\sqrt{2}}\left(Ua^{\dagger}_{1,t_1}U^{\dagger} - e^{i\alpha}Ua^{\dagger}_{1,t_1+\Delta_t}U^{\dagger}\right)|0\rangle = \\ = \frac{1}{2\sqrt{2}}(a^{\dagger}_{1,t_1} - e^{i\alpha}a^{\dagger}_{1,t_1+\Delta t} + ia^{\dagger}_{2,t_1} + ie^{i\alpha}a^{\dagger}_{2,t_1+\Delta t} + \\ -e^{i\beta}a^{\dagger}_{1,t_1+\Delta t} + e^{i(\alpha+\beta)}a^{\dagger}_{1,t_1-2\Delta t} - ie^{i\beta}a^{\dagger}_{2,t_1+\Delta t} + ie^{i(\alpha+\beta)}a^{\dagger}_{2,t_1+2\Delta t})\,|0\rangle \end{aligned} \tag{125}$$

a neater form is obtained writing the port specific result

$$|\psi_{b,1}\rangle = \frac{1}{2\sqrt{2}}\left(a^\dagger_{t_1} - e^{i\alpha}a^\dagger_{t_1+\Delta t} - e^{i\beta}a^\dagger_{t_1+\Delta t} + e^{i(\alpha+\beta)}a^\dagger_{t_1+2\Delta t}\right)|0\rangle \tag{126}$$

$$|\psi_{b,2}\rangle = \frac{i}{2\sqrt{2}}\left(a^\dagger_{t_1} + e^{i\alpha}a^\dagger_{t_1+\Delta t} - e^{i\beta}a^\dagger_{t_1+\Delta t} - e^{i(\alpha+\beta)}a^\dagger_{t_1+2\Delta t}\right)|0\rangle \tag{127}$$

Once more we want to work with the amplitudes on the temporal domain. The probability amplitude associated with the above states can be computed with the same procedure as before, bracketing the states above with $\langle 0|\, a(\omega)$ and Fourier transforming what is obtained.

$$\begin{aligned}\psi_1(t) = \frac{1}{2\sqrt{2}}\big[&F(t-t_1) - e^{i\alpha}F(t-t_1-\Delta t) + \\ -e^{i\beta}&F(t-t_1-\Delta t)) + e^{i(\alpha+\beta)}F(t-t_1-2\Delta t)\big]\,|0\rangle\end{aligned} \tag{128}$$

$$\begin{aligned}\psi_2(t) = \frac{i}{2\sqrt{2}}\big[&F(t-t_1) + e^{i\alpha}F(t-t_1-\Delta t) + \\ -e^{i\beta}&F(t-t_1-\Delta t) - e^{i(\alpha+\beta)}F(t-t_1-2\Delta t)\big]\,|0\rangle\end{aligned} \tag{129}$$

A quicker approach to the calculation is noting that we have derived the action of the interferometer 111, so we can directly apply it to the amplitude $\psi_0(t) = \frac{1}{\sqrt{2}}(F(t-t_1) + F(t-t_1-\Delta t))$, $\psi_0(t)$ being the amplitude associated to the state $\frac{1}{\sqrt{2}}(a^\dagger_{1,t_1} - e^{i\alpha}a^\dagger_{1,t_1+\Delta_t})\,|0\rangle$. In fact, this will be the standard approach to this type of computation henceforth, the first reason being calculation ease. However, there is a second reason to prefer working directly with amplitudes rather than creation operators on the vacuum. Indeed, having a look for example at equation 120, one notices that the phase depending on the path length does not appear in our state, as opposed to equation 108. In fact, the pase difference $e^{-i\omega_0\Delta t}$ is hidden in the notation – namely on the Δt subscript on the creation operator. When working with amplitudes, we can readily read this phase off the explicit form of the amplitutes instead.

Once again it is convenient to work with time shifted coordinates $\tau = t - t_1$. The amplitudes, modulo a global phase that does not interfere with the probabilities, are the following

$$\begin{aligned}\psi_1(\tau) = \frac{1}{2\sqrt{2}}\left(\frac{2}{\pi\tau_c^2}\right)^{1/4}\Big[&e^{-i\alpha}e^{-(\frac{\tau}{\tau_c})^2} - e^{-i\omega_0\Delta t}e^{-(\frac{\tau-\Delta t}{\tau_c})^2} + \\ -e^{-i(\alpha-\beta)}&e^{-i\omega_0\Delta t}e^{-(\frac{\tau-\Delta t}{\tau_c})^2} + e^{i\beta}e^{-2i\Delta}e^{-(\frac{\tau-2\Delta t}{\tau_c})^2}\Big]\end{aligned} \tag{130}$$

$$\begin{aligned}\psi_2(\tau) = \frac{i}{2\sqrt{2}}\left(\frac{2}{\pi\tau_c^2}\right)^{1/4}\Big[&e^{-i\alpha}e^{-(\frac{\tau}{\tau_c})^2} + e^{-i\omega_0\Delta t}e^{-(\frac{\tau-\Delta t}{\tau_c})^2} + \\ -e^{-i(\alpha-\beta)}&e^{-i\omega_0\Delta t}e^{-(\frac{\tau-\Delta t}{\tau_c})^2} - e^{i\beta}e^{-2i\Delta}e^{-(\frac{\tau-2\Delta t}{\tau_c})^2}\Big]\end{aligned} \tag{131}$$

The computation of the square module becomes much easier remembering that we are in the $\tau_c \ll \Delta t$ approximation. This means that any overlapping

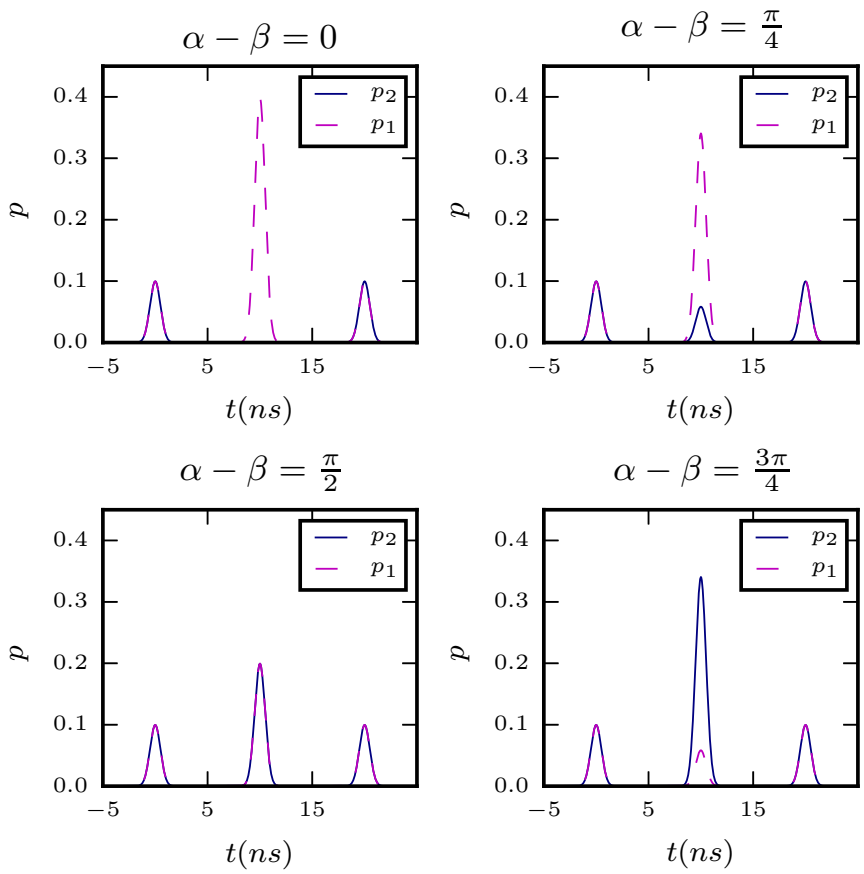

Figure 6: Probabilities at different phase values. Note how the two which-path peaks are not affected when changing the phase.

terms of the form $e^{-(\frac{\tau}{\tau_c})^2}e^{-(\frac{\tau-\Delta t}{\tau_c})^2}$, $e^{-(\frac{\tau-\Delta t}{\tau_c})^2}e^{-(\frac{\tau-2\Delta t}{\tau_c})^2}$ and $e^{-(\frac{\tau}{\tau_c})^2}e^{-(\frac{\tau-2\Delta t}{\tau_c})^2}$ are zero. The probability densities are

$$|\psi_1(\tau)|^2 = \frac{1}{8}\left(\frac{2}{\pi\tau_c^2}\right)^{1/2}\left[e^{-2(\frac{\tau}{\tau_c})^2} + e^{-2(\frac{\tau-2\Delta t}{\tau_c})^2} + 4e^{-2(\frac{\tau-\Delta t}{\tau_c})^2}\cos^2\left(\frac{\alpha-\beta}{2}\right)\right] \tag{132}$$

$$|\psi_2(\tau)|^2 = \frac{1}{8}\left(\frac{2}{\pi\tau_c^2}\right)^{1/2}\left[e^{-2(\frac{\tau}{\tau_c})^2} + e^{-2(\frac{\tau-2\Delta t}{\tau_c})^2} + 4e^{-2(\frac{\tau-\Delta t}{\tau_c})^2}\sin^2\left(\frac{\alpha-\beta}{2}\right)\right] \tag{133}$$

The first two terms are non interfering terms that integrated yield a total probability of $\frac{1}{4}$ to both amplitudes. As a result, there always is a total probability of $\frac{1}{2}$ that interference is *not* measured by this setup. The reason is that the photon can take 4 total paths to travel across this double umbalanced interferometer.

- short - short
- short - long
- long - short
- long - long

The first and the last possibile routes are indeed distinguishable with a time measurement. We have *which-path* information. On the other hand, from a temporal standpoint, a measurement happening when the photon takes one of the two remaining possibile courses cannot tell us whether the photon has crossed the short arm of the first interferometer and the long arm of the second or vice-versa, hence interference is measured. Schematically, keeping in mind the representation of the amplitudes for different values of the phase shown in figure 6

- short - short ⟵ first peak, *which-path*
- short - long ⟵ central peak, interference
- long - short ⟵ central peak, interference
- long - long ⟵ last peak, *which-path*

For completeness, one might want to compute the total probabilities observed at the two ports.

$$p_1 = \int_{-\infty}^{\infty} d\tau |\psi_1(\tau)|^2 = \frac{1}{4} + \frac{1}{2}\cos^2\left(\frac{\alpha-\beta}{2}\right) \tag{134}$$

$$p_2 = \int_{-\infty}^{\infty} d\tau |\psi_1(\tau)|^2 = \frac{1}{4} + \frac{1}{2}\sin^2\left(\frac{\alpha-\beta}{2}\right) \tag{135}$$

$$\tag{136}$$

In practise, in an experiment where the focus is to observe interference, one just integrates around the central peak, meaning that the $\frac{1}{4}$ terms are often forgotten about and the total probability one refers to is just

$$p_1 = \cos^2\left(\frac{\alpha-\beta}{2}\right) \tag{137}$$

$$p_2 = \sin^2\left(\frac{\alpha-\beta}{2}\right) \tag{138}$$

$$\tag{139}$$

This is possibile because there is no risk of ambiguity: which path events always happen away from the central interfering peak, provided that the coherence time is small enough compared to Δt. In conclusion, interference takes place at the central peak, with a phase that is modulated by the phase shifters of the two interferometers. Furthermore, the visibility is one.

1.10.2 Double unbalanced interferometer with different unbalancements

Here we assumed that the interferometers introduce the same delay on the longer arms. The more general case represented in figure 7 can be handled much in the same way as the previous one. Notation-wise, we still use a $\Delta t = l/c$ time shift for the initial interferometer, while we use $\Delta t' = l'/c$ for the second interferometer. l and l' are the length differences between longer and shorter arms respectively inside the first and the second unbalanced interferometers. We assume that both timeshifts are comparable in magnitude, and both are much larger than the coherence time. We also use the shorter notation $\tau = t - t_1$ and factor away any global time-shifts (like Δt_0), since those do not contribute to probabilities.

The second interferometer acts on the input state $F(\tau) - e^{i\alpha}F(\tau - \Delta t)$ as

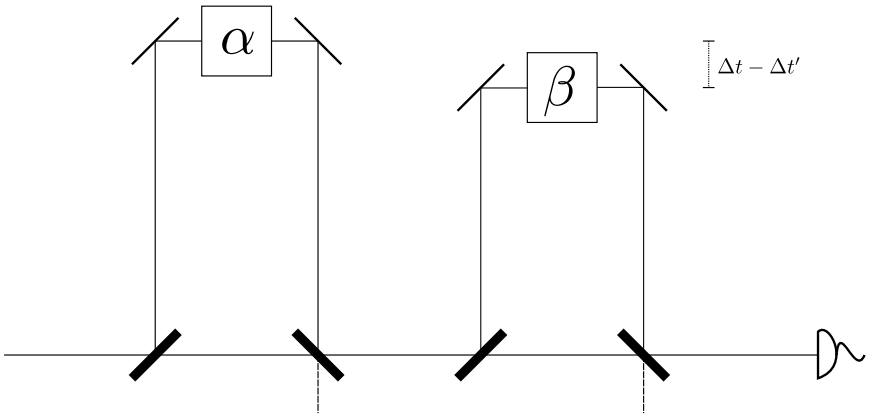

Figure 7: Two Mach Zehnder interferometers in series, with different unbalancements (greatly exaggerated in the figure). The setup is the same as the one considered before, except for the unbalancements.

$$\frac{1}{\sqrt{2}}\left(F(\tau) - e^{i\alpha}F(\tau - \Delta t)\right) \rightarrow$$
$$\frac{1}{2\sqrt{2}}\left(F(\tau) - e^{i\alpha}F(\tau - \Delta t) - e^{i\beta}F(\tau - \Delta t') + e^{i(\alpha+\beta)}F(\tau - \Delta t - \Delta t')\right) \tag{140}$$

when observed at the first port, and

$$\frac{1}{\sqrt{2}}\left(F(\tau) - e^{i\alpha}F(\tau - \Delta t)\right) \rightarrow$$
$$\frac{i}{2\sqrt{2}}\left(F(\tau) - e^{i\alpha}F(\tau - \Delta t) + e^{i\beta}F(\tau - \Delta t') - e^{i(\alpha+\beta)}F(\tau - \Delta t - \Delta t')\right) \tag{141}$$

at the second port. Explicitly, modulo a global phase,

$$\psi_1(\tau) = \frac{1}{2\sqrt{2}}\left(\frac{2}{\pi\tau_c^2}\right)^{1/4}\Big[e^{-i\alpha}e^{-(\frac{\tau}{\tau_c})^2} - e^{-i\omega_0\Delta t}e^{-(\frac{\tau-\Delta t}{\tau_c})^2} + \\ -e^{-i(\alpha-\beta)}e^{-i\omega_0\Delta t'}e^{-(\frac{\tau-\Delta t'}{\tau_c})^2} + e^{i\beta}e^{-i(\Delta t+\Delta t')}e^{-(\frac{\tau-\Delta t-\Delta t'}{\tau_c})^2}\Big] \tag{142}$$

$$\psi_2(\tau) = \frac{1}{2\sqrt{2}}\left(\frac{2}{\pi\tau_c^2}\right)^{1/4}\Big[e^{-i\alpha}e^{-(\frac{\tau}{\tau_c})^2} + e^{-i\omega_0\Delta t}e^{-(\frac{\tau-\Delta t}{\tau_c})^2} + \\ -e^{-i(\alpha-\beta)}e^{-i\omega_0\Delta t'}e^{-(\frac{\tau-\Delta t'}{\tau_c})^2} - e^{i\beta}e^{-i(\Delta t+\Delta t')}e^{-(\frac{\tau-\Delta t-\Delta t'}{\tau_c})^2}\Big] \tag{143}$$

The corresponding probability amplitudes are computed with the same assumptions as the previous case, and are given by

$$|\psi_1(\tau)|^2 = \frac{1}{8}\left(\frac{2}{\pi\tau_c^2}\right)^{1/2}\Big[e^{-2(\frac{\tau}{\tau_c})^2} + e^{-2(\frac{\tau-\Delta t-\Delta t'}{\tau_c})^2} + e^{-2(\frac{\tau-\Delta t}{\tau_c})^2} + e^{-2(\frac{\tau-\Delta t'}{\tau_c})^2} + \\ + 2e^{-(\frac{\tau-\Delta t}{\tau_c})^2}e^{-(\frac{\tau-\Delta t'}{\tau_c})^2}\cos\left(\omega_0(\Delta t'-\Delta t)+(\alpha-\beta)\right)\Big] \tag{144}$$

$$|\psi_2(\tau)|^2 = \frac{1}{8}\left(\frac{2}{\pi\tau_c^2}\right)^{1/2}\Big[e^{-2(\frac{\tau}{\tau_c})^2} + e^{-2(\frac{\tau-\Delta t-\Delta t'}{\tau_c})^2} + e^{-2(\frac{\tau-\Delta t}{\tau_c})^2} + e^{-2(\frac{\tau-\Delta t'}{\tau_c})^2} + \\ - 2e^{-(\frac{\tau-\Delta t}{\tau_c})^2}e^{-(\frac{\tau-\Delta t'}{\tau_c})^2}\cos\left(\omega_0(\Delta t'-\Delta t)+(\alpha-\beta)\right)\Big] \tag{145}$$

The first two terms of both equations correspond to which path measurements – two gaussian peaks situated respectively before ($\tau = 0$) and after ($\tau = \Delta t + \Delta t'$) the interfering part of the output wavepackets. Our interest lies in the middle part of the distribution, so that is what we are going to integrate over all times. The probability of finding a photon on the central peak is

$$p_1 = \int_{-\infty}^{\infty} d\tau|\psi_1(\tau)|^2 = \frac{1}{4}\left(1 + e^{-\frac{1}{2}\frac{(\Delta t-\Delta t')^2}{\tau_c^2}}\cos\left(\omega_0(\Delta t'-\Delta t)+(\alpha-\beta)\right)\right) \tag{146}$$

$$p_2 = \int_{-\infty}^{\infty} d\tau|\psi_2(\tau)|^2 = \frac{1}{4}\left(1 - e^{-\frac{1}{2}\frac{(\Delta t-\Delta t')^2}{\tau_c^2}}\cos\left(\omega_0(\Delta t'-\Delta t)+(\alpha-\beta)\right)\right) \tag{147}$$

This is an expression that has already been discussed: in short, we have interference with visibility less than 1. In general, an arm length difference between two unbalanced arms of the interferometers intrinsically degrades visibility. If one wants $\mathcal{V} \approx 1$, then the arms' lengths, while being both sufficiently larger than $c\tau_c$, must be chosen such that $l - l' \ll c\tau_c$. In the case where $\Delta t - \Delta t' \gg \tau_c$ interference is lost.

Intuitively, the loss of visibility occurs because crossing the *short-long* and *long-short* paths does not take the same time anymore: in mixed situations,

some path information can now be extracted from the experiment. This is because, even in the case where the two time shifts are only slightly different in length, if the photon takes longer than $\frac{\Delta t+\Delta t'}{2}$ to get to the detector, there is a larger chance that it travelled through the long arm of the interferometer with greater unbalancement, and vice-versa.

1.11 Basic review of the density operator formalism

When in quantum mechanics a state is a statistical ensemble of pure states, it is said to be a mixed state. The representation of this type of state is usually done via *density operators*. The state of the quantum system is a statistical mixture of an arbitrary number of pure states $|\psi_i\rangle$, $i \in [1, \ldots, n]$, with positive coeffients p_i such that $\sum_{i=1}^{n} p_i = 1$. A matrix called *density matrix* or *density operator* can be used to give a full desctiption of this ensemble, instead of the ket state formalism applied to pure states. The density operator for this system is

$$\rho = \sum_i p_i \left|\psi_i\right\rangle \left\langle\psi_i\right| = \sum_i p_i \rho_i \tag{148}$$

Here the terms density operator and density matrix are used interchangeably. Hower, we note that the term *density matrix* makes sense only after one has defined an orthonormal basis $|\varphi_n\rangle$, where $i = 1, \ldots, N$ so that the matrix elements can be computed as

$$\rho_{mn} = \left\langle\varphi_m\right| \rho \left|\varphi_n\right\rangle \tag{149}$$

note that the following hold

$$\rho^\dagger = \rho \tag{150}$$
$$\operatorname{tr} \rho = 1 \tag{151}$$
$$\tag{152}$$

and ρ is positive semi-definite. With this formalism, mean values are computed via traces: if O is an observable, then its mean value when the state of the system is given by $|\psi\rangle$ is

$$\langle A\rangle_\psi = \operatorname{tr}(A\rho) \tag{153}$$

For pure states, $p_i = 1$, and $p_j = 0$ for $j \neq i$, and the density operator is just $|\psi\rangle \langle\psi|$. When considering Hilbert spaces of dimension 2, that is, a qubit as introduced before, the density matrix provides a description that is equivalent to the Bloch sphere when considering only pure states, but also extends the formalism to mixed states. Let us parametrize the density matrix as

$$\rho = \frac{\mathbb{I} + S}{2} \tag{154}$$

where $\mathbb{I}$ is the 2 by 2 identity. Since ρ must be hermitian, we have the following parametrization for the S matrix

$$S = r_x \begin{pmatrix} 0 & 1 \\ 1 & 0 \end{pmatrix} + r_y \begin{pmatrix} 0 & -i \\ i & 0 \end{pmatrix} + r_z \begin{pmatrix} 1 & 0 \\ 0 & -1 \end{pmatrix} = \mathbf{r} \cdot \boldsymbol{\sigma} \tag{155}$$

the matrices σ_i are the well known Pauli matrices. $\boldsymbol{\sigma}$ is a vector of where each entry is one of these matrices, while (r_x, r_y, r_z) is a real vector $|r| \leq 1$ describing a point inside the unit ball in three dimensions. The equal sign holds for pure states, so that they are described by the unit sphere. When $r < 1$, the S matrix describes a mixed state instead.

1.12 Visibility and Predictability

Wavelike behavior is associated with inteference patterns, while particle-like behavior comes up anytime it is possibile to reconstruct with certainty the route that the quantum particle has undertaken, when a path-qubit is considered. An important result by Englert [11] introduced a concrete bound that quantifies quantum mechanical duality in a clear way. Precise definitions of *fringe visibility* and *distinguishability* were proposed, and, as it turns out, mixed situations where visibility and path distinguishability are not perfect satisfy a very specific inequality, along wth the ideal cases where distinguishability or visibility are perfect.

A Mach-Zehnder interferometer composed by a beam splitter and a beam merger is considered. The two alternative paths are labeled by quantum numbers $1, -1$, that is, the eigenvalues of the Pauli matrix σ_z. The beam merger (BM) has the same function of the beam splitter in the MZI: it recombines the rays after they travel through the two different arms. Furthermore, a different phase is applied to the different arms of the interferometer. Using the density matrix formalism, the BM and the BS are represented as acting on the density matrix ρ as

$$\rho \to e^{-i\frac{\pi}{4}\sigma_y}\rho e^{i\frac{\pi}{4}\sigma_y} \tag{156}$$

and the phase shifter is represented by

$$\rho \to e^{-i\frac{\varphi}{2}\sigma_z}\rho e^{i\frac{\varphi}{2}\sigma_z} \tag{157}$$

As an input state, a general mixed state is taken:

$$\rho^i = \frac{\mathbb{I} + \mathbf{r_i} \cdot \boldsymbol{\sigma}}{2} \tag{158}$$

the interferometer, after the beam merger that recombines the rays, outputs the final state ρ^f

$$\rho^f = \frac{\mathbb{I} + \mathbf{r_f} \cdot \boldsymbol{\sigma}}{2} \tag{159}$$

where, if (r_x, r_y, r_z) is the Bloch vector associated with the initial state, then

$$\mathbf{r}_f = \begin{pmatrix} -r_x \\ r_y \cos\varphi + r_z \sin\varphi \\ r_y \sin\varphi - r_z \cos\varphi \end{pmatrix} \tag{160}$$

represents the final state. For example, taking the pure state corresponding to $\mathbf{r}_{|0\rangle} = (0, 0, 1)$ as an input, the output state is $(0, \sin\varphi, \cos(\varphi))$, and the relative frequency of, say, measuring the value -1 rather than 1, is given by the operator $\frac{1}{2}(1 - \sigma_z)$. Probabilities are computed via the density matrix formalism with

$$p = \mathrm{tr}\left[\frac{1}{2}\left(1 - \sigma_z\right)\rho^f\right] \tag{161}$$

therefore, the probability that the detector corresponding to the path labeled -1 clicks, when the input state is given by the Bloch vector $r_{|0\rangle}$, is

$$p_{|0\rangle} = \frac{1}{2}\left(1 + \cos\varphi\right) = \cos^2\left(\frac{\varphi}{2}\right) \tag{162}$$

that is, the usual pure state interference pattern with maximum visibility. When a general mixed state is used as an input, the above is generalized as

$$\frac{1}{2}\left(1 - r_y \sin\varphi + r_z \cos\varphi\right) \tag{163}$$

The quantity

$$\mathcal{V}_0 = \sqrt{r_y^2 + r_z^2} \tag{164}$$

is defined as the *a priori* fringe visibility. The *predictability* of the system is a quantity that is associated to how well the experimenter can predict whether the quantum particle will take one route with respect to the other. For example, in a Mach-Zender interferometer without the second beam splitter before the detectors, we have minimal predictability, since the two probabilities associated with the two paths are $w_+ = \frac{1}{2}$ and $w_- = \frac{1}{2}$. Here, we define $\mathcal{P} = |w_+ - w_-|$, so that it will be 0 for fully unpredictable outcomes, and 1 when we know that only one of the two detectors will click. For the system considered here,

$$w_\pm = \mathrm{tr}\left[\frac{1}{2}\left(1 \pm \sigma_x\right)\rho^f\right] = \frac{1}{2}(1 \mp r_x) \tag{165}$$

so that

$$\mathcal{P} = r_x \tag{166}$$

For example, in the specific case of $r_{|0\rangle}$, we have a 0 predictability. Because of this definition, a relation between a priori visibility and predictability is derived when noting that for a Bloch vector $|\mathbf{r}| \leq 1$ [14]

$$\mathcal{V}_0^2 + \mathcal{P}^2 \leq 1 \tag{167}$$

where the equal sign holds for pure states. Predictability can be measured with which-way detectors inside the interferometer, for example, by placing two detectors on the two arms right after the first beam splitter. The total initial state of the system will be described by $\rho^i = \rho_Q^i \rho_D^f$, where Q refers to the quantum particle and D to the detectors. The which-path detectors evolve according to

$$\rho_D \to U_\pm \rho_D U_\pm \tag{168}$$

Where the plus sign holds when the quantum particle crosses the $+1$ path, while the minus sign when the path is -1. These which-path detectors are a part of the quantum system. Symmetric interferometers with maximal a priori fringe visibility are described by,

$$r_x = 0 \tag{169}$$

$$r_z + i r_y = e^{-i\theta} \tag{170}$$

Englert found that this states evolve inside the system coupled with which-path detectors as

$$r_x \to 0 \tag{171}$$

$$r_z + i r_y \to -e^{-i(\varphi-\theta)}\mathcal{C} \tag{172}$$

where $\mathcal{C}$ is a complex contrast factor depending only on the degrees of freedom of the detector

$$\mathcal{C} = \mathrm{tr}_D \left[U_-^\dagger \rho_D U_+\right] \tag{173}$$

and the visibility is taken as $\mathcal{V} = |\mathcal{C}|$. For the final state of the detectors, one must trace out the degrees of freedom relative to the quantum particles, which turns out to be

$$\rho_D = \mathrm{tr}_Q\, \rho^f = \frac{1}{2} U_-^\dagger \rho_D U_- + \frac{1}{2} U_+^\dagger \rho_D U_+ = \frac{1}{2}\rho_D^{(+)} + \frac{1}{2}\rho_D^{(-)} \tag{174}$$

In quantum mechanics, distinguishability between two states can be given in terms of the norm of their difference. Using the density matrix formalism, in this particular case,

$$\mathcal{D} = \frac{1}{2}\,\mathrm{tr}_D \left|\rho_D^+ - \rho_D^-\right| \tag{175}$$

With these definitions for visibility and distinguishability, Englert proved that

$$\mathcal{D}^2 + \mathcal{V}^2 \leq 1 \tag{176}$$

2 Locality and Hidden Variable Theories

2.1 Introduction

Let us consider two spatially separated observers, Alice and Bob, performing spin measurements on the singlet state of a system composed by a couple of spin $\frac{1}{2}$ particles (A and B). More specifically, the observer measures the value of the projection of the spin operator along a chosen axis. Suppose that Alice is the first to perform such a measurement: quantum theory predicts that regardless of the direction of the axis along which Alice choses to measure the spin of particle A, if Bob measures B along the same direction, he will obtain with certainty the opposite value of what Alice got. As soon as Alice measures A, she can infer with certainty Bob's spin value along the direction she chose to measure, provided that Bob will indeed perform a measurement along the same direction.

When considering the classical counterpart of this experiment no difficulties arise, as at the moment of separation the information about A and B is carried along the paths of the particles, and a classical measurement just draws this information out of the system. However, when A and B are two electrons in the singlet state, that is, a quantum mechanical system, their spin value along a certain direction is not defined until it is measured. When Alice performs a spin measurement, she does not "find out" the spin of the other particle, rather, she knows what Bob's measurement would yield if perfomed as described above. The two measurements are said to be *correlated*.

When assuming that the two observers are separated enough, it is very clear that quantum mechanics is in stark contrast with locality, as explained as follows. The notion of locality can be summarized by stating that, in a local theory, physical processes cannot have instantaneous consequences on some other parts of the system (this will be formalized in the next section). Quantum mechanics seems to imply that when Alice measures the spin of her particle, the fact that she performed a measurement would have to propagate instantly over to Bob's system, so that Bob's results will show correlations accordingly. This must happen regardless of his spatial separation with respect to Alice, because Alice can choose the settings of her measuring apparatus while the particle is in flight, and so can Bob, well after the particles initially separated (here we are still making the assumption that regardless what the observers do with their settings, they agree to always end up with their measurement axis aligned). The paradoxical nature of the system here described lies in the fact that quantum mechanics, taken as-is, appears to be a non-local theory. This result is Bohm's reformulation of the Einstein-Podolski-Rosen (EPR) paradox [10].

Because correlation seems to logically suggest that some sort of information is shared by the components of a system, one could suggest that this correlation between the two particles A and B is consequence of some sort of underlying interaction, over which the experimenters have no control over and/or knowledge of. At this stage, no particular request is made on this hidden interaction. EPR, after presenting the paradox, concluded that quantum mechanics must be incomplete (where *complete* has a specific meaning as defined in the famous paper), and that completing quantum mechanics with the addition of a hidden-variable theory would remove the paradox. Namely, they suggested that the problem might be fixed by the introduction of a set of hidden variables shared by both particles at the moment of separation and conjectured that if *locality*

were to be restored in quantum mechanics, it would be by means of a *local hidden-variable theory*. This means that, similarly to the classical case, some hidden information on the particles is indeed carried along their trajectories, and this fact is just not described by quantum mechanics.

In this chapter, the concept of *hidden-variable theory* will be treated with a mathematical approach, and a widely accepted definition of *locality* will be given. These two tools will be sufficient to show that regardless of whether quantum mechanics is a hidden variable theory or not, it cannot be local, contrary to the EPR conjecture.

2.2 Locality condition

Suppose that two spatially separated experimenters, Alice and Bob, perform measurements on two systems produced by a common source. The observers are free to choose what kind of measurement they want to perform on their system, and we label x the set of experimental settings chosen by Alice, and y the settings chosen by Bob. The possible outcomes for x and y are respectively labeled as a and b. For example, in the specific case described in the previous section, x and y are the two unit vectors denoting the direction along which the spin of two electrons in the singlet state is measured. In quantum mechanics, the outcomes of such a measurement are given by the eigenvalues of the matrices $\mathbf{x} \cdot \boldsymbol{\sigma}$, and $\mathbf{y} \cdot \boldsymbol{\sigma}$, where the components of the $\boldsymbol{\sigma}$ vector are the Pauli matrices σ_i (which the spin operator along the $\mathbf{x}$ unit vector $\frac{\hbar}{2}\mathbf{x} \cdot \boldsymbol{\sigma}$ is proportional to), hence $a = \pm 1$, $b = \pm 1$. For the time being, there is no need to restrict ourselves to this specific case.

Generally, a complete set of possible outcomes is associated to a probability distribution, which in turn depends on the experimental settings x and y. The outcomes a and b could be correlated, meaning that the probability $p(ab|xy)$ is not generally factorizable as $p(a|x)p(b|y)$. What we expect (and very reasonably, demand) from a local theory is that if there is any correlation between the measured values, it must be due to an interaction that happened in the past when the two system were in contact. As a consequence of this assumption, we can expand our notation by using a set of variables λ that fully take into account the correlations caused by the past interactions. Indeed, there must be a distance where the two particles cannot interact anymore, at the very least when Alice and Bob are spacelike separated. From Alice's point of view, the probability distribution associated to her experiment can only depend on her experimental setup x and on the past variables λ, and conversely, Bob's probability density depends on y and λ. In a local theory, Alice's measurements cannot be affected by the experimental choices y made by Bob, and the same must apply to Bob. As a result, a couple of outcomes is described by

$$a(x;\lambda) \tag{177}$$
$$b(y;\lambda) \tag{178}$$

because the two distributions are

$$p(a|x;\lambda) \tag{179}$$
$$p(b|y;\lambda) \tag{180}$$

Since by definition we factored out all correlations into the past variables λ, the total probabiliy is now factorizable with respect to the uncorrelated variables describing the experimental settings

$$p(ab|xy;\lambda) = p(a|x;\lambda)p(b|y;\lambda) \tag{181}$$

This reasoning in no way implies that the variables λ are under control, or even possible to know; after all, this is what a hidden variable theory implies. Interaction between the systems can be arbitrarily complex: the locality request 181 holds as long as the two systems stop interacting at some point, which is the case when the observers are sufficiently separated (we assume space-like separation from now on).

The actual value of the λs can vary for every run of the experiment, and we describe this by associating a normalized probability distribution $q(\lambda)$ to the past variables, where we made the assumption that q does not depend on x and y, since the experimental adjustments made by the observer cannot possibly have an influence on the source. The experimental distributions measured by Alice and Bob after many runs of the experiment are then

$$p(ab|xy) = \int d\lambda \; p(a|x;\lambda)p(b|y;\lambda) \tag{182}$$

where we can see that this description does indeed result in a correlated probability distribution, from the observers' standpoint. The product ab is defined as the correlation, and takes the form

$$E(x,y) = \int d\lambda \; a(x;\lambda) \; b(y;\lambda) \; q(\lambda) \tag{183}$$

A hidden variable theory is local when this equality holds (a detailed derivation of all of this formalism can be found in [3]). We could also take as alternative definitions 182 or 181. With this definition in mind, it is possible to investigate whether the correlations of quantum mechanics satisfy this condition. The short answer is no: in fact, Bell, in 1964 [4] demonstrated that local hidden variables theories cannot reproduce the correlations of quantum mechanics.

2.3 CHSH inequality

Here is presented the derivation of an inequality that holds for *any* local hidden-variable theory, in the specific case where the two sets of outcomes for the measurements, yet again performed by two experimenters Alice and Bob, are

$$a = \pm 1 = b \tag{184}$$

We stress that, while the result that will follow is of major interest when applied to the two spin $\frac{1}{2}$ system, at this stage the specific system (quantum mechanical or not) that is considered does not matter: the following derivation should hold regardless for any local theory as long as 184 holds.

Suppose that the complete description of the initial state is given by the set of hidden variables λ via the normalized probability density $q(\lambda)$ as defined in the section above. Alice's set of outcomes depends on her local variables x, because of locality, as well as on the hidden variables λ shared with Bob, whereas Bob's results depend on y and yet the same set of hidden variables

λ. The experimental settings of one of the experimenters does not affect the measurement of the other one. If the experimental outcomes are correlated, the reason for the correlation is all contained in the hidden variables, which in turn are local. The full dependence of the outcomes from the different variables are

$$a(x;\lambda) = \pm 1 \ , \ b(y;\lambda) = \pm 1 \tag{185}$$

Because the theory is assumed to be local, the correlations are defined as in 183.

These few premises by themselves suffice to derive a very powerful restriction on the correlations. Having said that, it is possibile introduce a more general hypothesis that takes into account experimental difficulties, so that an inequality that can be effectively used in actual, non idealized experiments, can be derived.

In practice, measurements never have perfect efficiency. Here we use a terminology associated with detectors for definiteness, but other measuring systems can be thought of (since we are dealing with an abstract system). For example, one of the two detectors may sometimes fail to register an event. When this is the case, we'll count a or/and b as 0. One can then supplement the theory by adding a new set of hidden variables μ and ν, so that $a = a(x;\lambda\mu)$ and $b = b(y;\lambda\nu)$ that take into account these experimental problems. In essence, the new variables are the ones responsible for the bad clicks on the detectors. These new sets of variables might not be under control, but because they only depend on the instruments, they must be local themselves, meaning that μ and ν have to be independent of b and a, respectively. As a result

$$|a(x;\lambda\mu)| \leq 1 \ , \ |b(y;\lambda\nu)| \leq 1 \tag{186}$$

from now we will refer to the experimental values obtained after many iterations of the experiment without changing the settings, so that the outcomes can be integrated over the set of hidden variables related to the two detectors, and the averaged out values are

$$\bar{a}(x;\lambda) = \int d\mu \ a(x;\lambda\mu) \tag{187}$$

$$\bar{b}(x;\lambda) = \int d\nu \ b(x;\lambda\nu) \tag{188}$$

It follows that 186 keeps holding for these, that is,

$$|\bar{a}| \leq 1 \ , \ \left|\bar{b}\right| \leq 1 \tag{189}$$

and the correlations relative to these averaged out experimental outcomes become

$$E(x,y) = \int d\lambda \ q(\lambda) \ \bar{a}(x;\lambda) \ \bar{b}(y;\lambda) \tag{190}$$

If x' and y' are two alternative experimental settings to x and y, we can write

$$E(x,y) - E(x,y') = \int d\lambda \ q(\lambda) \ [\bar{a}(x;\lambda) \ \bar{b}(y;\lambda) \ - \bar{a}(x;\lambda) \ \bar{b}(y';\lambda)] \tag{191}$$

Adding and subtracting the same quantity we get

$$E(x,y) - E(x,y') = \int d\lambda\ q(\lambda)\ \bar{a}(x;\lambda)\ \bar{b}(y;\lambda)\ [1 \pm \bar{a}(x';\lambda)\ \bar{b}(y';\lambda)] + \\ - \int d\lambda\ q(\lambda)\ \bar{a}(x;\lambda)\ \bar{b}(y';\lambda)\ [1 \pm \bar{a}(x';\lambda)\ \bar{b}(y;\lambda)] \tag{192}$$

using the triangle identity

$$|E(x,y) - E(x,y')| \leq \left| \int d\lambda\ q(\lambda)\ \bar{a}(x;\lambda)\ \bar{b}(y;\lambda)\ [1 \pm \bar{a}(x';\lambda)\ \bar{b}(y';\lambda)] \right| + \\ + \left| \int d\lambda\ q(\lambda)\ \bar{a}(x;\lambda)\ \bar{b}(y';\lambda)\ [1 \pm \bar{a}(x';\lambda)\ \bar{b}(y;\lambda)] \right| \tag{193}$$

the absolute values can be rearranged in the following way

$$|E(x,y) - E(x,y')| \leq \int d\lambda\ q(\lambda)\ \left|\bar{a}(x;\lambda)\ \bar{b}(y;\lambda)\right|\ \left|[1 \pm \bar{a}(x';\lambda)\ \bar{b}(y';\lambda)]\right| + \\ + \int d\lambda\ q(\lambda)\ \left|\bar{a}(x;\lambda)\ \bar{b}(y';\lambda)\right|\ \left|[1 \pm \bar{a}(x';\lambda)\ \bar{b}(y;\lambda)]\right| \tag{194}$$

using 189, the last expression is less then or equal to

$$\int d\lambda\ q(\lambda)\ [1 \pm \bar{a}(x';\lambda)\ \bar{b}(y';\lambda)] + \int d\lambda\ q(\lambda)\ [1 \pm \bar{a}(x';\lambda)\ \bar{b}(y;\lambda)] \tag{195}$$

and so is $|E(x,y) - E(x,y')|$. The absolute values have been dropped because the integrands are non negative anyway. Integrating the density functions we find

$$\int d\lambda\ q(\lambda)\ \bar{a}(x';\lambda)\ \bar{b}(y';\lambda) + \int d\lambda\ q(\lambda)\ \bar{a}(x';\lambda)\ \bar{b}(y;\lambda) + 2 \tag{196}$$

in conclusion,

$$|E(x,y) - E(x,y')| \leq 2 \pm (E(x',y') + E(x',y)) \tag{197}$$

which we can write in the neater and more common version

$$|E(x,y) - E(x,y') + E(x',y') + E(x',y)| \leq 2 \tag{198}$$

This is a generalization of the result first derived by CHSH [21]:

$$|E(x,y) - E(x,y')| \leq 2 - E(x',y') - E(x',y) \tag{199}$$

Commonly referred to as the Clauser-Horne-Shimony-Holt (CHSH) inequality. When a theory is local, and its observables take the values 186, then 197, 198 and 199 hold. J.S. Bell [4] was the first to derive this result for the specific case

of hundred-percent efficiency detectors, and showed that, in quantum mechanics, it is possible to choose a suitable set of measurement variables x and y in such a way that the inequality is violated. In other words, even supposing that quantum mechanics turned out to be a hidden variable theory, locality would not be restored by introducing a set of hidden variables, much to Einstein's disappointment.

2.4 Bell's theorem

Let us go back to the two spin $\frac{1}{2}$ example, with the system prepared so that the electrons are created at a point in space, and scatter in opposite directions towards Alice and Bob's detectors. These detectors perform spin measurement along an arbitrary axis. The spin operator along an arbitrary direction is $\mathbf{x} \cdot \boldsymbol{\sigma}$ (we forget the $\frac{\hbar}{2}$ factor for consistency with the notation used) for Alice, with $\mathbf{x}$ unit vector. Similarly, Bob's spin operator is $\mathbf{y} \cdot \boldsymbol{\sigma}$. Pauli matrices are given by

$$\sigma_1 = \begin{pmatrix} 0 & 1 \\ 1 & 0 \end{pmatrix}, \sigma_2 = \begin{pmatrix} 0 & i \\ i & 0 \end{pmatrix}, \sigma_3 = \begin{pmatrix} 1 & 0 \\ 0 & -1 \end{pmatrix} \tag{200}$$

so that the eigenvalues of the spin operator are ± 1, that is, the set of outcomes is the same as in the derivation above. As previosly anticipated, quantum mechanics is not a local hidden variable theory. To show this, it is sufficient to find an example of the violation of one of the inequalities derived in the previous section. Correlations are computed according to quantum theory as

$$E(\mathbf{x}, \mathbf{y}) = \langle (\boldsymbol{\sigma} \cdot \mathbf{x})(\boldsymbol{\sigma} \cdot \mathbf{y}) \rangle = -\mathbf{x} \cdot \mathbf{y} \tag{201}$$

one of the inequalities above becomes, in quantum theory,

$$B = |-\mathbf{x} \cdot \mathbf{y} + \mathbf{x} \cdot \mathbf{y'}| \mp |\mathbf{x'} \cdot \mathbf{y'} + \mathbf{x'} \cdot \mathbf{y}| \tag{202}$$

If u and v are two orthonormal vectors, by choosing the experimental settings as

$$\mathbf{x} = \mathbf{u} \tag{203}$$

$$\mathbf{x'} = \mathbf{v} \tag{204}$$

$$\mathbf{y} = \frac{\mathbf{u} - \mathbf{v}}{\sqrt{2}} \tag{205}$$

$$\mathbf{y'} = \frac{-\mathbf{u} - \mathbf{v}}{\sqrt{2}} \tag{206}$$

and picking the inequality with the plus sign, we get

$$B = 2\sqrt{2} > 2 \tag{207}$$

Hence the quantum mechanical correlation cannot be reproduced by a local hidden variable theory.

2.5 Quantum Entanglement

Quantum mechanical formalism describes a multipartite system composed by distinguishable particles as the tensor product of a number of subsystems $\mathcal{H}_i \ni |\varphi_i\rangle$ [17]; as a result, in general, the total Hilbert space is $\mathcal{H} = \otimes_{i=1}^{n} \mathcal{H}_i$. A pure state state of this type of system is described as

$$|\psi\rangle = \sum_{i_1,\ldots,i_n} c_{i_1,\ldots i_n} |\varphi_{i_1}\rangle \otimes \cdots \otimes |\varphi_{i_n}\rangle \tag{208}$$

$|\psi\rangle$ is entangled when it is not decomposable as the product of the states belonging to the individual subsystems $\mathcal{H}_i$, that is,

$$|\psi\rangle \neq |\varphi_1\rangle \otimes \cdots \otimes |\varphi_n\rangle, |\varphi_i\rangle \in \mathcal{H}_i \tag{209}$$

When a state can be written as such a product is said to be *separable* instead. The simplest example of an entangled basis for a Hilbert space is found considering a bipartite system where the dimension of both Hilbert spaces is 2. A common example is a system composed by two polarization encoded photons. In this case, $\mathcal{H}_1 \otimes \mathcal{H}_2$ is spanned by the 4 Bell states

$$\left|\Psi^{\pm}\right\rangle = \frac{1}{\sqrt{2}}(|H\rangle |V\rangle \pm |V\rangle |H\rangle) \tag{210}$$

$$\left|\Phi^{\pm}\right\rangle = \frac{1}{\sqrt{2}}(|H\rangle |H\rangle \pm |V\rangle |V\rangle) \tag{211}$$

which also maximally violate the CHSH equality.

When taking into account actual experimental scenarios, a more realistic description of quantum states is given by mixed states, described by the density matrix formalism discussed previously. A mixed state is separable when

$$\rho = \sum_i p_i \rho_1^i \otimes \cdots \otimes \rho_n^i \tag{212}$$

and is entangled otherwise.

2.6 Quantum entanglement and Bell inequalities

Let us focus on the two dimensional system of the two observers Alice and Bob. Quantum mechanical measurements performed by Alice and Bob can be characterised by a set of positive operator valued measure (POVM) elements $M_{a|x}$ and $M_{b|y}$, acting respectively on Alice's and Bob's Hilbert spaces $\mathcal{H}_A$ and $\mathcal{H}_B$. The number of POVM elements is D, and it needs not to be the same as the dimension of the Hilbert space. A POVM defined on Alice's subspace must satisfy the following

$$M_{a|x} \geq 0 \tag{213}$$

$$\sum_{a=1}^{D} M_{a|x} = \mathbb{I}_A \tag{214}$$

$$M_{a|x} M_{a'|x} = \delta_{aa'} M_{a|x} \tag{215}$$

and same applies to $M_{b|y}$. By tracing these operators over a state described by some density matrix, one obtains the probability of the measurements. For example if the state is given by the density matrix ρ_{AB},

$$p(ab|xy) = \mathrm{tr}\left((M_{a|x} \otimes M_{b|y})\rho_{AB}\right) \tag{216}$$

If the two dimensional system is separable, states can be described with

$$\rho_{AB} = \sum_i p_i \rho_A^i \otimes \rho_B^i \tag{217}$$

and the probability above becomes

$$\begin{aligned} p(ab|xy) &= \mathrm{tr}\left(\sum_i p_i M_{a|x}\rho_A^i \otimes M_{b|y}\rho_B^i\right) = \\ &= \sum_i p_i \,\mathrm{tr}\big(M_{a|x}\rho_A^i\big)\,\mathrm{tr}\big(M_{b|y}\rho_B^i\big) = \\ &= \sum_i p_i p(a|x;i)p(b|y;i) \end{aligned} \tag{218}$$

which is of the local form, only with a sum in place of the integral in 182. Because separable states all exhibit local behavior, violation of Bell inequalities must necessarily be a property of entangled states. The specific relation between non-local behavior and entanglement, however, is a very complex problem, especially for mixed states and higher dimensional spaces. For pure states, it was shown that the above relation can be reversed, so that any pure entangled state admits a set of local measurements that violate a Bell inequality. The proof has been derived for a bipartite system on two-dimensional Hilbert spaces by Capasso, Fortunato, and Selleri [7], and by Gisin and Home and Selleri [13, 16] for bipartite states of arbitrary Hilbert space dimension. When considering mixed states, the problem becomes much harder to treat, and it is beyond the scope of this work anyway. Nevertheless, we note an interesting result by Werner [40], who found a class of mixed entangled states which admit a local hidden variable description for any local measurement.

3 Delayed-choice experiments

3.1 Wheeler's delayed-choice gedanken experiment

The delayed-choice gedanken experiment is arguably the most effective way to highlight the puzzling nature of quantum mechanics, and how some naive interpretations of the physical processes must be abandoned. A modern formulation was given by Wheeler [41], although other earlier versions that address essentially the same problem can be found in literature. Wheeler proposed the scheme represented in figure 8, based on a Mach-Zehnder interferometer.

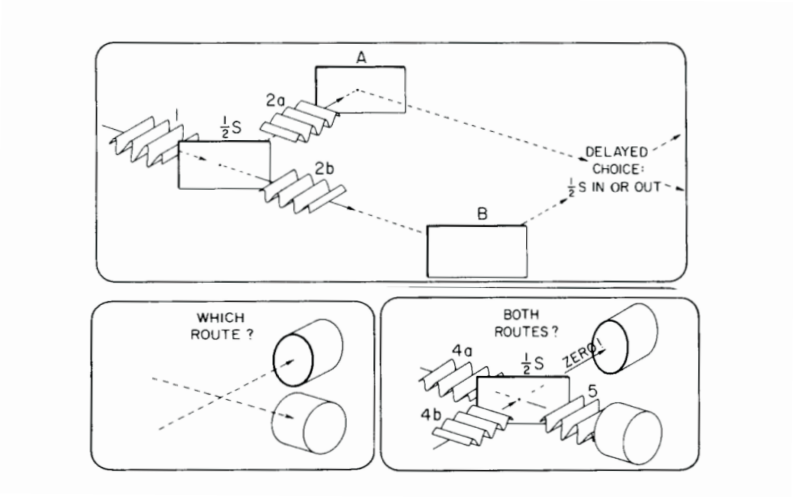

Figure 8: The original scheme proposed by Wheeler. Picture taken from [41]. The setup is a MZI, where the option of removing the last beam splitter is considered. Half silvered mirrors are $\frac{1}{2}S$, while A and B are mirrors.

With reference to figure 8, a half silvered mirror (beam splitter) may or may not be placed on the right-hand side, before the exit of the interferometer. This allows the experimenter to choose which kind of experiment he wants to perform, namely if he wants to highlight the wave-like or particle-like nature of quantum mechanics. Indeed –assuming 100% efficiency for the detectors– in absence of the beam splitter the detectors click with equal probability, providing which-path information. When a beam splitter identical to the first one is positioned as shown in figure 8, the path difference can be chosen so that the phase of the interferometer is a multiple integer of the photon wavelength, so that only one detector will click and the maximum of interference is obtained.

Wheeler proposed to choose whether the second beam splitter is placed or not *after* the photon crossed the first beam splitter, so that the experimental settings are chosen when the photons are already inside the interferometer, where the physical processes are supposed to take place. Because standard quantum mechanics does not distinguish between a situation where the last BS is inserted with a delay, or was alredy there in the first place, this scheme would rule out the "naive" interpretation that the photon travels one or both routes according to whether the second mirror is in place or not. This is challenging

because, if we insist on describing the photon as behaving as a wave or a particle, according to the kind of measurement that is perfomed, Wheeler's scheme would imply that by acting on the last beam splitter, it is possibile to modify properties of the photon that have already been decided in the past. In Wheeler's words,

> Thus one decides the photon shall have come by one route or by both routes after it has already done its travel.

A particularly interesting version of the experiment is one where the interferometer is large enough to make sure that there is space-like separation between the entry of the photon in the MZI and the experimenter's choice to keep or remove the second beam splitter. When this is the case, one can safely assume that, even if there is some sort of way for the photon to acquire the information regarding the status of the second mirror, it could not be relativistically causal, which is a typical behavior of non local theories. In the following, experimental adaptations of Wheeler's gedanken experiment, with varying degrees of faithfulness to the original scheme will be briefly outilned, some of which are very recent. Wheeler's hypothesis is experimentally confirmed in all of these experiments. However, some variants of the gedanken-experiment itself will be discussed first.

3.2 Quantum erasure

Scully and Drühl [35, 34] proposed a very interesting variant of the Wheeler's delayed-choice experiment, introducing the concept of a quantum "erasure". This proposal was made with the intention of suggesting a real world implementation of Wheeler's proposal, but later gained its place as a kind of delayed-choice experiment in its own right. A quantum eraser is a device (more precisely, a physical process) that can act on an quantum system by "erasing" which path or interference information. The delayed-choice operational mode is then obtained by controlling the timing of the erasure event, as described as follows.

The system that was proposed originally is a pair of atoms located at two sites (1 and 2). These atoms are pumped by a faint light pulse, which excites them one at a time. Photons are observed at a detector and, depending on the energetic configuration of the atoms, the detectors can show an interfering or non interfering pattern. Figure 9(a) is a representation of the system; the two interfering (or not) photons are γ_1 and γ_2. Three systems were considered. When the two atoms have only two energy levels as in 9(b), light pulses l_1 impinge on the atoms, realizing the energy transition from the ground state to the highest energy ($b \to a$). The system subsequently emits photons (γ) associated to the $a \to b$ de-excitation, which is the same for both atoms. In other words, the state of the system is given by

$$|b\rangle_1 |b\rangle_2 (|\gamma_1\rangle + |\gamma_2\rangle) \tag{219}$$

Because the states $|\gamma_1\rangle$ and $|\gamma_2\rangle$ are not orthogonal, the square module will feature an interference term. In this setup the experimenter has no way to know which of the two atoms has emitted the γ photon, interference is observed when the photons are both detected on the screen.

Which-path information can be registered if, as in figure 9(c) the two atoms have three energy levels. Atoms are excited by the resonant light l_1 as before,

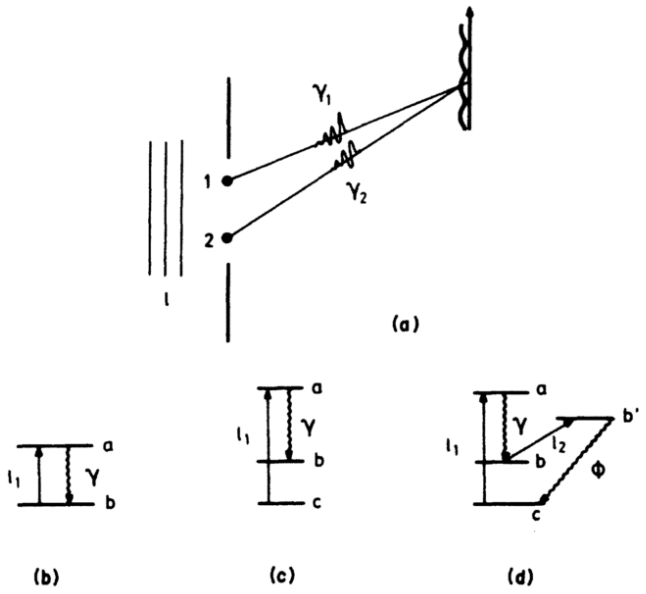

Figure 9: The three different atomic configurations considered proposed by Scully and Drühl. Picture taken from [35]

but after the $c \to a$ transition, atoms de excite to the b energy level. In ket notation

$$|b\rangle_1 |c\rangle_2 |\gamma_1\rangle + |c\rangle_1 |b\rangle_2 |\gamma_2\rangle \tag{220}$$

And the products $\langle b|c\rangle_1$ and $\langle b|c\rangle_2$ in the square module are zero because $|b\rangle$ and $|c\rangle$ are orthogonal, so that there is no interfering term on the detection probability. Since after the emission the atoms are now in two different states, namely, one at the ground state c and the other at level b, distinguishability is obtained and the experimenter knows which one of the two atoms has emitted the γ photon, and consequently obtains which-path information.

The system in figure 9(d) is the one where the quantum eraser is implemented. Light pulses l_2 are also pumped along l_1 on the system. This additional light l_2 is resonant as well, but with a different transition $b \to b'$, as represented in the figure. The second light source is assumed to always trigger this second transition. Furthermore, the b' is strongly coupled to the ground state c, so that the $b' \to c$ transition fast. The photon associated with the new transition is ϕ, while γ still refers to the photon emitted by $a \to b$. The whole transition of an atom is then described by $c \to a \to b \to b' \to c$. The final state of both atoms is c so that *the internal states* of the atoms do not provide which-path information anymore. However, the final state of the system comprises a "signal" photon γ, which will interfere or not depending on how the experimenter makes measurements on the "information carrying" photon ϕ. It was shown, on the same paper, that the which-path information is inherited by the ϕ photon, so that the system as it is now will exhibit which-path behavior regardless

whether the information is experimentally retrieved from ϕ or not. However, and this is where the "erasure" happens, if a measurement that does not inform the observer about the spatial origin of the ϕ photon is performed (hence erases this information), which-path information is lost and interference is restored at the screen.

Rather than discussing the actual implementation proposal for this system (we will see a more modern take on the experiment later), we emphasize how all this lends itself to a delayed-choice mode: the system is split in two parts, the actual signal, that might show fringes or a non interfering pattern, and, at the same time, a separate part that allows the experimenter to observe quantum mechanical complementarity over the first part of the system. Scully and Drühl themselves proposed to combine this scheme with the delayed-choice paradigm by erasing the information after the photons have been registeres at the detector.

3.3 Entanglement swapping

A very relevant example of the combination of Bell measurements and the delayed-choice paradigm is delayed-choice entanglement swapping. Much like in the wave/particle case, quantum mechanical systems can present separability/entanglement duality. Two pairs of polarization entangled photons 1&2 and 3&4 are produced from different sources. Suppose that the initial state is the product of two antisymmetric Bell states

$$|\psi\rangle = \left|\Psi^-\right\rangle_{12} \left|\Psi^-\right\rangle_{34} \tag{221}$$

$|\Psi^-\rangle_{12}$ represents the Bell state $\frac{1}{\sqrt{2}}(|HV\rangle - |VH\rangle)$ relative to the first pair, and similarly for the second product state. In entanglement swapping three observers are considered: Alice, Bob, and Victor. Each generated pair sends one photon to Victor so that he can detect two photons simultaneously, and the remaining two photons are sent respectively to Alice and Bob. The scheme is

- $1 \rightarrow$ Alice
- $4 \rightarrow$ Bob
- $2\&3 \rightarrow$ Victor

Even though the photons recieved by Alice and Bob belong to two different pairs to begin with, this scheme allows for Victor to have an impact on the correlations between 1 and 4 or, more specifically, entanglement can be "swapped" from the two original pairs to the 2&3 and 1&4 pairs.

Since Victor recieves two photons at once, the quantum system over which he perfoms measurements is two dimensional. As a result, he can choose to perform measurements with respect to an entangled or separable base. In the former case Victor makes a Bell-state measurement (BSM) while the latter base choice is separable-state measurement (SSM). Let us assume that Alice and Bob, as well as Victor, can freely choose their measurement base. As a first scenario we consider that Victor chooses the separable base

$$\{|H\rangle_2 |H\rangle_3, |H\rangle_2 |V\rangle_3, |V\rangle_2 |V\rangle_3, |V\rangle_2 |H\rangle_3\} \tag{222}$$

In Victor's system, each of these polarization states has $\frac{1}{4}$ probability. When a measurement projects the state in either of those four states, the photons detected at Alice and Bob are projected accordingly to

$$|H\rangle_1 |H\rangle_4 , |H\rangle_1 |V\rangle_4 , |V\rangle_1 |V\rangle_4 , |V\rangle_1 |H\rangle_4 \tag{223}$$

with $\frac{1}{4}$ probability (for example, if Victor measures $|H\rangle |H\rangle$ then Alice must be in the $|V\rangle$ state and Bob too, etc). With this basis choice, Alice and Bob's results are not correlated. Nevertheless, The initial state can also be written as

$$|\psi\rangle = \frac{1}{2}\left(\left|\Psi^+\right\rangle_{14}\left|\Psi^+\right\rangle_{23} - \left|\Psi^-\right\rangle_{14}\left|\Psi^-\right\rangle_{23} - \left|\Phi^+_{14}\right\rangle\left|\Phi^+\right\rangle_{23} - |\Phi_-\rangle_{14}\left|\Phi^-\right\rangle_{23}\right) \tag{224}$$

This algebric manipulation shows how Alice and Bob correlations behave when Victors is performing measurement on the alternative, entangled, base

$$\{\left|\Psi^+\right\rangle_{23} , \left|\Psi^-\right\rangle_{23} , \left|\Phi^+\right\rangle_{23} , \left|\Phi^-\right\rangle_{23}\} \tag{225}$$

Specifically, each one of Victor's results still have a probability of $\frac{1}{4}$, but they project Alice and Bob's state to the entangled states

$$\left|\Psi^+\right\rangle_{14} , \left|\Psi^-\right\rangle_{14} , \left|\Phi^+\right\rangle_{14} , \left|\Phi^-\right\rangle_{14} \tag{226}$$

meaning that a perfect correlation between two photons (1 and 4), that were created from independent sources, is created *without having them directly interact*. Entanglement passed from the 1&2, 3&4 configuration, to 1&4, 2&3. This is a very baffling and counter intuitive aspect of quantum mechanical behavior, interesting in its own right. Still, Peres suggested [28] that a delayed-choice scheme could be employed on top of this already curious protocol by having Victor's measurement happen *after* Bob and Alice's detections. Having Victors measurements change Alice and Bob correlation *well after* their respective photons have been registered as events at the detector adds a new level of "quantum counterintuitiveness" to the phoenomenon.

Furthermore, this scheme shows a less obvious complementary behavior than just wave/particle, that is, separability/entanglement. The delayed-choice paradigm, applied to which-path/interference behavior emphasizes how paradoxical conclusions are found if one accepts the description where a photon *is* either wave or particle, and behaves accordingly. The delayed-choice version of the entanglement swapping protocol, similarly, allows for a similar paradox to surface when entanglement or separability are assumed to be properties that the quantum system *has*.

3.4 Experimental realizations of different delayed-choice schemes

Having discussed various elaborations of the delayed-choice gedanken experiments, it is important to emphasize that all the proposed schemes imply, more or less explicitly, that some requirements are met. These requirements can be summarized as

- the choice is free, or random

  As long as the choice is predetermined, we cannot rule out that photons already have all the informations they need to behave as either a particle or a wave, given some delayed-choice experimental setup.

- the emission event and the choice are space-like separated

  The timing of the choice should be made in such a way that it must be impossibile for a light-speed signal starting at the choice event to send information back to the photon, so that the latter can adjust its behavior (particle or wave like) accordingly. In other words, there cannot be any causal relation between the entry of the photon into the interferometer and the choice, hence the two events must be space-like separated. Also space-like separated must be the the choice and interference detection events. It might seem like a given that this should not constitute a problem because photons travel at light-speed, but actual experiments can introduce delays of various nature on the path of the photon, not to mention that there might be some uncertainty on the choice time. Further complications are due to the fact that there always is a time delay between the choice and its physical realization on the system (like inserting a BS, detecting a photon, etc.). This is actually a very non trivial problem on some experiments.

- the experiment is perfomed with single photons.

  Semi-classical theory of light does not clash with Wheeler's scheme, because light is seen propagating as a classical wave at all times, and only acts as a particle on the detectors. Furthermore, both detectors are continuously "clicking", so that the effect is not purely quantum mechanical.

While failing to meet one of the three requirements does not mean that an experiment is not worth doing, simultaneously satisfying all three of those is certainly very appealing. In the following discussion of some experimental realizations, it should be clear how much effort has been dedicated by various experimental groups to recreate said conditions.

3.4.1 Wheeler's delayed-choice experiments

Wheeler's delayed-choice gedanken experiment was first realized experimentally by [2], [15]. Hellmuth and collaborators used a Mach-Zehnder interferometer where the light source was an attenuated picosecond laser emitting on average less than 0.2 photons per pulse, that were delayed by two 5m glass fibers. The setup is represented in figure 10. The decision whether to extract which path information or to observe interference was made by means of opening or closing a shutter (a combination of a polarizer and a Pockels cell) placed on the upper arm of the interferometer. When the shutter was closed, only the photons travelling through the lower arm of the MZI could reach the photomultipliers at the end, thus revealing which-path information –the experimenter knows that they could only have passed through the lower arm. Keeping the shutter open, both arms were available routes, and the interference pattern was revealed. The 20ns delay provided by the glass fibers allowed for a delayed-choice operating mode, where the shutter was opened only after the photons crossed the beam splitter. This experiment did not use single photons and the the shutter could

only be opened. This means that only particle like behavior was tested, and no random choice could be made.

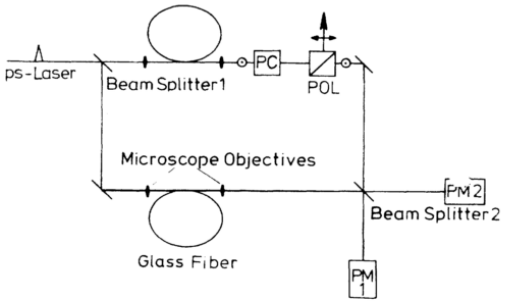

Figure 10: Sketch of the experimental setup used by Hellmuth and colleagues. When the shutter composed of POL+PC is "closed", the photons travel through the lower arm. Picture taken from [15]

An early realization of a delayed-choice experiment using single photon states can be found in [2]. The mechanism exploited for the production of single photon pairs was spontaneous parametric down conversion (SPDC) in a $LiIO_3$ crystal. SPDC is now the standard method to generate pairs of entangled photons. Figure 11 is a representation of the experimental scheme: one of the photons, which are both linearly polarized, acts as a trigger for a Pockels cell placed inside a Sagnac interferometer, where the relative phase of the interfering signal is governed by tilting one of the mirrors inside the interferometer. The other photon is the signal that may exibit wave or particle like behavior. Delayed-choice conditions were realized by delaying the signal photon with respect to the activation of the cell by using an optical fiber.

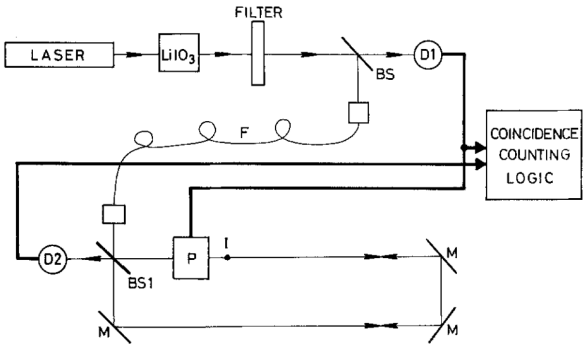

Figure 11: The setup used by Baldzuhn and colleagues. Picture taken from [2]

The activation time of the Pockels was controlled via electronic delays in order to activate the cell when the signal photon was already inside the interferometer. Furthermore, a second delaying element (a 10 meters long monomode

fiber) is added to the signal photon to compensate for the switching time of the Pockels cell. When the PC is not activated, the interferometer should exhibit which-path behavior, while its (delayed) activation can rotate the polarization of the signal photon in such a way that interference is obtained. This experiment did not provide space-like separation between the choice event and the entrance of the photon in the interferometer.

A Wheeler experiment implementing at the same time single photon states, random choice and space-like separation between the choice event and the entry event was realized by Jacques and colleagues [18, 19], by means of a 48 meter long interferometer, corresponding to a delay of about $160ns$. This experiment is arguably the most faithful to the original scheme proposed by Wheeler. The choice was randomly made by controlling a fast electo-optical modulator (EOM) operating at two voltages. These two voltages give the two different which-path and interfering configuration of the interferometer, and are randomly chosen by means of a quantum random number generator (QRNG) based on the noise of a white light beam. The base scheme is the same as a the Mach-Zehnder interferometer considered by Wheeler, but polarizing beam splitters were used instead of half silvered mirrors. This means that which-path information or interference is measured with polarization measurements, rather than using the position of the detector that clicked, as in Wheeler's proposal. The last beam splitter is actually composed by a combination of a half-wave plate, a polarizing beam splitter (PBS), an EOM connected to the QRNG oriented at $\pi/8$ with respect to the incoming polarizations, and a Wollaston prism, used to separate the polarization into two different orthogonal components directed at two detectors. Depending on the voltage randomly supplied from the QRNG, the EOM can either mix the polarizations (acting as a half-wave plate) and show interference, or leave them untouched, providing which path information. Single photon emission and random choice are triggered by two synchronized signals: the operation of the QRNG itself is electronically delayed by $80ns$, plus an additional delay of $40ns$ needed to drive the EOM. The random number generator is placed at the output port of the interferometer, so that the photon enters the future light cone of the choice event only when it is about halfway through the interferometer, which is after it passed the first PBS.

3.4.2 Quantum erasure experiments

Delayed-choice of wave or particle like behavior can also be observed in quantum erasure experiments. A first example of this is [23], based on the work of Scully [34]. A schematic layout is shown in figure 12. When a pair of photons is generated in the region at the right of the slits by means of a β-Barium borate crystal (via type-I SPDC), one photon propagates to the left passing either through slit A or B. At the same time the other photon is scattered in the opposite direction towards a moving detector. After passing through A (B) the photon crosses the beam splitter BSA (BSB) and is reflected to either the top (bottom) detector or the beam splitter in the middle (BSM) with equal probability. If BSA or BSB click, wich path information is known: the photon came from either A or B. The detector on the right acts accordingly, showing the typical particle pattern. If the two detectors in the middle click instead, wich path information is erased, and D_0 presents the interference pattern. The choice happens at the first beam splitter that the photon propagating to the

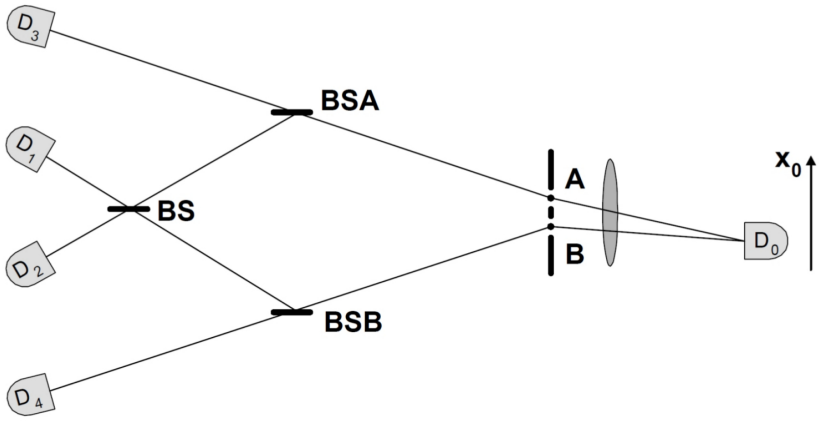

Figure 12: Layout of the experiment performed by Kim et al. Photons propagating to the left can either pass through slit A or B, while the other photon belonging to the pair is sent to the moving detector on the right. Image from [23]

left encounters (BSA or BSB). The experiment was set so that the distance from the crystal and the beam splitters was 2.3 m longer than the distance from the crystal to the detector on the right so as to establish that the choice at the beam splitter is actually made after the measurement on D_0. This setup does not provide space-like separation between the choice and the measurement.

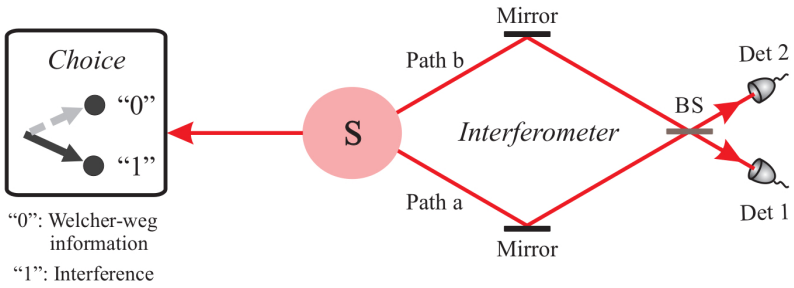

Figure 13: Schematics of the more recent experiment performed by Ma et al. with space-like separation achieved. The right-hand side represents detectors with a 144km separation from the source S. Image taken from [26]

Complete space-like separation between the quantum erasure and all relevant interference events was obtained by Ma and colleagues in 2013 [26]. The layout of the quantum eraser is fairly different from [23], see figure 13. The choice was implemented by choosing a polarization basis for the measure. Photon pairs are created with entanglement between the polarization and path degrees of freedom. The "system" photon is sent to the interferometer, while the "environment" photon is the which-path information carrier, and is sent to

a polarization analyzer well separated spatially from the interferometer. Because polarization and path are entangled, the environment photon carries path information that can be extracted with a measurement in an appropriate polarization base. If, however, the polarization of this photon is measured on a different base, this information is lost. This experiment has been done by the same group in various spatial configurations. The laboratories in Vienna provided a 55 meter long optical fiber, while in a later realization a free-space link was used in the Canary Island from La Palma and Tenerife reaching the remarkable distance of 144km.

3.4.3 Entanglement swapping experiments

Delayed entanglement swapping has also been investigated, and confirmed, experimentally. The first experimental work on entanglement swapping was realized by [20], but did not implement neither space-like separation nor freedom of choice at Victor. Victor's measurement was delayed by about $50ns$ with two optical fibers through which photons 2 and 3 traveled (the scheme of the experiment is essentially the same of the theoretical discussion in the previous section, so we use the same terminology). Alice's and Bob's detectors were placed side by side, and detected the photons 1 and 4 about $20ns$ after the emission of the double pair. The separation between them and Victor was about 2.5, about $8ns$. Victor's measurement was in the time-like future of Alice and Bob's. A free-choice system was not implemented, and only Bell state measurements were performed.

An more complete experimental proof was performed in [27]. Random choice between BSM and SSM was made by means of a quantum random number generator. The delay at Victor was obtained using a $104m$ long optical fiber. The decision and detection events at Victor were only in the time-like future of Alice and Bob.

4 Taking the delayed-choice scheme to space

4.1 Introduction

Quantum mechanics has been extensively tested within regimes bounded by the distances available on Earth. While many aspects of quantum mechanics (fortunately) do not require experiments involving large distances, in some cases being able to increase the spatial dimension of the quantum system is necessary to highlight phenomena that may or may not come into play only at larger scales. The experimental efforts discussed in the previous chapter should underline this necessity. Although the focus of the dicussion has been mainly delayed-choice type experiments, many aspects of fundamental quantum mechanical behavior has yet to be tested over large distance scales.

One of the main reasons why there is much interest dedicated to this kind of large scale quantum experiments (as discussed for example in [33, 32]) is that, over large scale, relativistic effects – both Special and General – are to be taken into consideration. So far, a delayed-choice scheme has never been tested under such conditions, although space-like separation has been indeed reached in some of the experiments above. It is clear that establishing experiments into space using satellites would allow to probe fundamental quantum mechanics on unprecedented scales. A starting point for this new generation of experiments is low Earth orbit, but in the future one can reasonably expect that distance scales might be pushed even further. Among the fields that would certainly benefit from satellite based experiments is the study of quantum entanglement and Bell tests [9], where spacelike separated events are often mandatory. Furthermore, we already showed that the delayed-choice paradigm and quantum entanglement often go hand-in-hand. In general, distances in the order of 1000km would make it substantially easier for an experimental setup to achieve spacelike separation.

In any case, quantum mechanical tests in space are not by any means limited to delayed-choice (which nevertheless is the focus of this work). For example, under certain conditions, reference frames in relative motion can affect entangled states by modifying the polarization correlations [29]. Special relativistic effects also include phase shifts induced on single photon superposition states (as we will see), that could in principle be measured when the the velocities are those provided by LEO satellites. Earthbound experiments performed with static detectors managed to reach separations as large as 144km for quantum communication experiments, which is about how far as it is currently feasible on Earth. How entangled systems behave when in relative motion has been investigated as well [24]. However, this has been achieved with much smaller systems ($55m$) than static experiments. Furthermore, it has been argued [32] that speeds nearer light speed are needed to to draw more reliable conclusions about relativistic effects, and unfortunately detector speeds in earthbound experiments cannot exceed $10^{-6}c$ [37]. The speeds and distances accessible to space based tests can also shed light on the quantum mechanical paradoxes that arise from the various interpretations of the collapse of the wave function, specifically in the case where two reference frames disagree on who measured first. The needed spatial separation and relative velocity can easily be achieved using satellites.

On a more technological standpoint, it is well worth noting that lately a lot of effort has been made to envisage space based quantum key distribution

(QKD) protocols, which heavily rely on quantum entanglement. While quantum encrypted communication on the ground is possible, the distances that can be reached are limited, due to the intrinsic losses of optical fibers. If QKD protocols are realized with satellites, the services can be extended to global scale [5]. Clearly, to realize a fully functioning QKD protocol based in space, one must first explore all the possible complications that might affect the protocol, such as the ones mentioned earlier.

Here we present a first effort to measure an overwhelmingly well established quantum phoenomenon: photon interference at a single photon. This test has been performed by the Quantum Future group from Padova at the Matera Laser Ranging Observatory [39]. Good visibility for quantum interference as been achieved, and in this chapter a quick review of how this has been done will be presented. In addition, we will give particular emphasis on a special relativist effect that affects the wavepackets. The possibility of measuring interference over an Earth-satellite system, makes the possibility of a delayed-choice experiment very concrete, so that the later part of this chapter will be dedicated to a possibile delayed-choice scheme which borrows many aspects from the following.

Another crucial test for our purposes that has been been performed, by the same group, is the experimental proof that photon polarization is preserved over satellite distances [38], because in the final setup we will be using the photons' polarization degree of freedom, as well as time.

4.2 Overview of the MLRO experiment

The assumption that quantum superposition of states is preserved over long distances when propagating under idealized conditions might seem as a safe bet, but an actual test of this presents many difficulties at hand. Here we will briefly outline such test, performed at the Matera Laser Ranging Observatory, of the Italian Space Agency.

Interference was measured with a two-way type of interferometer that makes use of temporal mode superpositions. We will see that besides the various techical difficulties that can arise when using such a complex experimental setup, an interesting theoretical aspect that needs to be taken care of will come up. Namely, the satellite velocity introduces a relative phase to the wavefunction of the interfering photon. The next section will be dedicated to the derivation on this effect. Here we present a short overview of the experiment.

The interferometer is a two-way setup: a system composed by a single unbalanced Mach-Zehnder interferometer and a mirror. The mirror reflects the photons, that enter the interferometer once more on their way back. The temporal modes are superimposed during the second crossing, and interference is observed at one of the two ports. However, in this case, the mirrors where the photons are reflected back towards Earth are mounted on satellites in orbit. Although we will sometimes refer to these with the term "mirror", the satellites actually mount *retroreflectors*. Contrary to a planar mirror, a retroreflector always reflects elecromagnetic radiation with an angle that is the opposite of the angle of incidence. This is of unvaluable importance, since it means that we do not have to concern ourselves with the angle of the satellite. These kind of

satellites have been launched into orbit, for geodynamical studies, from as early as 1976 (LAGEOS-1).

Input light is a strong laser, with a repetition rate of $100MHz$, which is subsequently attenuated to get a mean photon number per pulse, at the recieving telescope, of the order of 10^{-3}, thus obtaining single photon interference. Different satellites have been employed in this experiment, and single photon interference has been measured with visibilities up to 67%. The satellites used to perform the interference measurements are: Ajisai (1600 to 2500 km), Stella (1100 to 1500 km), and Beacon-C (1200 to 1500 km).

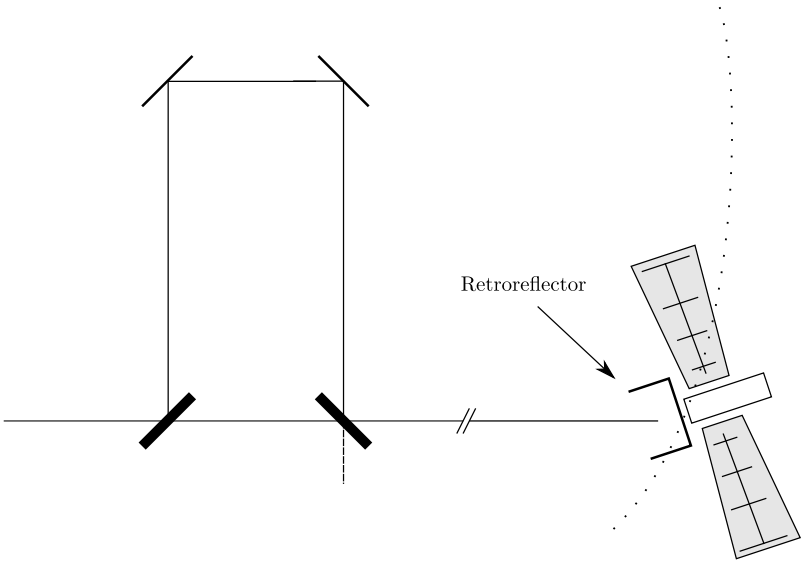

Figure 14: Schematic representation of the experimental setup. A MZI on earth is combined with sending-back retroreflectors which are mounted on satellites in orbit.

Schematically, the time-bin encoded state undergoes the following transformations

- the first passage through the interferometer creates a superposition of the state that crossed the longer ($|L\rangle$) and shorter path ($|S\rangle$) path, and we transmit the output of port 1 to a satellite (hence the minus sign due to double reflection at the beam splitters)

$$|\psi\rangle = \frac{1}{\sqrt{2}}(|L\rangle - |S\rangle) \tag{227}$$

- a relative phase is aquired by the state during the time of flight, before re-entering the MZI. In first approximation, the relative phase is due to the motion of the satellite. Specifically, if the wavefunction is seen as two wavepackets temporally separated by Δt, as in the introductory sections, one can estimate that in first approximation, the phase shift is $\gamma \approx \frac{2\pi}{\lambda}(2\Delta x)$, with Δx is the distance by which the satellite has travelled during the Δt time interval.

$$|\psi'\rangle = \frac{1}{\sqrt{2}}(|L\rangle - e^{i\gamma}|S\rangle) \tag{228}$$

- the photon crosses the interferometer once again. The beam splitter introduces two new possible routes, and the base for the total Hilbert space describing all the possible spatial modes is given by

$$\{|L\rangle|L\rangle, |S\rangle|S\rangle, |S\rangle|L\rangle, |L\rangle|S\rangle\} \tag{229}$$

  Interference is observed at the second port, hence the global i factor due to two single reflections inside the MZI

$$|\psi''\rangle = \frac{i}{2}(|L\rangle(|L\rangle + |S\rangle) - e^{i\gamma}|S\rangle(|L\rangle + |S\rangle)) = \tag{230}$$

$$= \frac{i}{2}(|L\rangle|L\rangle + |L\rangle|S\rangle - e^{i\gamma}|S\rangle|L\rangle - e^{i\gamma}|S\rangle|S\rangle) = \tag{231}$$

  the qubit is time encoded, so that we distinguish states with time measurement. As far as time measurements are concerned, $|S\rangle|L\rangle$ and $|L\rangle|S\rangle$ are the same state, since a time measurement cannot tell apart the two possibilities shorter first - longer last, and vice versa.

- three distinguishable states are obtained, corresponding to the 3 different travel times $S-S$, $L-L$ and $S-L$. Transition probabilities with the states $|S\rangle|S\rangle$ and $|L\rangle|L\rangle$ give $\frac{1}{4}$ and $\frac{1}{4}$, while the transition probability with the remaining state $|L\rangle|S\rangle$ are modulated by the phase

$$|\langle LS|\psi\rangle|^2 = \sin^2(\frac{\gamma}{2}) \tag{232}$$

The phase γ is due to the relative speed between satellite and ground, which varies along the trajectory. As a result, the intereference pattern will not be constant over time. In the next section we will see a more careful model of the experiment, and we will see that the simple model sketched above can be improved.

The unbalancement of the interferometer was $\approx 1m$ (so that $\Delta t \approx 3ns$), while the coherence time $\approx 80ps$. This ensures that the $|L\rangle$ and $|S\rangle$ states are orthogonal, since their scalar product is $\approx e^{-(\frac{\Delta t}{\tau_c})^2} \approx 0$. As far as satellite tracking is concerned, precision measurements on satellite position and speed are crucial, since they are necessary to the knowledge of the phase and expected arrival time of the photons. This is why the experiment has been performed at a laser ranging observatory. Laser ranging observation stations can achieve precision measurement up to the millimeter order in the position of retroreflector satellites, by means of measuring the round trip time of a powerful pulsed laser beam.

A single photon detector is used to measure interference during the passage of a satellite. The data acquired over a passage is then divided between different values of the phase $\gamma(t) \mod 2\pi$. The phase values that have been considered constructive interference are $\frac{4}{5}\pi \leq \gamma \mod 2\pi \leq \frac{6}{5}\pi$, while, for destructive interference, $\frac{-1}{5}\pi \leq \gamma \mod 2\pi \leq \frac{1}{5}\pi$. Since a pulsed laser has been

used, and the time resolution at the detector is sufficiently high ($\approx 80ps$), a three-gaussian-peak distribution is expected. Ideally (we assume the distribution normalized to 1), the central peak has null area when interference is destructive, and $\frac{1}{2}$ when interference is constructive. The remaining peaks that contribute to the total distribution as which-path information should both contribute to the total probability with two constant areas of $\frac{1}{4}$ that do not change while the phase γ spans different values. In practise, the central interfering part of the histograms obtained were fitted with a distribution that takes into account an experimental visibility less than one, that is, $p = \frac{1}{2}(1 - \mathcal{V}_{exp}\cos\gamma(t))$. Interference was measured with different experimental visibilities depending on the satellite: $\mathcal{V}_{exp} = 67 \pm 11\%$ for Beacon-C, $\mathcal{V}_{exp} = 53 \pm 13\%$ for Stella and $\mathcal{V}_{exp} = 38 \pm 4\%$ for Ajisai.

4.3 Relativistic correction due to mirror movement

The setup of the experiment is treated as a *two-way* interferometer. A more general setup has been treated in the introductory section. Schematically, the system is composed by one interferometer, which the photon will cross twice, and a moving mirror. Here we model a propagating gaussian wavepacket as

$$\psi_0(t) = e^{i\omega_0(t-x)}e^{-(\frac{t-x}{\tau_c})^2} \tag{233}$$

representing a gaussian wavepacket propagating along x axis on from left to right, with its peak located at $x = 0$ when $t = 0$. Note that throughout this whole computation we always consider one port of the interferometer at a time, and to simplify the notation we drop normalization factors. The interferometer acts on the wavefunction by splitting ψ_0 in two distinct wavepackets, as previously derived. To avoid self interaction of the photon $\tau_c \ll \Delta t$, so that the two split wavepackets are separated enough. The action of the interferometer upon the first passage of the wavepacket through the interferometer is

$$\psi(t) \to \psi(t) - \psi(t - \Delta t) \tag{234}$$

where port 1 has been chosen as the output outlet that will send photons toward the mirror, hence the minus sign due to the double reflection on the beam splitters. A second simplification has been made on the above formula: equation 111 has an additional time shift due to Δt_0, which is the common travel time shift between the arms of the interferometer. Later on in the derivation of the total probability, obtained by integrating the amplitudes over all times, one can see that the probability does not depend on this time shift. This is true in general, since the matrix associated to the *common time shift* operator is a phase multiplied by the identity. The amplitudes are still technically changed by such a transformation, but the change is nothing but a common transposition of the wavepacket on the positive direction of the t axis. One can see the omission of Δt_0 as a change on the reference frame, that centers the "earlier" peak on a new time $\tilde{t}$ when $\tilde{t} - x = 0$. This description, while simplifying our calculation, keeps useful quantities such as, say, round trip time, implicit. Having said that, note that if we would want to restore the more verbose description we could always retrace the steps of the calculation where said omissions have been made. In the following we will keep the transformations implicit for ease of computation. After exiting the interferometer the amplitude has the following form

$$\psi_1(t) = [e^{-(\frac{t-x}{\tau_c})^2} - e^{i\omega_0\Delta t}e^{-(\frac{t-x-\Delta t}{\tau_c})^2}]e^{i\omega_0(t-x)} \tag{235}$$

The photon at this point is travelling towards the mirror. It is convenient to move to the reference frame of the mirror, since the photon's reflection on it, in this frame, will be described by a much more convenient equation than its non transformed counterpart. Here we simplify the computation by considering only the radial component of the speed of the mirror with respect to the interferometer. If $\boldsymbol{\beta}$ represents the instantaneous velocity of the satellite, which we consider constant for the time being, to a first approximation, one can only consider its projection on the direction connecting $\boldsymbol{\beta}$ and the interferometer back on Earth. Basically, we are considering a one-dimensional motion. Here we use $\beta_{radial} = \beta$. Using the Lorentz transformation connecting the two frames,

$$\gamma = \frac{1}{\sqrt{1-\beta^2}} \tag{236}$$

$$t' = \gamma(t - \beta x) \tag{237}$$

$$x' = \gamma(x - \beta t) \tag{238}$$

we get the following relations between the Earth's (x, t) and the satellite's coordinates (t', x'):

$$x - t = \gamma(1-\beta)(t' - x') = \alpha(t' - x') \tag{239}$$

where $\alpha \equiv \gamma(1-\beta)$ has been defined. Rewriting the amplitude in this new set of coordinates we obtain the satellite's description of an incoming photon

$$\psi_1'(t') = [e^{-\alpha^2(\frac{t'-x'}{\tau_c})^2} - e^{i\omega_0\Delta t}e^{-(\frac{\alpha(t'-x')-\Delta t}{\tau_c})^2}]e^{i\omega_0\alpha(t'-x')} \tag{240}$$

This is where the coordinate change makes things easier: the reflection, as seen from the mirror, is simply given by the transformation

$$x' \to -x' \tag{241}$$

because the mirror is not moving in this reference frame. Applying this to the wavepacket we find

$$\psi_2'(t') = [e^{-\alpha^2(\frac{t'+x'}{\tau_c})^2} - e^{i\omega_0\Delta t}e^{-(\frac{\alpha(t'+x')+\Delta t}{\tau_c})^2}]e^{i\omega_0\alpha(t'+x')} \tag{242}$$

At this point the equation above describes the amplitude travelling back towards the MZI in the mirror's reference frame. Because interference is eventually observed at the interferometer, another Lorentz transformation is needed to go back to the initial reference frame. This second transformation is the same as before, with velocity $-\beta$

$$t = \gamma(t' + \beta x') \tag{243}$$

$$x = \gamma(x' + \beta t') \tag{244}$$

hence

$$t' + x' = \gamma(1-\beta)(t+x) = \alpha(t+x) \tag{245}$$

We apply this transformation to the wavefunction ψ_2' to come back to Earth's reference frame, right before the photon crosses the interferometer once more.

$$\psi_2(t) = [e^{-\alpha^4(\frac{t+x}{\tau_c})^2} - e^{i\omega_0\Delta t}e^{-(\frac{\alpha^2(t+x)-\Delta t}{\tau_c})^2}]e^{i\omega_0\alpha^2(t+x)} \tag{246}$$

the action of the interferometer on the wavepacket observed from port 1 is given by 234. Hence, the final result for port 1 is

$$\begin{aligned}\psi_2^1(t) = [e^{-\alpha^4(\frac{t+x}{\tau_c})^2} - e^{i\omega_0\Delta t}e^{-(\frac{\alpha^2(t+x)-\Delta t}{\tau_c})^2} \\ -e^{i\omega_0\alpha^2\Delta t}e^{-\alpha^4(\frac{t+x-\Delta t}{\tau_c})^2} + e^{i\omega_0\Delta t(1+\alpha^2)}e^{-(\frac{\alpha^2(t+x)-\Delta t(\alpha^2+1)}{\tau_c})^2}]e^{i\omega_0\alpha^2(t+x)}\end{aligned} \tag{247}$$

while, at port 2, we must use $\psi(t) \to i\left(\psi(t) + \psi(t-\Delta t)\right)$

$$\begin{aligned}\psi_2^2(t) = i[e^{-\alpha^4(\frac{t+x}{\tau_c})^2} - e^{i\omega_0\Delta t}e^{-(\frac{\alpha^2(t+x)-\Delta t}{\tau_c})^2} \\ +e^{i\omega_0\alpha^2\Delta t}e^{-\alpha^4(\frac{t+x-\Delta t}{\tau_c})^2} - e^{i\omega_0\Delta t(1+\alpha^2)}e^{-(\frac{\alpha^2(t+x)-\Delta t(\alpha^2+1)}{\tau_c})^2}]e^{i\omega_0\alpha^2(t+x)}\end{aligned} \tag{248}$$

Note that although we have been neglecting normalization factors, it does not mean that they are not affected by coordinate changes. This global change comes from the fact that the commutation relations of the creation and annihilation operators are

$$\left[a_t, a_{t'}^\dagger\right] = \delta\left(t - t'\right) \tag{249}$$

hence, when a transformation is defined on the times, the relation $\delta(f\left(z - z_i\right)) = \sum_i \frac{\delta(z-z_i)}{\left|\frac{\partial f}{\partial z}\right|_{z_i}}$, where z_i are the zeroes of the function $f\left(z\right)$, must be used. If one wants to have a normalized commutation rule as in 249 in the new set of coordinates, the transformation must necessarily rescale the amplitudes. Nevertheless, this is an overall normalization factor over the amplitude as a whole, which we have been neglecting.

Before computing the detection probabilities, we can check that when the mirror is not moving we get the same action as a two-way interferometer. A two-way interferometer with a still mirror is just a double interferometer where all the phases are the same, hence setting $\alpha = \beta$ in the formulas for detection probability of a double interferometer (derived in the earlier sections) we get that, on the central interfering peak, the detection probabilities for ports 1 and 2 are 1 and 0 (here we are not counting which-path events), i.e. perfectly constructive and destructive interference. Indeed, when the mirror is not moving, then $\alpha = 1$ and the second and third terms on the above equation are summed at port 1 (constructive interference), while they cancel out when observing interference from port 2 (destructive interference).

If we want the probability densities, we should use the fact that after the square module, the only overlapping terms that do not vanish are those of the form $e^{-\alpha^4(\frac{t+x-\Delta t}{\tau_c})^2}e^{-(\frac{\alpha^2(t+x)-\Delta t}{\tau_c})^2}$, while every other overlapping term is separated by at least Δt, so it does not interfere because of $\tau_c \ll \Delta t$

$$\begin{aligned}\left|\psi_1^2(t)\right|^2 = e^{-2\alpha^4(\frac{t+x}{\tau_c})^2} + e^{-2(\frac{\alpha^2(t+x)-\Delta t(\alpha^2+1)}{\tau_c})^2} + \\ + e^{-2(\frac{\alpha^2(t+x)-\Delta t}{\tau_c})^2} + e^{-2\alpha^4(\frac{t+x-\Delta t}{\tau_c})^2} + \\ + 2e^{-\alpha^4(\frac{t+x-\Delta t}{\tau_c})^2} e^{-(\frac{\alpha^2(t+x)-\Delta t}{\tau_c})^2} \cos\left(\omega_0 \Delta t(1-\alpha^2)\right)\end{aligned} \tag{250}$$

$$\begin{aligned}\left|\psi_2^2(t)\right|^2 = e^{-2\alpha^4(\frac{t+x}{\tau_c})^2} + e^{-2(\frac{\alpha^2(t+x)-\Delta t(\alpha^2+1)}{\tau_c})^2} + \\ + e^{-2(\frac{\alpha^2(t+x)-\Delta t}{\tau_c})^2} + e^{-2\alpha^4(\frac{t+x-\Delta t}{\tau_c})^2} + \\ - 2e^{-\alpha^4(\frac{t+x-\Delta t}{\tau_c})^2} e^{-(\frac{\alpha^2(t+x)-\Delta t}{\tau_c})^2} \cos\left(\omega_0 \Delta t(1-\alpha^2)\right)\end{aligned} \tag{251}$$

In this coordinates, evaluating the above at $x = 0$ we get two well separated peaks at $t = 0$ and $t = \Delta t(\alpha^2 + 1) \geq \Delta t$. The interference term is located between these two peaks. Furthermore, if we define $\Delta t' \equiv \alpha^{-2}\Delta t$ the equalities above become much more meaningful. For instance, at port 1,

$$\begin{aligned}\left|\psi_1^2(t)\right|^2 = e^{-2\alpha^4(\frac{t}{\tau_c})^2} + e^{-2\alpha^4(\frac{t-\Delta t-\Delta t'}{\tau_c})^2} + \\ + e^{-2\alpha^4(\frac{t-\Delta t}{\tau_c})^2} + e^{-2\alpha^4(\frac{t-\Delta t'}{\tau_c})^2} + \\ + e^{-\alpha^4(\frac{t-\Delta t}{\tau_c})^2} e^{-\alpha^4(\frac{t-\Delta t'}{\tau_c})^2} \cos\left(\alpha^2\omega_0(\Delta t' - \Delta t)\right)\end{aligned} \tag{252}$$

This is exactly the probability amplitude of a double interferometer where

- the two unbalanced arms have different unbalancement length (namely $c\Delta t$ and $c\Delta t'$)
- the coherence time of the input wavepackets time is rescaled: $\tau_c' = \alpha^{-2}\tau_c$
- the central frequency of the wavepacket is also rescaled: $\omega_0' = \alpha^2\omega_0$

This means that special relativity has an effect on observation times, spread of the wavepackets, and frequency of the wavepackets. Also, the visibility is not one anymore, like on the simpler analysis of the previous section.

Because we are only interested in interference, we just integrate the central peak $|\psi_{i,int}|^2$ to get

$$p_1 = \int_{-\infty}^{\infty} d\tau |\psi_{1,int}(\tau)|^2 = \frac{1}{2}\left(1 + e^{-\frac{1}{2}\alpha^4\frac{(\Delta t-\Delta t')^2}{\tau_c^2}} \cos\left(\alpha^2\omega_0(\Delta t' - \Delta t)\right)\right) \tag{253}$$

$$p_2 = \int_{-\infty}^{\infty} d\tau |\psi_{2,int}(\tau)|^2 = \frac{1}{2}\left(1 - e^{-\frac{1}{2}\alpha^4\frac{(\Delta t-\Delta t')^2}{\tau_c^2}} \cos\left(\alpha^2\omega_0(\Delta t' - \Delta t)\right)\right) \tag{254}$$

where the normalization has been chosen so that $p_1 + p_2 = 1$. It is not particularly useful to constantly have both amplitudes at sight, so we just pick the second port from now on. The second port is also more accessible experimentally because port 1 is where the photons enter the interferometer. If one

writes the above in the form $p = \frac{1}{2}(1 - \mathcal{V}\cos\varphi)$, phase and visibility become, using $\alpha^2 = \frac{1-\beta}{1+\beta}$

$$\varphi = \omega_0 \Delta t \frac{2\beta}{1+\beta} \tag{255}$$

$$\mathcal{V} = \exp\left\{-2\left(\frac{\Delta t}{\tau_c}\frac{\beta}{1+\beta}\right)^2\right\} \tag{256}$$

The radial velocity of the satellite changes during the passage of the satellite, but the formulas above do not depend explicitly on the time t. Technically, the Lorentz transformations that have been employed above are not valid in this case: $\beta = \beta(t)$, meaning that the motion is accelerated and the two reference frames are non inertial. In practise, the reflection time of the photon is so small that the motion of the satellite can be considered uniform, and the transformations are indeed valid for any time t. The above is then generalized via $\beta \to \beta(t)$, where $\beta(t)$ is the velocity profile of the satellite over one passage, as obtained via laser ranging techniques. As a result, the phase becomes time dependent and interference is modulated by the variation of the radial velocity of the satellite with respect to the ground.

It should also be noted that there is a competing effect on the visibility between the time shift / coherence time ratio and the $\Delta t - \Delta t'$ difference. Were it not for the motion of the satellite, the time shift difference would be null and visibility would be perfect (ideally). The faster the satellite moves, the larger the relativistic effect on times is. Typical values for β in satellite experiments never exceed values as large as 10^{-4} and are around 10^{-5} in most cases, so that only taking the first order of β in the above formulas is perfectly reasonable for our purposes. Using on the above formula $\Delta t \approx 3ns$ and $\tau_c \approx 150ps$, $\beta = 10^{-4}$ and $\beta = 10^{-5}$, the visibilities are 99.9% and 99.99%, rendering the theoretical visibility drop undetectable as compared to the overall drop we have seen in the previous section due to mixed experimental reasons. Putting these two last consideration together, the following is the final result

$$\varphi(t) \approx 2\omega_0 \Delta t \beta(t) \tag{257}$$

$$\mathcal{V} \approx 1 \tag{258}$$

As long as the theoretical visibility drop is small compared to the experimental one, the simplified description of the interferometer of the previous section is indeed an accurate one, provided that we use as $\gamma = \varphi(t)$ for the phase.

4.4 Experimental realization of an interferometer with which-path/interfering operational modes

The experimental results presented in the previous sections are very encouraging from the experimental perspective of the realization of a space based delayed-choice scheme, because they show how both interference and polarization are experimentally preserved – at the quantum level – over the long distances involved with ground-satellite systems. In the following, we present an experimental setup that with some changes can be used for a delayed-choice

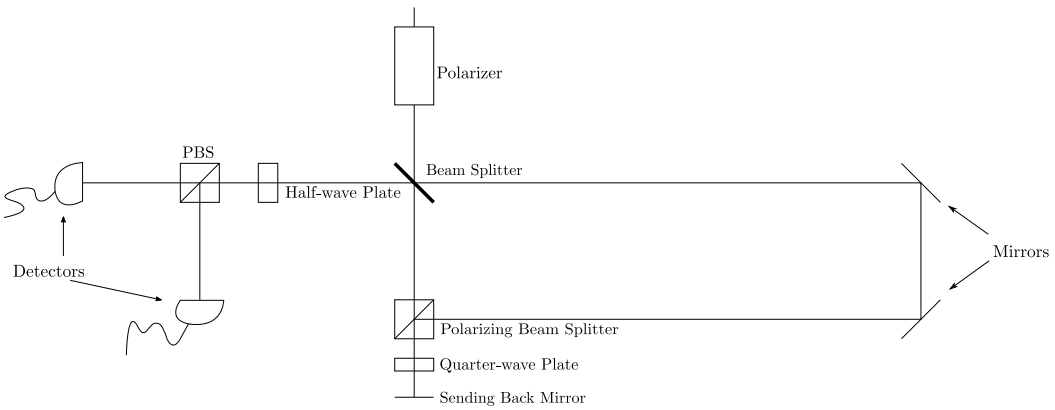

Figure 15: Photons in the $|+\rangle$ polarization state enter the MZI from the top and are split by the first beam splitter (BS), and the beam is brought together again by a polarizing beam splitter (PBS), which transmits the horizontally polarized component of light, and reflects the vertical part. A quarter-wave plate (QWP) is placed before the mirror (M) so that photons cross the latter twice before re entering the PBS. This QWP-M-QWP systems turns horizontal and vertical polarizations into one another. Interference is observed recombining the temporal and polarization modes of the beam. Temporal modes are superimposed when the photon crosses the PBS for the second time, while the superposition of the polarization states is achieved by placing a combination of a half-wave plate and another PBS in series. Interference is thereby measured at the two detectors.

type of test. An earthbound interferometer was realized at Luxor laboratories in Padova. Here we present the details of the design and a description of the experimental realization. Later on we will see how this setup can accommodate a delayed-choice operational mode keeping in mind that very large distances will be involved when using laser ranging techniques.

4.4.1 Idealized scheme of the interferometer

The interferometer considered is a two-way scheme where both time-bin and polarization degrees of freedom are combined to observe interference. Figure 15 is an idealized representation of the experiment. We will first carry out the calculations relative to this idealized scheme and, after that, we will discuss some of the necessary experimental adjustments that need to be made on the setup.

Input states are diagonally polarized: $|+\rangle = \frac{1}{\sqrt{2}}(|H\rangle + |V\rangle)$ or $|-\rangle = \frac{1}{\sqrt{2}}(|H\rangle - |V\rangle)$. In the following computation the state $|+\rangle$ is assumed. After the first non polarizing beam splitter the temporal part of the state is a mixture of the longer $|L\rangle$ and shorter $|S\rangle$ temporal modes, while the polarization part of the wavefunction is not affected. The wavefunction in ket notation is given by

$$\frac{1}{\sqrt{2}}\left(|S\rangle + i\,|L\rangle\right)|+\rangle \tag{259}$$

We are only interested on the port of the PBS that leads to the mirror because the other port directs the beam outside the interferometer. A photon on the $|S\rangle$ state must be transmitted to be sent to that region of the interferometer, while a photon in the $|L\rangle$ state needs to be reflected. This is because the PBS transmits horizontal polarizations and reflects vertical polarizations. Thus, writing down the transformations using only the port we need

$$|S\rangle\,|+\rangle = \frac{1}{\sqrt{2}}\,|S\rangle\left(|H\rangle + |V\rangle\right) \to \frac{1}{\sqrt{2}}\,|S\rangle\,|H\rangle \tag{260}$$

and

$$|L\rangle\,|+\rangle = \frac{1}{\sqrt{2}}\,|S\rangle\left(|H\rangle + |V\rangle\right) \to \frac{i}{\sqrt{2}}\,|L\rangle\,|V\rangle \tag{261}$$

hence, on the wavefunction considered,

$$\frac{1}{2}\left(|S\rangle\,|H\rangle - |L\rangle\,|V\rangle\right) \tag{262}$$

Transformations defined strictly on just the polarization leave the temporal part of the wavefunction untouched, so that any time we have a polarization transformation we can use, for example, Jones matrix notation. The horizontally polarized state is $\left(\begin{smallmatrix}1\\0\end{smallmatrix}\right)$, and the matrix associated with a QWP at an angle of $\pi/4$ with the horizontal axis is $\frac{1}{2}\left(\begin{smallmatrix}1+i & 1-i\\ 1-i & 1+i\end{smallmatrix}\right)$. Upon crossing the waveplate, for the horizontal polarization

$$\frac{1}{2}\begin{pmatrix}1+i & 1-i\\ 1-i & 1+i\end{pmatrix}\begin{pmatrix}1\\0\end{pmatrix} = \frac{1+i}{2}\begin{pmatrix}1\\-i\end{pmatrix} = \frac{1+i}{2}\,|R\rangle \tag{263}$$

whereas

$$\frac{1}{2}\begin{pmatrix}1+i & 1-i\\ 1-i & 1+i\end{pmatrix}\begin{pmatrix}0\\1\end{pmatrix} = \frac{1-i}{2}\begin{pmatrix}1\\i\end{pmatrix} = \frac{1-i}{2}\,|L\rangle \tag{264}$$

for vertical polarization. Therefore we use the following on the wavefunction

$$|H\rangle \to \frac{1+i}{2}\,|R\rangle \tag{265}$$

$$|V\rangle \to \frac{1-i}{2}\,|L\rangle \tag{266}$$

which becomes

$$\frac{1}{2}\left(\frac{1+i}{2}\,|Short\rangle\,|R\rangle - \frac{1-i}{2}\,|Long\rangle\,|L\rangle\right) \tag{267}$$

The reflection on the mirror inverts the direction of propagation while leaving the polarization vector invariant. This means that right polarizations are turned into left, and vice-versa, and after reflection the wavefunction is given by

$$\frac{1}{2}\left(\frac{1+i}{2}\,|S\rangle\,|L\rangle - \frac{1-i}{2}\,|L\rangle\,|R\rangle\right) \tag{268}$$

the quarter wave plate is crossed once again. The outcome is therefore computed with the same matrix as before. For right polarization

$$\frac{1}{2}\begin{pmatrix} 1+i & 1-i \\ 1-i & 1+i \end{pmatrix}\frac{1+i}{2}\begin{pmatrix} 1 \\ -i \end{pmatrix} = \frac{2(1+i)(1-i)}{4}\begin{pmatrix} 0 \\ 1 \end{pmatrix} = |V\rangle \tag{269}$$

and, for left polarization

$$\frac{1}{2}\begin{pmatrix} 1+i & 1-i \\ 1-i & 1+i \end{pmatrix}\frac{1-i}{2}\begin{pmatrix} 1 \\ i \end{pmatrix} = \frac{2(1-i)(1+i)}{4}\begin{pmatrix} 1 \\ 0 \end{pmatrix} = |H\rangle \tag{270}$$

In fact, the configuration HWP-Mirror-HWP is often used in real world applications as a way to switch from H to V polarization states and vice versa. The wavefunction after the second passage through the wave plate is

$$\frac{1}{2}\left(|S\rangle|V\rangle - |L\rangle|H\rangle\right) \tag{271}$$

The vertically polarized part of the wavefunction is now associated with the short path. Vertical polarization is reflected when crossing the PBS, so that vertically polarized photons will be directed towards the longer path. Similar reasoning applies to the horizontally polarized part of the wavefunction.

$$\frac{1}{2}\left(i|S\rangle|L\rangle|V\rangle - |L\rangle|S\rangle|H\rangle\right) \tag{272}$$

Only one of the two ports of the BS is used, so there appears a $\frac{1}{\sqrt{2}}$ factor on the wavefunction, and a phase factor i due to the reflection:

$$\frac{1}{2\sqrt{2}}\left(i|S\rangle|L\rangle|V\rangle - i|L\rangle|S\rangle|H\rangle\right) \tag{273}$$

Since the states $|L\rangle|S\rangle$ and $|S\rangle|L\rangle$ are not distinguishable with a time measurement, we can rewrite the above as

$$\frac{i}{2}|LS\rangle\left(|V\rangle - |H\rangle\right) \tag{274}$$

At this point, the state is still distinguishable: while the time ambiguity due to the total round trip time appeared, there still is polarization as a distinguishing factor [1]. A half wave plate and another polarizing beam splitter can mix polarizations, so interference appears at the detectors. If the HWP is placed at a $\pi/8$ angle with respect to the horizontal polarization, its Jones matrix is $\frac{1}{\sqrt{2}}\left(\begin{smallmatrix} 1 & 1 \\ 1 & -1 \end{smallmatrix}\right)$ and its action on $|H\rangle$ and $|V\rangle$ is

$$|H\rangle \to \frac{1}{\sqrt{2}}\left(|H\rangle + |V\rangle\right) \tag{275}$$

$$|V\rangle \to \frac{1}{\sqrt{2}}\left(|H\rangle - |V\rangle\right) \tag{276}$$

[1] here we are making the assumption that the measurement is made on the $\{|H\rangle, |V\rangle\}$ base. Strictly speaking, a measurement on any non orthogonal base would indeed restore interference. In this system we are filtering the results with a second PBS right before the detectors, that corresponds to performing a measurement on the $\{|H\rangle, |V\rangle\}$ base.

so that, after the waveplate, the state is purely vertical, because

$$\frac{1}{4}\left(|H\rangle - |V\rangle - (|H\rangle + |V\rangle)\right) = -\frac{1}{2}|V\rangle \tag{277}$$

As a result, after the final PBS, the state will always be reflected and never transmitted. If I is the transmission port, and II is the reflection port, and photodetectors are placed after each port, we would observe constructive interference at II, while destructive interference at I. The role of the ports is inverted when the HWP is placed a $-\pi/8$ angle with respect to the horizontal polarization axis. This is therefore the interfering configuration of the setup. If the detectors are connected to an oscilloscope, a single-gaussian peak distribution is expected.

The wavefunction has not been normalized to keep track of the total losses due to the fact that we discard 2 output ports. As a result, the total signal is halved twice, and the total probability here adds up to 1/4. Contrary to the two-way setup where only normal beam splitters are employed, the output is purely interfering, rather than just a mixture. This is because we restricted the possibile paths by means of the PBS and the deviation of the photons to different paths is not randomly governed by non-polarizing beam splitters anymore. Losses due to the geometry of the apparatus are comparable to the two-way interferometer without polarizing beam splitters. Indeed, on the two-way interferometer seen in the previous section, signal is discarded 2 times: the first time when the photons are on their way toward the mirros, after crossing the interferometer for the first time, while the second time when observing interference from just one of the two ports. The total signal is then damped by a $\frac{1}{2} \cdot \frac{1}{2}$ factor. Furthermore, if one is only interested on the interfering part of the signal, one must keep in mind that interference makes up only half the signal, so another $\frac{1}{2}$ factor on the total probability must be considered. As a result, the portion of interfering signal, as compared to the input, is lowered by a 1/8 factor.

Which-path behavior is obtained with a simple change on the interferometer above, that is, either removing the QWP or placing its optical axis parallel to the horizontal or vertical polarization axis. Equation 271 does not hold anymore, and needs to be substituted with

$$\frac{1}{2}\left(|S\rangle|H\rangle - |L\rangle|V\rangle\right) \tag{278}$$

The horizontal component is now transmitted by the PBS and takes the shorter path, while vertical polarization is reflected and the corresponding part of the wavefunction takes the longer route on its way back. We obtain a wavefunction that has two well distinct time components, instead of the mixing that occurs with the other configuration.

$$\frac{1}{2}\left(|S\rangle|S\rangle|H\rangle - |L\rangle|L\rangle|V\rangle\right) \tag{279}$$

No changes to the last part of the configuration are made, so that after the HWP the wavefunction is

$$\begin{aligned}&\frac{1}{4}\left(|S\rangle|S\rangle\left(|H\rangle+|V\rangle\right)-|L\rangle|L\rangle\left(|H\rangle-|V\rangle\right)\right)=\\&\frac{1}{4}\left(\left(|S\rangle|S\rangle-|L\rangle|L\rangle\right)|H\rangle+\left(|S\rangle|S\rangle+|L\rangle|L\rangle\right)|V\rangle\right)\end{aligned}\tag{280}$$

Both detectors will have their signal characterised by the two different trip times $t(LL)$ and $t(SS)$. Double gaussians peaked at two different time values are expected at *both* detectors, where the time difference is given by $t(LL)-t(SS)$.

Because a simple change on the setup as the turning of the quarter-wave plate can be used as a toggle for interference, the setup lends itself to a delayed-choice version (with a minor change, as will be discussed on the next sections). Also, the similarity with the already tested setup for the MLRO experiment that was presented in the previous section makes it very manageable from an experimental standpoint since many of the practical difficulties that might arise when implementing this on a space version would be already taken care of. Still, the above is an idealization of the interferometer, and the actual experimental realization slightly differs.

4.4.2 Experimental objectives

The main goal is to realize the interferometer described above, and test both which-path and the interfering configuration. Furthermore, an assessment of the experimental visibility of interference corresponding to the latter operational mode is extracted. A pulsed laser beam with the same wavelength as the laser available at the MLRO ($532nm$) is used as the light source.

4.4.3 Modifications on the idealized configuration

A delayed-choice experiment cannot be realized in the laboratory, because of the optical elements used and the distances involved. Because we need to test the two operating modes and provide a visibility estimate, a laser beam is used instead of single photons, as opposed to the idealized case. The coherence length of the laser is shorter than the length of the 1 meter unbalancement to avoid interference between the delayed pulses. The time difference introduced by the unbalancement will be of the order of few nanoseconds, as the detectors will confirm.

To make sure that the divergence of the laser is the same when the beams are recombined at the PBS, two pairs of lenses are placed on the longer arm of the interferometer; this evens out the different divergence that the beam traveling through the longer arm acquires with respect to the shorter path. The lenses need to be adjusted making sure that the two light spots, relative to short path and long path exiting the interferometer from the secondary port of the first PBS have the same diameter, both near the port and from a distance of $\approx 2m$.

Another complication is that the phase between $|H\rangle$ and $|V\rangle$ before crossing the HWP is not π as in the ideal case above, because additional phase effects that are not under direct control build up. This is mostly due to the mirrors, that upon reflection add a relative phase between the two polarizations. As a result, the wavefunction in the interfering case before entering the HWP is

$$\frac{1}{\sqrt{2}}\left(|V\rangle - e^{i\varphi}|H\rangle\right) \tag{281}$$

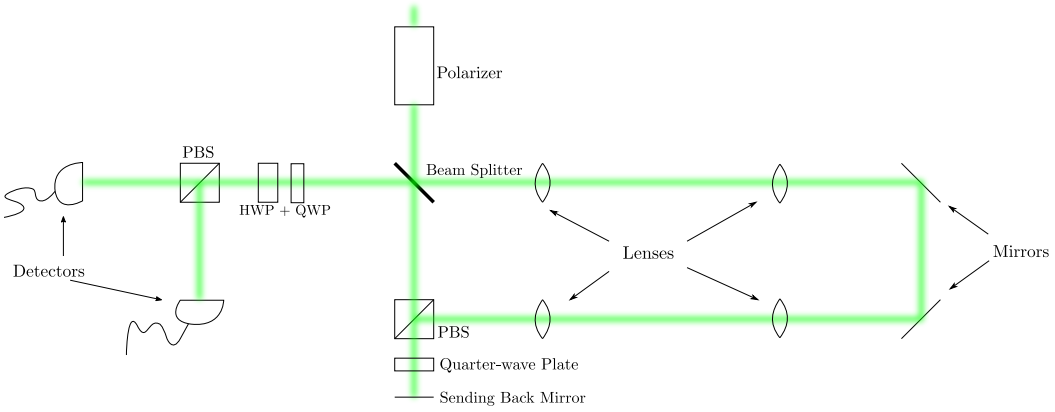

Figure 16: A more accurate representation of the actual interferometer realized. Note the addition of a second QWP and the 4 lenses system.

If one wants to detect interference at the maximum/minumum, an additional QWP must be placed right before the HWP to fix the phase before entering the HWP-PBS detection system. Figure 16 represents this adjusted setup.

4.4.4 Methodology of the realization

The input laser generates a beam with too much intensity for our purposes ($10mW$), because it might saturate the detectors and it is a bit too bright to look at for extended periods, especially when aligning the laser beam. The light is therefore attenuated right at the output of the laser with a 3 orders of magnitude filter, which still gives plenty of light to both comfortably align the laser and drive the detectors with sufficient power. Furthermore, during the alignment process the detectors are not connected, so the filters are easily taken out (unscrewed) and replaced with lighter filters if ever needed.

A polarizer is also placed at this stage, to feed the interferometer a diagonally polarized state. After that, the light is reflected by three mirrors before entering the interferometer. For alignment purposes only two mirrors are really needed; the third one just makes the interferometer more reacheable and manageable.

The first BS, the two mirrors, the 4 lenses and the PBS are all mounted on the same frame, although this only simplifies the alignment process and does not solve it. The beam splitter is a half sivered mirror with a diameter of 2 inches resting inside a cubic box solidal with the frame; the BS can be rotated and moved inside the box with some freedom. The angle must be at a $\pi/4$ with respect to incident light, thus ensuring that the reflected part of the beam is deviated by a $\pi/2$ angle with respect to transmitted light. Furthermore, the BS must be placed inside its rest in such a way that reflected light impinges on the

first two lenses of the longer arm right in the center, so as to minimize aberrations. All the lenses are solidal with the frame, so that they are automatically aligned to each other, and can only be moved in one direction parallel to the laser beam. This degree of freedom is needed to properly adjust the divergence of the ray traveling through the long arm.

The mirrors in the longer path are mounted on two boxes, also solidal to the main structure, that accommodates a V-shape configuration, approximately at a $\pi/4$ angle with the light beam and at a $\pi/2$ angle with each other. Fine adjustments can be made on the mirrors by rotating two knobs controlling the two rotational degrees of freedoms of each mirror around the vertical and horizontal axis with respect to the main frame. These are adjusted so that the beam crosses the second pair of lenses in the middle.

After the lenses, light in the longer beam reaches the PBS. The PBS is in a completely analogous configuration as the BS, and is adjusted with the same criteria as the latter. At this point, light coming from the shorter and longer paths exits the interferometer from the two ports of the PBS. The port that leads to the outside mirror is the port that transmits light from the shorter path and reflects light from the longer one. A QWP solidal with the frame is placed at this port, perpendicularly to the laser beam, with its optical axis at an angle of $\pi/4$ with respect to the horizontal polarization axis when one wants to observe interference. The reflective mirror is solidal with the optical table, and is adjusted at a perpendicular angle with the beam by superimposing the reflected beam with the incoming beam.

The other exit of the interferometer is not of direct use in the experimental scheme, but is actually very useful for the calibration of the two pairs of lenses, as described previously. Furthermore, light coming out of this port is eventually used as a stable trigger signal for the oscilloscope, since the various configurations of the interferometer (interfering and non interfering) do not affect its output in any way, which is always non interfering.

At this point, if all the pieces are aligned correctly, the ingoing and outgoing beams should be well superimposed all over their paths inside the interferometer. As already stated, to observe interference one can place, in this order, a QWP, a HWP, and another PBS before the detectors. Instead of a PBS, a Glan-Thompson polarizer has been used, since it is a rotating polarizing beam splitter that also features a secondary exit to observe the part of light that has been reflected. The fact that this PBS can be rotated also helps with fine adjustments of the horizontal plane of polarization at the output. When this is simply operated as a polarizer, the secondary output is closed, and interference is still detected.

In fact, one can continuously rotate the polarizer from the horizontal to the vertical position to see the single gaussian signal at the oscilloscope continuosly variate from a mininum of interference to a maximum. This also makes it easier to pinpoint the maximum and minimum values of intensity that will be used to provide the experimental visibility.

Another optical element that can be continuously rotated in order to observe mixed behavior is the QWP before the sending-back mirror. The two cases where the waveplate is at a 0 and $\pi/4$ angle with the light beam are just the extreme cases of a transformation that gradually mixes the polarizations and the time degrees of freedom to different extents. This behavior was indeed observed experimentally, and the output of the oscilloscope is represented in figure 20.

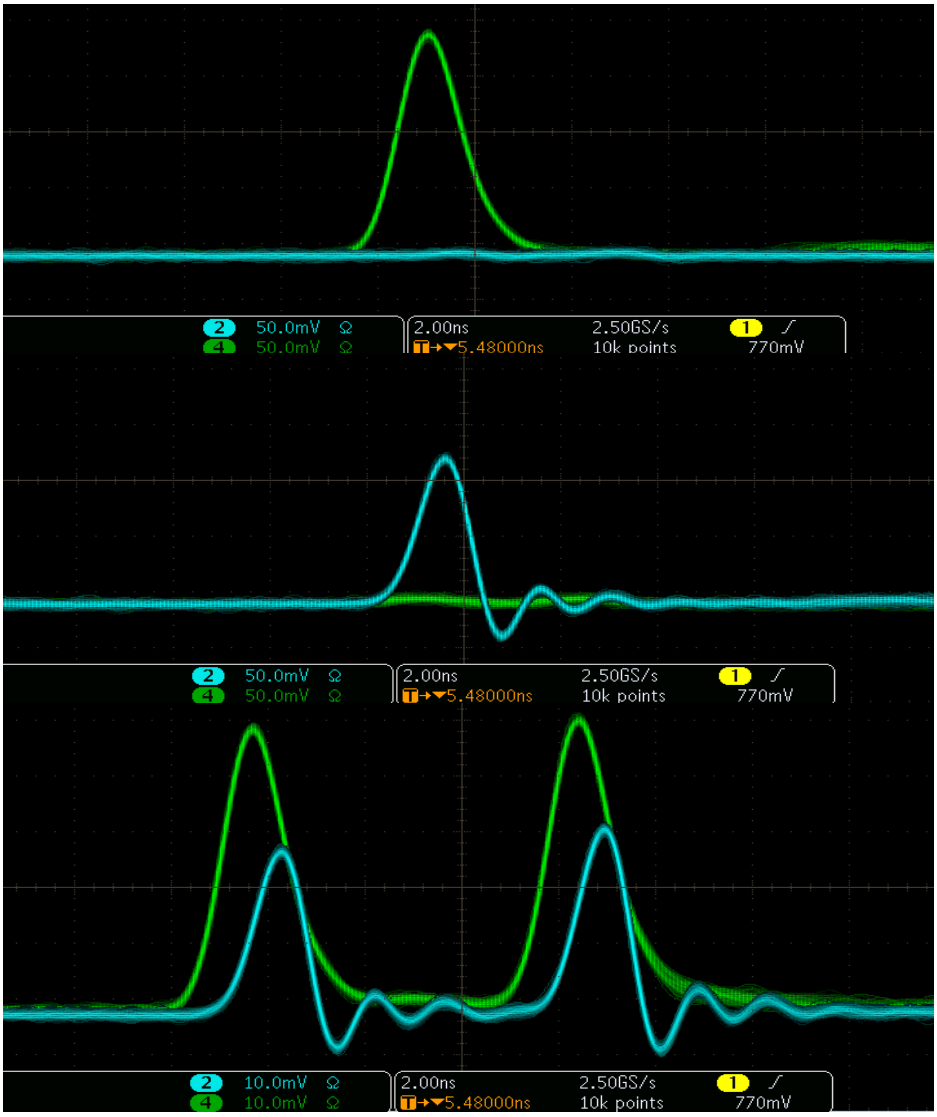

Figure 17: Three screenshots from the oscilloscope, connected to the two detectors simultaneously operating after ports I and II. From top to bottom: constructive/destructive interference at ports I and II, destructive/constructive interference, which path signal. The arrival times of the peaks are slightly shifted because the detectors are placed at different distances from the two exit ports of the polarizer. The signal is triggered with the non interfering laser pulses coming out of the unused port after the first PBS; note that the interfering peak corresponds to an intermediate time of arrival, between the peaks corresponding to the short-short and long-long paths.

4.4.5 Fine Tuning

Before placing the photodetectors after the QWP-HWP-polarizer series, we made sure that the light spot which will eventually be fed to the photodiodes

must show interference. If the two interfering light beams are aligned more or less correctly, the typical interference fringes of two laser beams must appear on a screen (see figures 18 and 19 for reference). Finer alignment is achieved with a careful manipulation of the knobs of the two mirrors mounted on the frame. Alignement is complete when, instead of an interference pattern, a solid spot can be seen on the screen instead of interference patterns.

When the alignement process is complete, the detectors are placed in position, and the whole interfering spot is focalized with lenses on their active area of about $1mm^2$. Real time signal analysis is provided by an oscilloscope, which the detectors are connected to.

The oscilloscope characterizes the temporal properties of the signal, and the intensity of the various peaks. Better alignement of the first QWP is obtained by making sure that the oscilloscope reproduces, in the two cases,

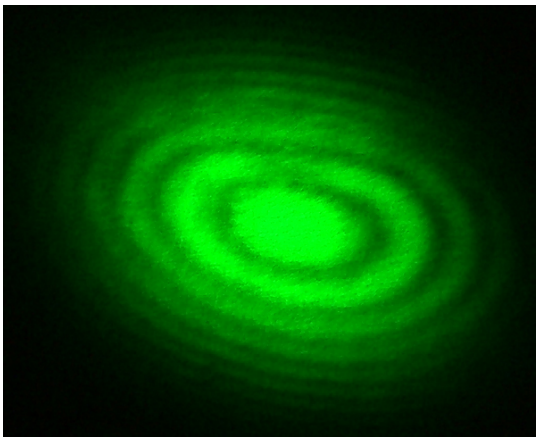

Figure 18: Circular interference fringes. Source: Wikimedia commons

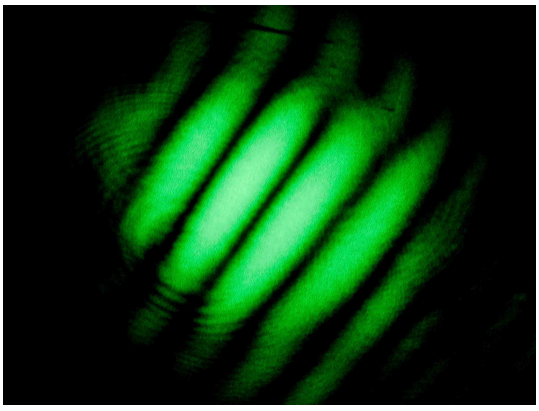

Figure 19: Linear interference fringes. Source: Wikimedia commons

- which-path configuration: two well distinct peaks relative to the short-

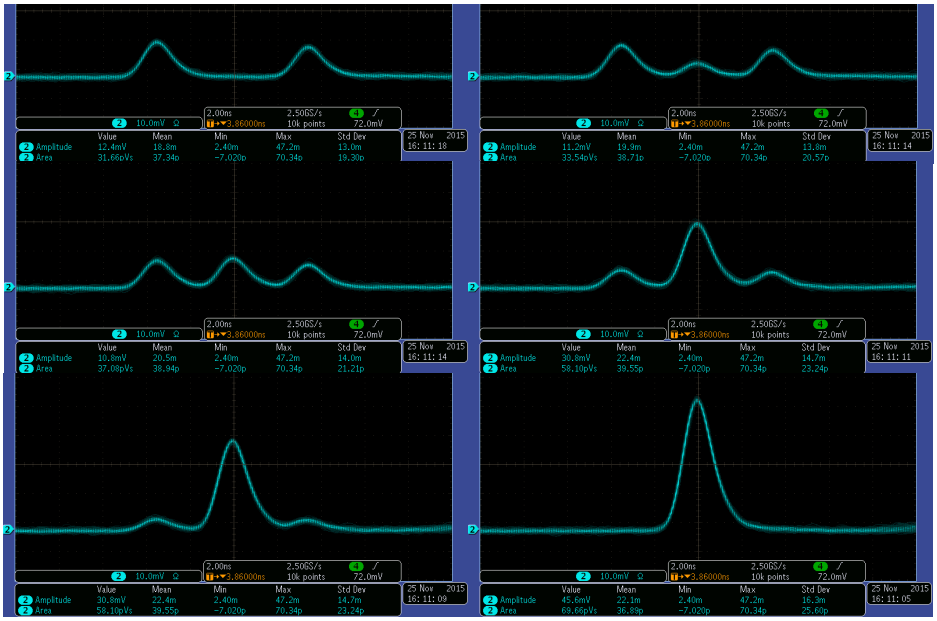

Figure 20: Signal at the oscilloscope when the QWP is not parallel either to the horizontal or the diagonal polarization axis. The central peak corresponds to the interfering part of the signal. The two peaks are non interfering, and their timing indeed corresponds to either the short-short or the long-long path. The first image represent the purely which-path configuration, while the last is the interfering configuration

short and long-long passages; no central peak (short-long passage) can be seen between these two

- interfering configuration: only one single peak corresponding to the long-short and short-long passages is observed

When in interfering configuration, the last quarter-wave plate is rotated in order to observe a minimum of interference from port I, rather than just an intermediate intensity.

4.4.6 Data acquisition

Visibility was computed fitting every peak of the output of the interferometer with the exponentially modified gaussian distribution

$$f_i\left(t;\lambda,\mu,\sigma\right)=A_i\frac{\lambda}{2}e^{\frac{\lambda}{2}\left(2\mu+\lambda\sigma^2-2t\right)}\left(1-\operatorname{erf}\left(\frac{\mu+\lambda\sigma^2-t}{\sqrt{2}\sigma}\right)\right) \tag{282}$$

where $\operatorname{erf}\left(u\right)$ is the error function, defined by

$$\operatorname{erf}\left(u\right)=\frac{2}{\sqrt{\pi}}\int_0^u du' e^{-u'^2} \tag{283}$$

and A_i gives the area of the i-th peak on the data. The distribution is the convolution of a gaussian and an exponential, and takes into account both the gaussian form of laser pulses, and the exponential discharge of the photodiodes. Experimental visibility is thereby estimated as

$$\mathcal{V}_{exp} = \frac{A_{constr} - A_{destr}}{A_{constr} + A_{destr}} \tag{284}$$

where $A_{constr/destr}$ are the areas under the fitted functions in the constructive and destructive case. From figure 17 we can see how one of the two detectors, while roughly showing the expected output at port II, is not well behaved enough to provide a valid visibility estimate. It was still worth mounting it so as to show the simultaneous relationship of the outputs at both ports. Using the detector at port I, the visibility estimate is derived by fitting the raw output of the oscilloscope shown in figure 21, using only port I, in both constructive and destructive case. Constructive and destructive configurations are found by rotating the HWP. The fit results are in table 2

	SS	SL/LS	LL
Constructive	-	1.000 ± 0.005	-
Destructive	-	0.028 ± 0.002	0.016 ± 0.002
Which-Path	0.236 ± 0.003	-	0.248 ± 0.003

Table 2: Fit results for the areas of the Gaussians appearing in the oscilloscope, normalized to the largest area $A_{constr} = 0.335 \pm 0.002$. Errors are given by the least square method used for the fits.

The experimental visibility is therefore given by

$$\mathcal{V} = 94.6\% \pm 0.1\% \tag{285}$$

4.5 Comments on the result

A realistic model of the polarizing beam splitters used in the experiment should account for the different transmission and reflection coefficients. Transmitted light is horizontally polarized with very good approximation, while reflections retain a horizontally polarized component. This is described by changing the transformation law of the PBS as

$$|V\rangle \to it_V |V\rangle |Refl\rangle \tag{286}$$

$$|H\rangle \to t_H |H\rangle |Transm\rangle + ir |H\rangle |Refl\rangle \tag{287}$$

where $|Refl\rangle$ and $|Transm\rangle$ are the spatial modes relative to the reflected and transmitted part of the beam. Only non-negligible coefficients have been written down in the formulas above. The phase of the states is assumed to be unchanged by the PBS, so all the coefficients are real. Their square module must give the percentage of the beam that is reflected or transmitted. For example, if horizontally polarized light of intensity I_0 impinges on a PBS, at

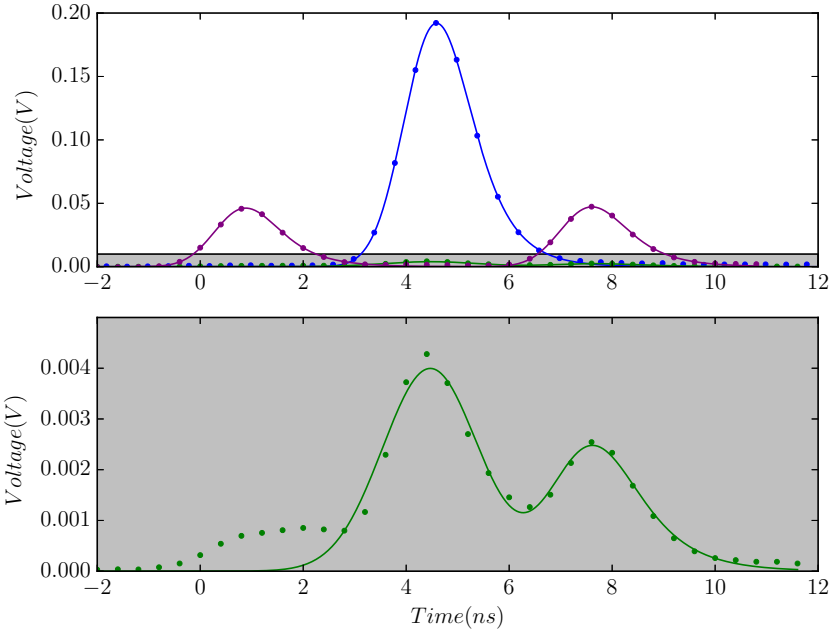

Figure 21: Data taken from the interferometer representing which-path, destructive, and constructive interference, along with the corresponding exponential gaussian fits. The second plot represents the zoomed in area from the grey box in the first plot.

the transmission port the intensity is $I_T = I_0 t_H^2$ while at the reflection port the intensity is $I_R = I_0 r^2$.

When this model is applied to the experimental scheme above, we find that before the HWP and the Glan-Thompson, the wavefunction is given by

$$\frac{i}{2}\left[t_H t_V \left|LS\right\rangle \left(\left|V\right\rangle - \left|H\right\rangle\right) - r\left|LL\right\rangle \left(\left|V\right\rangle + \left|H\right\rangle\right)\right] \tag{288}$$

Because the short-long part of the wavefunction is still proportional to $|V\rangle - |H\rangle$, visibility is not affected by the non ideality of the Polarizing beam splitters. Some signal corresponding to the long-long travel time appears at the detectors. This peak is observed along with the central one in the case of destructive interference, with area $A_{long-long} \approx 0.005 Vns$, as shown in figure 21.

The experimental factor with the largest impact on the visibility is the alignement of the light beams. By looking at the interfering spot that is sent into the detectors when interference is destructive, the signal does not appear as a completely dark spot. Rather, *on average*, the signal on the screen is darker than any other configuration. This is because the two interfering beams are not perfectly plane waves, and they are not perfectly superimposed.

A good improvement on visibility is obtained by occluding the lighter areas of the destructive spot by means of an iris. It was possibile to postselect a

dark spot with a diameter of $\approx 1mm$, which was focalized on the detectors. The visibility obtained this way was $\approx 98\%$. This procedure was applied on a slightly different setup, where the PBS and the BS are inverted. More details on this different setup will be given in one of the next sections. Because with this method much better visibility has been achieved, we conclude that the less-than-one value for the visibility obtained with the whole spot is primarily due alignement, rather than other physical effects.

4.6 Space based delayed-choice version

In delayed-choice experiments, a "switch" is performed that allows the experimenter to trigger the two complementary aspects of quantum states. In our case, this switch would have to be in place of the first quarter wave plate. Indeed, the cumulative effect of the $\lambda/4$ waveplate at a $\pi/4$ angle, upon double passage of the photon is the exchange of the polarization states with respect to their temporal part:

$$|H\rangle |S\rangle \rightarrow |V\rangle |S\rangle \tag{289}$$
$$|V\rangle |L\rangle \rightarrow |H\rangle |L\rangle \tag{290}$$

This is the same effect of a $\lambda/2$ waveplate at a $\pi/4$ angle with respect to the horizontal polarization axis, granted that it is crossed only once (two passages would get the polarizations back to their original configurations). Ideally, in a delayed-choice experiment, one wants to change the experimental setup from a which-path detector to an interferometer, or vice versa, as late as possible. Physically, the manipulation that allows this behavior change, in this interferometer, is the polarization swap above described: if polarizations are swapped, interference is measured, while if they are left untouched, which-way information is recorded. With the QWP method, this switch is clearly inefficient, since it takes the whole round trip time of the photon to be realized. But if a HWP is put in place right before the photon enters the interferometer for the second time, almost all the round trip time is used as a delay. Since the time delays provided by the Earth-satellite distance are, for example, about 10 milliseconds for a satellite distance of $1500km$, no "artificial" retarders like optical fibers are needed to delay light.

The practical implementation of the switch is not a mechanical one. Instead, a liquid crystal variable waveplate operating at two switchable configurations can be used. These configurations are defined by the *retardance* δ. The phase introduced between the components parallel to the slow and fast axis is expressed in terms of multiples of the wavelength, so that, for a HWP we have $\delta = \frac{1}{2}$, (π, a half wavelength) and for a QWP $\delta = \frac{1}{4}$ ($\pi/2$, a quarter of a wavelength). The two configurations needed for operating a delayed switch are $\delta = \frac{1}{2}$, needed to exchange the polarizations of the two temporal modes, and $\delta = 0$, needed to leave the polarizations untouched. Retardance values for the liquid crystals waveplates available at the laborarory (Thorlabs LCC-1221a) range from about 0 to about 0.75, so using an integer multiple of the wavelength to not switch polarizations is not an option.

Different retardance values are obtained by driving the waveplate with different voltages with a voltage controller that can supply up to about $25V$. The

dependence of the retardance from the voltage $\delta(V)$ must be determined experimentally. A quick estimate of the voltage value needed to operate at $\lambda/2$ can be obtained by using, in this order, a polarizer, the LCWP, and another polarizer, aligned as follows. The axis of the first polarizer is diagonal, the LCWP horizontal, and the last polarizer is parallel to the first one. Voltage is gradually applied to the LCWP until no light comes out of the second polarizer; this means that diagonally polarized light has been rotated by a $\pi/2$ angle, which is the effect of a $\lambda/2$ waveplate at a $\pi/4$ angle with the polarization axis of the incident beam.

If one wants to reconstruct the whole $\delta(V)$ dependence instead, a more thorough calibration system is needed. The system is a series of optical elements, namely, a continuous-wave laser, a fixed polarizer that polarizes laser light diagonally, the LC-waveplate with the slow axis aligned horizontally that introduces a phase $2\pi\delta$ between the horizontal and vertical polarization axes and another polarizer. The last polarizer is mounted on a computer controlled rotator at a variable angle θ. A power meter is also connected to the computer, so that angle-intensity data can be acquired automatically. This allows for a complete analysis of the behavior of the variable waveplate. The expected intensity, as a function of the retardance and the angle of the rotating polarizer is

$$I(\theta, \delta) = \frac{I_0}{2} \left(1 + \cos\left(2\pi\delta\right) \sin\left(2\theta\right)\right) \tag{291}$$

where the angle of the first polarizer is fixed at $\pi/4$ and I_0 is the intensity after the first polarizer. This is derived by using input photons with Jones vector proportional to $\frac{1}{\sqrt{2}} \left(\begin{smallmatrix} 1 \\ 1 \end{smallmatrix}\right)$, the matrix for a arbitrarily oriented polarizer and $\left(\begin{smallmatrix} 1 & 0 \\ 0 & e^{-2i\pi\delta} \end{smallmatrix}\right)$ for the LCWP parallel to the horizontal axis. Substituting $\theta = \pi/4$ and $\delta = \frac{1}{2}$ in 291 validates the procedure described above to estimate the $\lambda/2$ voltage. A single acquisition is made when the voltage (thus δ) is fixed. The rotator gradually changes the angle of the polarizer, saving a power measurement for each angle, thus the experimental values are expected to represent the function above. The acquisitions are subsequently fitted with the function for each value of the voltage, and the retardance corresponding to each value of the voltage is estimated. This estimate, unfortunately, shows that even at the maximum voltage, a single LCWP cannot be operated as a 0-order retarder, because of a small offset $\delta \approx 0.05$. The problem is solved by using a pair of LCWPs instead. If their two slow axes are parallel, then the total matrix associated with the waveplates in series is

$$\begin{pmatrix} 1 & 0 \\ 0 & e^{-2\pi i(\delta_1+\delta_2)} \end{pmatrix} \tag{292}$$

meaning that $\delta_1 + \delta_2$ must add up to $\frac{1}{2}$ when the switch occurs, and to 1 when it does not. If the slow axes are crossed instead, the total Jones matrix is

$$e^{-2\pi i\delta_1} \begin{pmatrix} 1 & 0 \\ 0 & e^{-2\pi i(\delta_2-\delta_1)} \end{pmatrix} \tag{293}$$

and the difference must be chosen as $\delta_2 - \delta_1 = \frac{1}{2}$ for the polarization swap, while they must be set at the same value when the polarizations are left untouched (the overall phase has no physical effect).

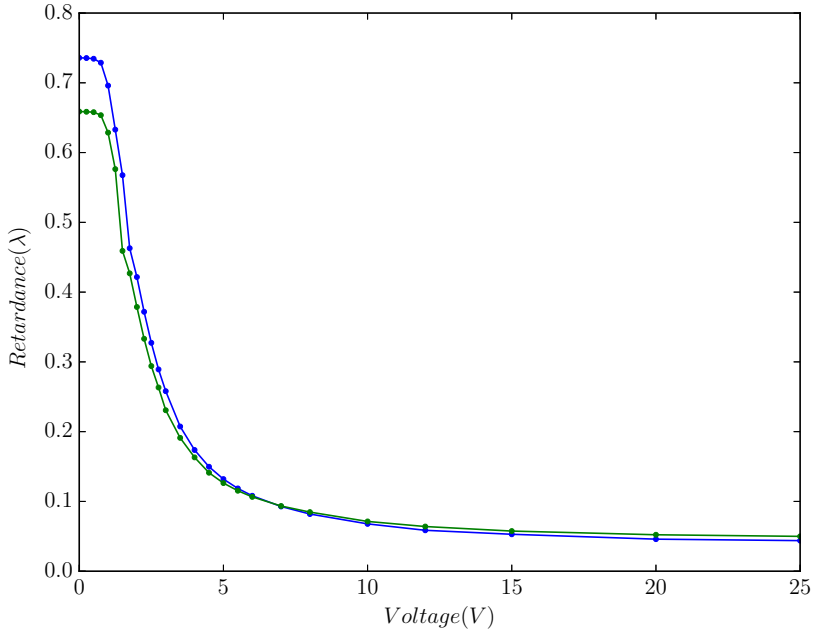

Figure 22: Two liquid crystal wave plates are available at the laboratory. The figure represents the retardance values obtained from the fit results with the procedure described above, for the two LCWPs, at different voltages. Note the offset when $25V$ are supplied.

Another parameter that must be taken into account is the switching time. Liquid crystals behave in such a way that transitions from higher to lower voltage (lower to higher retardance) take longer time than the opposite. The nominal values of the waveplates for high-to-low are of the order of $10ms$ while low to high are 2 orders of magnitude less than that. For the configuration chosen here, we must firstly choose whether we want to perform a $which-path \rightarrow interference$ switch or the opposite, and then adjust the parameters as needed. Furthermore, another thing that should be considered is that the fall time is shortened by a larger voltage change. For the time being, a preliminary estimate on the rise and fall times was performed. The results agree with the nominal values.

Because the sending-back mirror would be on a satellite, interference is not expected to be stable as the case of the laboratory realization, because during the round trip the photons will acquire the same Doppler induced relative phase as the MLRO experiment previously discussed. As a result, interference is expected to be modulated by the Earth-satellite relative speed.

4.7 Alternative setup

A similar delayed-choice scheme can be realized with a simple modification to the setup discussed earlier. This employs the same optical elements used so far.

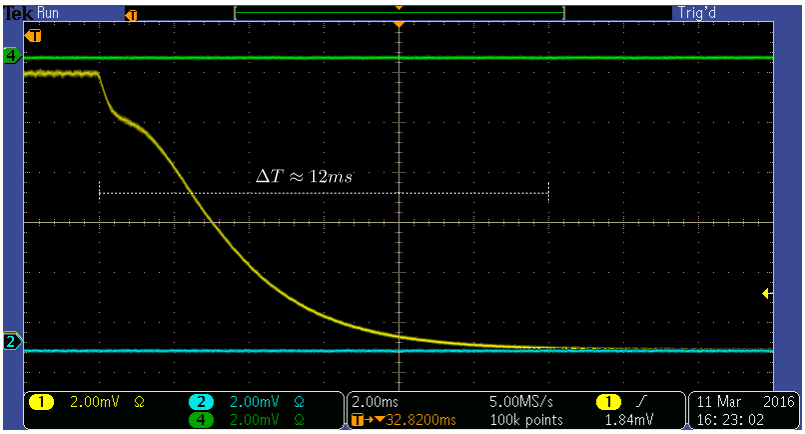

Figure 23: Rough estimate on the fall times of the LCWP.

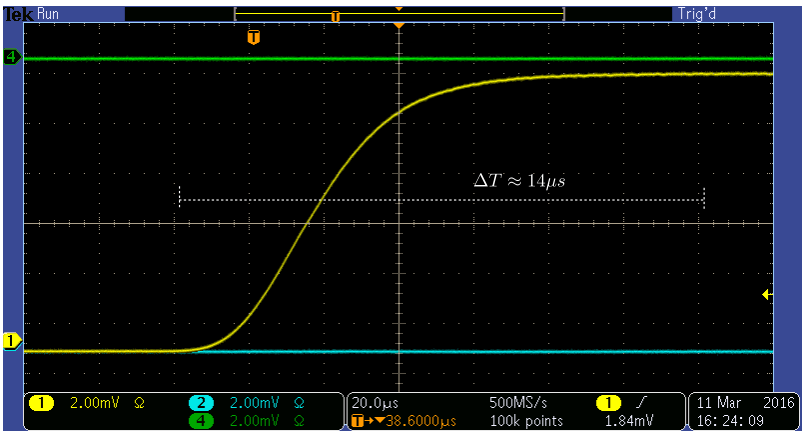

Figure 24: Rough estimate on the rise time of the LCWP.

The calculations are carried out once more in an idealized fashion, leaving out the possible kinematic phase of the satellite and the additional mirror phases, since we have already learned how to introduce these phases at need when discussing practical implementations.

The variant of the previous setup has the BS and the PBS inside the frame of the interferometer switched. The $|+\rangle$ state after the PBS is then transformed to

$$|+\rangle \to \frac{1}{\sqrt{2}} \left(|S\rangle |H\rangle + i |L\rangle |V\rangle \right) \tag{294}$$

Photons are recombined at the BS, and the new state after the port that leads to the mirror is given by

$$\frac{1}{2} \left(|S\rangle |H\rangle - |L\rangle |V\rangle \right) \tag{295}$$

Leaving the LCWP doublet off, photons reach the satellite and come back to the interferometer without changing the polarization state. The BS is crossed once again, so that before crossing the PBS the state is

$$\begin{aligned} &\frac{1}{2\sqrt{2}}\left(|S\rangle\left(|S\rangle|H\rangle - |L\rangle|V\rangle\right) + i|L\rangle\left(|S\rangle|H\rangle - |L\rangle|V\rangle\right)\right) \\ &= \frac{1}{2\sqrt{2}}\left(|S\rangle|S\rangle|H\rangle - |S\rangle|L\rangle|V\rangle + i|L\rangle|S\rangle|H\rangle - i|L\rangle|L\rangle|V\rangle\right) \end{aligned} \tag{296}$$

if the photons are observed from the port of the PBS that leads to the detectors, the wavefunction is transformed to

$$= -\frac{i}{2\sqrt{2}}\left(|S\rangle|L\rangle|V\rangle - |L\rangle|S\rangle|H\rangle\right) \tag{297}$$

which leads to interference if we use a HWP and a PBS before the detectors. Carrying out the same calculation with the pair of LCWPs acting as a HWP on the photons that are returning to the interferometer, a which-path measurement is performed instead.

The difference between this and the BS-first setup is that when the variable waveplates are either not in place, or set to induce a 0 phase shift, we have interference, while which-way information is detected when these are set so as to act as a HWP.

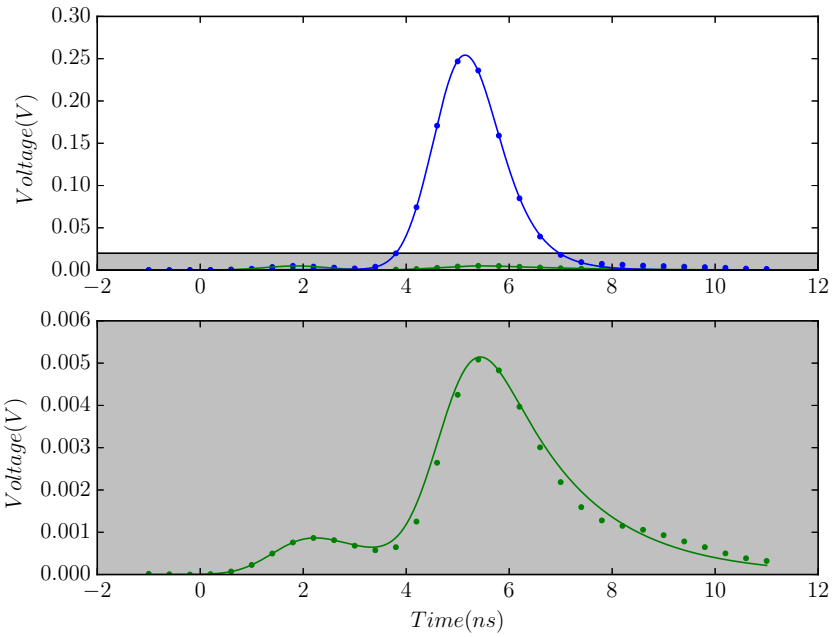

Figure 25: Experimental data and fits for constructive (green line) and destructive (blue line) interference. The grey area is the detail of the first plot.

This setup was tested in the laboratory and, as compared to the PBS-first setup, a similar visibility value ($\approx 93\%$) was obtained when focusing the whole interfering spot into the photodetectors.

	SS	SL/LS
Constructive	0.017 ± 0.002	1.000 ± 0.008
Destructive	0.006 ± 0.004	0.034 ± 0.002

Table 3: Fit results for the areas of the Gaussians appearing in the oscilloscope, normalized to the largest area $A_{constr} = 0.428 \pm 0.003 nsV$.

Experimental visibility estimated with the areas on table 3 is $\mathcal{V} = 93.3\% \pm 0.1\%$.

When taking into account the non ideality of the polarizing beam splitters, using 287, the final state before entering the last polarizer is

$$\frac{i}{2}\left[|LS\rangle\left(-r^2|H\rangle - t_V^2|V\rangle + t_H^2|H\rangle\right) - irt_H|SS\rangle|H\rangle + irt_H|LL\rangle|H\rangle\right] \quad (298)$$

which is quite different from the BS-first setup. Two horizontally polarized peaks corresponding to the short-short and long-long times appear. The peak corresponding to the shortest travel time can be seen in figure 25, while the delayed peak corresponding to the longest path is harder to see, because it seems to be concealed by the response function of the photodetector.

The expected visibility computed with the areas of the $|LS\rangle$ peaks is not exactly one, as the previous case, but

$$\frac{2T_H^2 t_V^2}{T_H^4 + t_V^4} \quad (299)$$

where $T_H^2 \equiv t_H^2 - r^2$. The greater the difference between T_H and t_V is, the more visibility deteriorates.

The coefficients were measured in the laboratory: t_V^2 was found to be *at least* 95%, while $t_H^2 - r^2$ was found to be *at the most* $98\% = 99\% - 1\%$. These two values therefore constitute a worst case scenario estimate for the visibility drop. Using the formula above, we get that $\mathcal{V} \approx 99.995\%$, which constitutes the maximum visibility drop that could be observed with the PBS that have been used in the experiment.

As previously stated, for this setup an iris was placed after the last polarizer so that the analysis could be restricted to the part of the signal with better contrast between constructive and destructive configuration. This improves visibility from $\approx 93\%$ to $\approx 98\%$. The $\approx 0.005\%$ maximum error due to the non ideality of the polarizing beam splitters can be safely neglected, because it is three orders of magnitude smaller than the alignement error.

In table 4 and figure 26 experimental data relative to this last visibility estimate is reported. In this case, $\mathcal{V} = 97.6\% \pm 0.2\%$

	SS	SL/LS
Constructive	-	1.000 ± 0.007
Destructive	0.0120 ± 0.0006	0.01249 ± 0.0008

Table 4: Fit results for the areas of the Gaussians appearing in the oscilloscope, normalized to the largest area $A_{constr} = 2.47 \pm 0.02 nsV$.

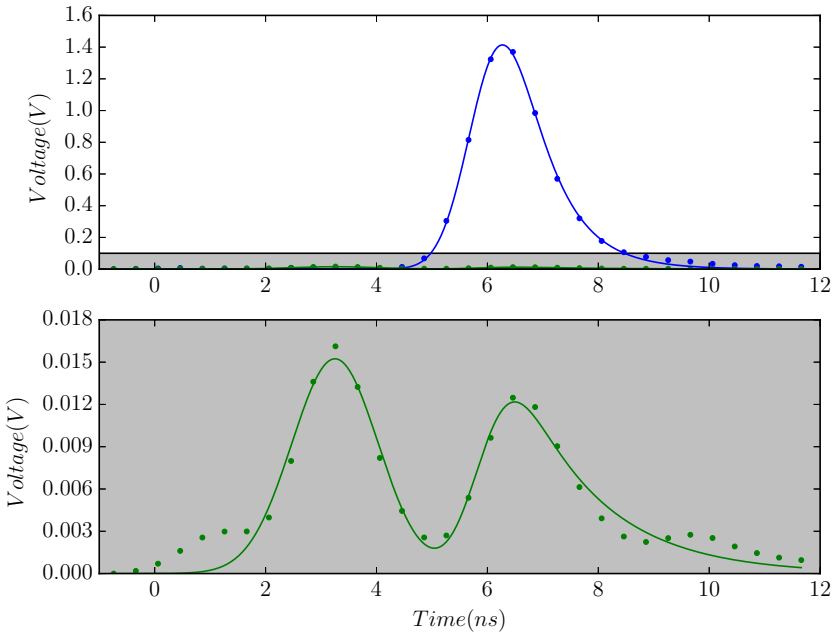

Figure 26: Oscilloscope data when the iris was set in place to optimize the contrast between constructive and destructive signal.

5 General Relativistic effects

5.1 Introduction

Up until now, the main focus has been placed on delayed-choice type experiments. However, taking test of fundamental quantum mechanics to space automatically opens up many different possibilities. Among these, a particularly appealing route is to envision experiments specifically designed to highlight the interplay between QM and General Relativity. Lately, much attention has been dedicated to this topic, as discussed for example in [31, 43, 42]. This is because while General Relativity tests have come a long way since the first experimental verifications, there is still much to be experimentally demonstrated at the quantum level.

Interaction between gravity and Quantum Mechanics has been first measured with interferometric techniques by Colella, Overhauser, and Werner in [8]. Neutrons crossed an interferometer with two different paths under different gravitational potential, and the phase shift induced by the latter is measured. The gravitational potential which the neutron wavefunction is coupled with, however, is the classical Newtonian potential. In this case the predictions made by General Relativity and Newtonian gravitation are the same, therefore, it is not possibile to take the experiments as either proving or disproving General Relativity at the quantum level. COW-like experiments evolved over time, making it possibile to reach a precision on measurements of the gravitational acceleration g of $\frac{g}{\Delta g}$ 10^{-9} [30]. Still, as emphasized in works like [31], a *quantum* test of General Relativity as opposed to Newtonian gravity has yet to be performed. Zych and colleagues proposed interferometric experiments that would confirm genuinely General gravitational effects, such as gravitational time dilation. One of these is *matter wave* based, while the other comprises the use of photons. We note that, while a matter based experiment would necessarily have to demonstrate a *proper time* shift to confirm the influence of general relativity, a photon based test that can detect single photon / gravitational potential interaction – even just a Newtonian potential – would have to be considered a success in its own rights, without necessarily a direct measurement of a shift of the proper time, because newtonian gravity does not predict the coupling of massless particles to the potential. Such an experiment would then constitute a good proof of the mass-energy equivalence, which is of fundamental importance in General relativity. The ideal experimental scenario, though, would have both effects showing: proper time shift and photon coupling to the gravitational field.

In the following we show how a time-bin encoded qubit can potentially be exploited to observe a gravitational effect on a single photon wavepacket, where an Earth-satellite system is once again used. Because of the motion satellite, relative speeds must be taken into account in the computation, so that the final result will present special relativistic effects as well as gravitational.

5.2 Possibily measurable effects on a one-way setup

Photons are sent to a satellite in the same way as the MLRO experiment, but the setup considered is not a two way interferometer. Instead of reflecting the photon by means of a retroreflector, a second unbalanced interferometer with the same time unbalancement Δt as the first one is mounted on an orbiting satellite,

where interference is measured. The goal is to estimate how and to what extent the photon is affected by the interaction with the Earth's gravitational field. In general, the metric is written as

$$c^2 d\tau^2 = ds^2 = g(x)_{\mu\nu} dx^\mu dx^\nu \tag{300}$$

from now on we set $c = 1$. We adopt the notation with greek indices $\mu = 0, \ldots, 3$, associating the temporal index to the 0 index, while we use latin indices only for spatial indices $i = 1, 2, 3$. The metric tensor $g_{\mu\nu}$ is a function of the coordinates $x^\mu = (t, x^i)$. The proper time τ is the time measured according to a clock in free fall. In general, to get the metric associated to a particular system, one must solve Einstein's equations. The general soulution for our simple case (spherical distribution of mass) is the Schwarzschild metric

$$g_{00} = 1 - 2\varphi \tag{301}$$

$$g_{0i} = 0 \tag{302}$$

$$g_{ij} = -\delta_{ij} + \frac{2\varphi}{1 + 2\varphi} \frac{x_i x_j}{r^2} \tag{303}$$

Where the gravitational potential is $\varphi = \varphi(r) = -\frac{MG}{r}$. G is Newton's gravitational constant, M is the Earth's mass, and r is the distance from the origin of the coordinate system, where the center of the Earth is located. qubits are transmitted from a point placed somewhere in the gravitational field at $\mathbf{x_1}$ in motion with velocity $\boldsymbol{\beta_1} = \frac{d\mathbf{x_1}}{dt}$, with $\beta_1 = |\boldsymbol{\beta_1}|$. Substituting these coordinates in 300, using 303, one finds

$$\frac{d\tau_1}{dt_1} = \sqrt{1 + 2\varphi_1 - \beta_1^2 \left(1 - \frac{2\varphi_1}{1 + 2\varphi_1} \cos^2 \theta_1\right)} \tag{304}$$

where θ_1 is the angle between $\mathbf{x_1}$ and $\boldsymbol{\beta_1}$. φ_1 is short for $\varphi(|\mathbf{x_1}|)$. The same equation holds for a second point located at $\mathbf{x_2}$, also in motion ($\boldsymbol{\beta_2}$). If the emission event occurs at point $(t_1, \mathbf{x_1})$, and the emission event at $(t_2, \mathbf{x_2})$, when S_1 emits a frequency ω_1 that is recieved at point 2, the general relativistic prediction for the frequency shift is [1]

$$\omega_2 = \omega_1 \frac{dt_1}{dt_2} \sqrt{\frac{1 + 2\varphi_1 - \beta_1^2 (1 - \frac{2\varphi_1}{1+2\varphi_1} \cos^2 \theta_1)}{1 + 2\varphi_2 - \beta_2^2 (1 - \frac{2\varphi_2}{1+2\varphi_2} \cos^2 \theta_2)}} \tag{305}$$

To simplify the calculation, we can assume a 1-dimensional motion. Point 2 represents a satellite falling at constant speed β_2 towards the center of the Earth. Point 1 is placed on the surface of the Earth on the line connecting 2 and O, the origin of the coordinate system. The speed of the point on Earth (1) is negligible, so the formula above becomes

$$\omega_2 = \omega_1 \frac{dt_1}{dt_2} \sqrt{\frac{1 + 2\varphi_1}{1 + 2\varphi_2 - \beta^2 (1 - \frac{2\varphi_2}{1+2\varphi_2})}} \approx \omega_1 \frac{dt_1}{dt_2} \sqrt{\frac{1 + 2\varphi_1}{1 + 2\varphi_2 - \beta^2}} \tag{306}$$

Typical values for β^2 and φ for a LEO satellite are both in the order of 10^{-10}, so there really is no need here to carry out a calculation for all orders, since we can safely consider just the first order of respectively β and φ.

The derivative $\frac{dt_1}{dt_2}$ represents the relationship between the coordinate times of reception and emission, in Schwarzschild coordinates. In general, the computation is more complicated than just the case of the Doppler shift we have seen earlier. This is because photons are deflected by Earth's gravitational field, and, in principle, that interaction should be accounted for. Admittedly, the computation is fairly easy in the case of the one dimensional motion here. However, we are tackling this problem with a first order approach, and one can show that the complete calculation would yield a correction in the order of $\varphi\beta \approx 10^{-14}$ (as pointed out in [1]), which we would have discarded anyway. Thus, for the follwing, we can use the flat Minkowsky metric to get $\frac{dt_1}{dt_2}$, in conjunction with the fact that for a photon the interval equals to zero.

$$ds^2 = dt^2 - dr^2 = 0 \tag{307}$$

$$\Rightarrow dt = \pm dr \tag{308}$$

the + solution is chosen because the photon is traveling from earth to the satellite, hence increasing its distance from the origin O

$$\Rightarrow t_2 = t_1 + r_2 - r_1 \tag{309}$$

the motion of the satellite described with Schwarzschild coordinates is $r_2(t_2) = r_0 - \beta t_2$, where r_0 is the position of the satellite at time $t_2 = 0$. If β is positive, the satellite is falling towards the Earth. Also, uniform motion has been assumed. The motion of the emission point is $r_1 = r_T$, with r_T Earth's radius. By differentiating 309 with these constraints on the motion, we get

$$\frac{dt_1}{dt_2} = 1 + \beta \tag{310}$$

Note that the 2-dimensional computation where the satellite is still in uniform motion but is moving towards a generic direction, has β replaced with the projection of the velocity on the radial direction. For our purposes we continue with the 1-dimensional case. The final result for the frequency shift under said approximation is obtained substituting the above in 306

$$\omega_2 = \omega_1(1+\beta)\sqrt{\frac{1+2\varphi_1}{1+2\varphi_2-\beta^2}} \tag{311}$$

The special relativistic Doppler frequency shift is recovered evaluating this expression far from the gravitational source where $\varphi_{1/2} = 0$, and we get $\omega_2 = \omega_1\sqrt{\frac{1+\beta}{1-\beta}}$. We define

$$\alpha_G = \frac{\omega_2}{\omega_1} \tag{312}$$

The propagation of a a wavepacket is described by the phase $\omega(t-x)$. For a description of the same wavepcket in the two coordinate systems which measure the redshifted frequencies ω_1 and ω_2, we can use the fact that $\omega(t-x)$ is observer independent [6], so that, for the two coordinate systems,

$$\omega_1(\tau - x) = \omega_2(\tau' - x') \tag{313}$$

which can be inverted to find out the transformation between $\tau - x$ and $\tau' - x'$. Both Earth and the satellite will measure times according to their clocks (here respectively τ and τ'). We can carry out a similar calculation as in the case where we worked out the sole Doppler effect on the outgoing wavepackets from the interferometer to the satellite, provided that we promote times to proper times. Consistently with the notation used in the previous chapters, we use a notation where the primed coordinates refer to the satellite's frame, and the regular ones to Earth's. With this notation $\tau - x = \frac{\omega'}{\omega}(\tau' - x') = \frac{\omega_2}{\omega_1}(\tau' - x') = \alpha_G(\tau' - x')$ (cfr 239). The wavefunction as seen from Earth, after passing through the interferometer, is given by (omitting normalizations)

$$\psi_1(\tau) = [e^{-(\frac{\tau - x}{\tau_c})^2} - e^{i\omega_0 \Delta t} e^{-(\frac{\tau - x - \Delta t}{\tau_c})^2}] e^{i\omega_0(\tau - x)} \tag{314}$$

while, right before entering the satellite's interferometer, in coordinate system of the satellite,

$$\psi_1'(\tau') = [e^{-\alpha_G^2(\frac{\tau' - x'}{\tau_c})^2} - e^{i\omega_0 \Delta t} e^{-(\frac{\alpha_G(\tau' - x') - \Delta t}{\tau_c})^2}] e^{i\omega_0 \alpha_G(\tau' - x')} \tag{315}$$

Using the fact that the interferometer is mounted on the satellite is a perfect copy of the one on Earth, we write down its action on the wavepacket in the new coordinate system. If interference is being observed from the second port, the wavefunction is modified according to

$$\psi_2'(\tau') = i(\psi_1'(\tau') + \psi_1'(\tau' - \Delta t)) \tag{316}$$

so, at the second port of the interferometer on the satellite, the wavefunction is

$$\begin{aligned} \psi_2'(\tau') = i[e^{-\alpha_G^2(\frac{\tau' - x'}{\tau_c})^2} - e^{i\omega_0 \Delta t} e^{-(\frac{\alpha_G(\tau' - x') - \Delta t}{\tau_c})^2} \\ + e^{i\omega_0 \alpha_G \Delta t} e^{-\alpha_G^2(\frac{\tau' - x' - \Delta t}{\tau_c})^2} - e^{i\omega_0 \Delta t(1 + \alpha_G)} e^{-(\frac{\alpha_G(\tau' - x') - \Delta t(\alpha_G + 1)}{\tau_c})^2}] e^{i\omega_0 \alpha_G(\tau' - x')} \end{aligned} \tag{317}$$

We can set $\Delta t' \equiv \frac{\Delta t}{\alpha_G}$, and rewrite the above

$$\begin{aligned} \psi_2'(\tau') = i[e^{-\alpha_G^2(\frac{\tau' - x'}{\tau_c})^2} - e^{i\omega_0 \Delta t} e^{-\alpha_G^2(\frac{\tau' - x' - \Delta t'}{\tau_c})^2} \\ + e^{i\omega_0 \alpha_G \Delta t} e^{-\alpha_G^2(\frac{\tau' - x' - \Delta t}{\tau_c})^2} - e^{i\omega_0 \alpha_G(\Delta t + \Delta t'))} e^{-\alpha_G^2(\frac{(\tau' - x') - \Delta t - \Delta t')}{\tau_c})^2}] e^{i\omega_0 \alpha_G(\tau' - x')} \end{aligned} \tag{318}$$

As usual, the time-bin qubit is assumed to be perfectly encoded, so overlapping terms in the square module vanish.

$$\begin{aligned} |\psi_1|^2(\tau') = e^{-2(\alpha_G \frac{\tau'}{\tau_c})^2} + e^{-2(\alpha_G \frac{\tau' - \Delta t - \Delta t'}{\tau_c})^2} + \\ + e^{-2(\alpha_G \frac{\tau' - \Delta t}{\tau_c})^2} + e^{-2(\alpha_G \frac{\tau' - \Delta t'}{\tau_c})^2} + \\ - 2e^{-(\alpha_G \frac{\tau' - \Delta t}{\tau_c})^2} e^{-(\alpha_G \frac{\tau' - \Delta t'}{\tau_c})^2} \cos(\alpha_G \omega_0(\Delta t' - \Delta t)) \end{aligned} \tag{319}$$

The non interfering peaks are the first two terms because their integration yields equal and constant values, while the last three give rise to interference with less-than-one visibility. Integrating the probability density, and restoring normalization, the total probability is

$$p = \frac{1}{2}(1 - \mathcal{V}\cos\Phi) = \frac{1}{2} + \frac{1}{2}\left(1 - e^{-\frac{1}{2}\left(\frac{\Delta t' - \Delta t}{\tau_c'}\right)^2}\cos\left(\omega_0'\left(\Delta t' - \Delta t\right)\right)\right) \tag{320}$$

where the $\frac{1}{2}$ term comes from the integration of the two non-interfering peaks. This overall contribute to the probability can be omitted as long as we refer just to the interference probability (we might have just as well integrated over the central peak). The above is the same interference pattern of two unbalanced interferometers in series with different unbalancements Δt and $\Delta t'$, crossed by a beam with the following parameters adjusted

- coherence time $\tau_c' = \alpha_G^{-1}\tau_c$
- central frequency $\omega_0' = \alpha_G\omega_0$
- unbalanced arms time shifts Δt and $\Delta t' = \Delta t/\alpha_G$

where the first two substitutions describe the redshift of the laser as seen from the satellite.

Visibility and phase Φ are, expressed in terms of β and φ_1,

$$\mathcal{V} = e^{-\frac{1}{2}(1+\beta)^2\frac{1+2\varphi_1}{1+2\varphi_2-\beta^2}\left(\frac{\Delta t}{\tau_c}\right)^2} \tag{321}$$

$$\Phi = \omega_0(1-\alpha_G)\Delta t = \omega_0\left(1 - (1+\beta)\sqrt{\frac{1+2\varphi_1}{1+2\varphi_2-\beta^2}}\right)\Delta t \tag{322}$$

If the motion does not take place in one dimension, the most straightforward generalization of the result is derived considering that the motion takes place on a plane instead. Let θ be the angle between $\boldsymbol{\beta}$ and the vector $\mathbf{x_2} - \mathbf{x_1}$, connecting the satellite to the point of observation on Earth. Still in the approximation of uniform motion

$$\frac{dt_1}{dt_2} = 1 - \beta\cos\theta \tag{323}$$

Since the approximations made on the second factor of expression 306 are still valid, the generalized result, to the first order in β and $\varphi_{1,2}$ is

$$\begin{aligned}\Phi &= \omega_0\left(1 - (1-\beta\cos\theta)\sqrt{\frac{1+2\varphi_1}{1+2\varphi_2-\beta^2}}\right)\Delta t \\ &\approx (-\beta\cos\theta + \frac{\beta^2}{2} - (\varphi_2 - \varphi_1))\omega_0\Delta t\end{aligned} \tag{324}$$

Alternatively, a calculation based on the spectral amplitudes as a function of the frequencies could have been been perfomed. Since the relativistic transformation here is defined on the frequencies, this method might be preferred.

As a double check, as well as completeness, the main points of the calculation are reported.

The amplitude after the first interferometer is,

$$\psi_1(\omega) = e^{-\left(\frac{\omega-\omega_0}{2\sigma}\right)^2}\left(1 - e^{-i(\omega-\omega_0)\Delta t}\right) \tag{325}$$

frequencies are transformed according to 311, so that right before entering the second interferometer, the wavepacket is

$$\psi_1'(\omega) = e^{-\left(\frac{\omega'/\alpha_G-\omega_0}{2\sigma}\right)^2}\left(1 - e^{-i(\omega'/\alpha_G-\omega_0)\Delta t}\right) \tag{326}$$

Interference is detected at the satellite, observing at port 2. The second interferometer transforms the wavepacket as seen in the introductory chapters

$$\begin{aligned}\psi_2'(\omega) = e^{-\left(\frac{\omega'/\alpha_G-\omega_0}{2\sigma}\right)^2}\Big(1 - e^{-i(\omega'/\alpha_G-\omega_0)\Delta t} + \\ +e^{-i(\omega'-\omega_0)\Delta t} - e^{-i(\omega'-\omega_0)\Delta t}e^{-i(\omega'/\alpha_G-\omega_0)\Delta t}\Big)\end{aligned} \tag{327}$$

And the probability density function is

$$\begin{aligned}|\psi_2|^2(\omega') = e^{-\left(\frac{\omega'/\alpha_G-\omega_0}{2\sigma}\right)^2}\Big(2 - 2e^{i(\omega'-\omega_0)\Delta t} + 2e^{i(\omega'/\alpha_G-\omega_0)\Delta t} + \\ -e^{i(\omega'+\omega'/\alpha_G-2\omega_0)\Delta t} - e^{i(\omega'/\alpha_G-\omega')\Delta t} + c.c.\Big)\end{aligned} \tag{328}$$

with c.c. denoting complex conjugation. After integration over all frequencies, three vanishing terms are obtained because the coherence time σ^{-1} is much smaller than Δt. These terms are

$$4\sqrt{2\pi\sigma^2}\alpha_G e^{-\frac{(\alpha_G\Delta t\sigma)^2}{2}}\cos\left(\omega_0(\alpha_G-1)\Delta t\right) \tag{329}$$

$$-4\sqrt{2\pi\sigma^2}\alpha_G e^{-\frac{(\Delta t\sigma)^2}{2}} \tag{330}$$

$$-2\sqrt{2\pi\sigma^2}\alpha_G e^{-\frac{(\Delta t(1+\frac{1}{\alpha_G})\sigma)^2}{2}}\cos\left(\omega_0\left(\frac{1}{\alpha_G}-1\right)\Delta t\right) \tag{331}$$

$$\tag{332}$$

The only non vanishing term is

$$-2\sqrt{2\pi\sigma^2}\alpha_G e^{-\frac{(\Delta t(1-\alpha_G)\sigma)^2}{2}}\cos\left(\omega_0\left(\alpha_G-1\right)\Delta t\right) \tag{333}$$

so the total probability, after normalization, is

$$p = \frac{1}{2} + \frac{1}{2}\left(1 - e^{-\frac{(\Delta t(1-\alpha_G)\sigma)^2}{2}}\cos\left(\omega_0\left(\alpha_G-1\right)\Delta t\right)\right) \tag{334}$$

and substituting $\Delta t' = \Delta t/\alpha_G$ we get the same result of the previous calculation, as expected.

5.3 Comments on the result

The same result as equation 320 has been derived in [43] for a different setup, where the use of a single Mach-Zehnder interferometer is proposed. The two arms are placed at different heights, so that photons traveling through them interact with two different gravitational potentials. The possibility of realizing an equivalent experiment which is ground-satellite based was also suggested.

The result of this section emphasizes how the speed of the satellite is an effect that cannot be neglected for this type of experimental test. For a numerical estimate on the effect, we can consider circular orbit, in which case the phase shift becomes

$$\approx (-\beta \cos\theta - \frac{3}{2}\varphi_2 + \varphi_1))\omega_0 \Delta t \tag{335}$$

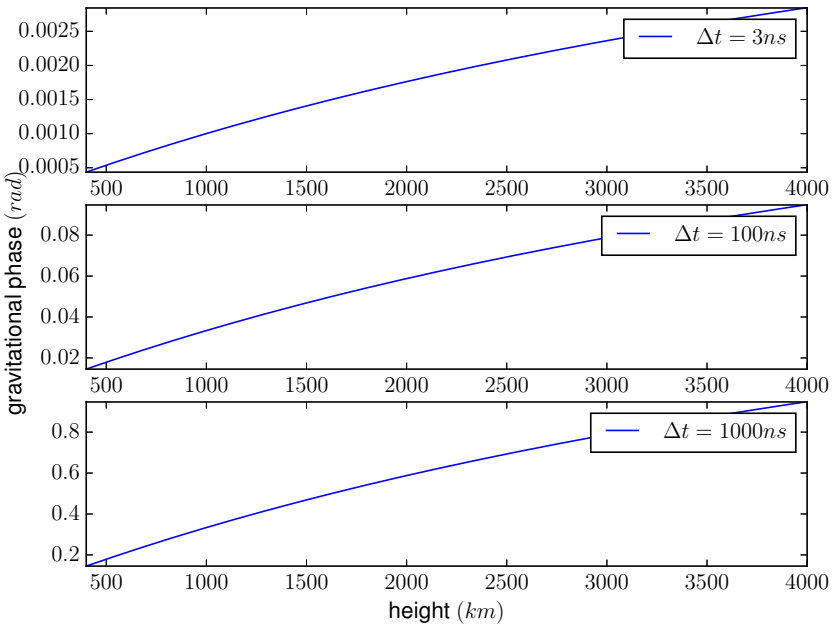

Figure 27: Gravitational contribute $(\varphi_1 - \varphi_2)\,\omega_0 \Delta t$ to the phase shift for different values of the time delay at different heights, for the wavelength $\lambda = 532nm$.

5.4 General relativistic effects on two-way setups

Gravitational effects do not affect a two-way MLRO type of experiment when considering the first order in β and φ. To understand why, it is not strictly necessary to redo all our calculations, because by now we have developed a shorthand for treating this kind of problem. All the important physics at work on this kind of computations can be summarized by the transformation that the frequencies undergo, from the second that the wavepacket enters the first

interferometer, to the time when interference it is eventually observed at the detectors. Hence we omit every direct transformation on the wavepackets, which at this point are just cumbersome and unnecessary.

We will be using 305 as the general formula for frequency transformations, here re-written again for reference (where terms in the order of $\beta^2\varphi_{1,2}$ have been neglected).

$$\omega' = \omega \frac{1+\beta'\cos\theta'}{1+\beta\cos\theta}\sqrt{\frac{1+2\varphi-\beta^2}{1+2\varphi'-\beta'^2}} \tag{336}$$

where β', φ' refer to the reciever, and β, φ to the emitter. For simplicity, the motion is assumed one-dimensional, so that θ and θ' are either 0 or π.

- the photon exits from the first interferometer and bounces off the satellite. The only element in motion in the system is the satellite, with velocity $\beta' = \beta$,

$$\omega' = \omega(1-\beta)\sqrt{\frac{1+2\varphi}{1+2\varphi'-\beta^2}} \tag{337}$$

- the photon is transmitted back to Earth and frequencies are observed with respect to Earth's clocks. The emitter and reciever roles are inverted. The angle also changes: $\theta' = -\theta$

$$\omega'' = \omega' \frac{1}{(1+\beta)}\sqrt{\frac{1+2\varphi'-\beta^2}{1+2\varphi}} = \omega\frac{1-\beta}{1+\beta} \tag{338}$$

- interference is detected. The interference pattern detected back at the interferometer is not affected by the gravitational potentials, and measurements have the same outcome as the case where gravitational effects are neglected. The interference pattern is obtained by taking the formula for a double interferometer with different unbalancements, and substituting all the relevant quantities with their transformations induced by the frequency shifts here derived.

5.5 Comments on the result

We conclude that in a two way interferometer, when photons are sent back with a satellite, no gravitational effects can be measured to the first order, and the sole Doppler shift affects measurements. Higher order effects do appear in the term $\frac{dt_1}{dt_2}$, for example, when considering the radial motion of a rocket launched from Earth. The rocket's speed couples with the gravitational field, and effects of the order $\beta\varphi(r)$ appear, because the altitude of the satellite changes during the motion. In other words, the reflection of the two wavepackets on the satellite happens at two different heights, that is, at two different gravitational potentials. The same effect is present when the satellite is in elliptical orbit, which provides a motion of the satellite through different values of the gravitational field, although sufficiently large radial speeds might be difficult to achieve.

However, since the effect has yet to be measured experimentally, it might be best to focus on experimental possibilities that predict the effect at the first order.

6 Conclusions

An interferometer that can in principle be taken as-is to be employed as the earthbound part of a space based version of the famous delayed choice experiment was realized in the laboratory. Which-path behavior and interference were observed to a very good degree. Specifically, the assessment of interference visibility, which was done after careful alignement of the setup, yields a value of $\approx 95\%$. A comparable value of $\approx 93\%$ was obtained with an alternative setup which has the BS and the PBS inverted. We suggest the hypotesis that the main cause for less-than 100% percent visibility is linked to alignement imperfections due to the fact that the superposition of the wavefronts of two light beams is slightly off. This could be corrected with the use of more precise optical components, if needed.

As far as theoretical computations are concerned, a good formalism to deal with space-based interferometric measurements was pointed out, which allows to take into account both special relativistic contributes and general relativistic corrections to the amplitude describing the photons involved with this kind of experiments. Two different setups, which are candidates for the measurement of single photon gravitational redshift, were analyzed with this formalism. The setup with one interferometer on the ground and the other on the satellite, in principle, constitutes a good way to observe this effect by means of a phase measurement, to the first order in the gravitational potentials. This is especially true if the interferometer is allowed to introduce a time delay in the order of few microseconds (this may be achieved with optical fibers), which would mean that the gravitational contribution to the phase would be in the order of the radian, as shown in figure 27.

Acknowledgements

I would like to express my sincere gratitude to Professors Paolo Villoresi and Giuseppe Vallone for the unvaluable advice and support that was given to me throughout this whole work, both when working in the laboratory, and with the writing process itself. It is also thanks to their immense expertise that I got introduced in the best possibile way to such an exciting field I had virtually no prior knowledge of.

I would also like to thank all my labmates for their infinite patience in helping me with essentially everything related to the experimental part of this work, and for many engaging discussions on aspects very relevant to my thesis. I also thank them for welcoming me as their peer.

Lastly, I would like to thank all my family, particularly my mom and dad, for supporting me in so many different ways during these years.

References

[1] RS Badessa, RL Kent, JC Nowell, and CL Searle. A doppler-cancellation technique for determining the altitude dependence of gravitational red shift in an earth satellite. *Proceedings of the IRE*, 48(4):758–764, 1960.

[2] J. Baldzuhn, E. Mohler, and W. Martienssen. A wave-particle delayed-choice experiment with a single-photon state. *Zeitschrift f??r Physik B Condensed Matter*, 77(2):347–352, 1989.

[3] J. S. Bell. *Speakable and Unspeakable in Quantum Mechanics*, volume 57. 1989.

[4] John S Bell. On the einstein podolsky rosen paradox, 1964.

[5] JP Bourgoin, E Meyer-Scott, Brendon L Higgins, B Helou, Chris Erven, Hannes Huebel, B Kumar, D Hudson, Ian D'Souza, Ralph Girard, et al. A comprehensive design and performance analysis of low earth orbit satellite quantum communication. *New Journal of Physics*, 15(2):023006, 2013.

[6] De Bruschi, Tim Ralph, and Ivette Fuentes. Spacetime effects on satellite-based quantum communications. *arXiv preprint arXiv: ...*, pages 1–13, 2013.

[7] V Capasso, D Fortunato, and F Selleri. Sensitive observables of quantum mechanics. *International journal of theoretical physics*, 7(5):319–326, 1973.

[8] R. Colella, A. W. Overhauser, and S. A. Werner. Observation of gravitationally induced quantum interference. *Phys. Rev. Lett.*, 34:1472–1474, Jun 1975.

[9] David Edward Bruschi, Carlos Sabín, Angela White, Valentina Baccetti, Daniel K L Oi, and Ivette Fuentes. Testing the effects of gravity and motion on quantum entanglement in space-based experiments. *New Journal of Physics*, 16:1–16, 2014.

[10] Albert Einstein, Boris Podolsky, and Nathan Rosen. Can quantum-mechanical description of physical reality be considered complete? *Physical review*, 47(10):777, 1935.

[11] Berthold-Georg Englert. Fringe Visibility and Which-Way Information: An Inequality. *Phys. Rev. Lett.*, 77(11):2154–2157, 1996.

[12] Mark Fox. *Quantum Optics: An Introduction: An Introduction*. OUP Oxford, 2006.

[13] Nicolas Gisin. Bell's inequality holds for all non-product states. *Physics Letters A*, 154(5):201–202, 1991.

[14] Daniel M Greenberger and Allaine Yasin. Simultaneous wave and particle knowledge in a neutron interferometer. *Physics Letters A*, 128(8):391–394, 1988.

[15] T. Hellmuth, H. Walther, A. Zajonc, and W Schleich. Delayed-choice experiments in quantum interference. *Physical Review A*, 35(6):2532–2541, mar 1987.

[16] Dipankar Home and Franco Selleri. Bells theorem and the epr paradox. *La Rivista del Nuovo Cimento (1978-1999)*, 14(9):1–95, 1991.

[17] Ryszard Horodecki, Micha Horodecki, and Karol Horodecki. Quantum entanglement. *Reviews of Modern Physics*, 81(2):865–942, jun 2009.

[18] Vincent Jacques, E Wu, Frédéric Grosshans, François Treussart, Philippe Grangier, Alain Aspect, and Jean-François Roch. Experimental realization of wheeler's delayed-choice gedanken experiment. *Science*, 315(5814):966–968, 2007.

[19] Vincent Jacques, E Wu, Frédéric Grosshans, François Treussart, Philippe Grangier, Alain Aspect, and Jean-François Roch. Delayed-choice test of quantum complementarity with interfering single photons. *Physical review letters*, 100(22):220402, 2008.

[20] Thomas Daniel Jennewein. *Quantum communication and teleportation experiments using entangled photon pairs*. na, 2002.

[21] Richard a. Holt John F. Clauser, Michael A. Horne, Abner Shimony. Proposed Experiment To Test Local Hidden-Variable Theories. *Phys. Rev. Lett.*, 23(15):880–884, 1969.

[22] R Clark Jones. A new calculus for the treatment of optical systemsi. description and discussion of the calculus. *JOSA*, 31(7):488–493, 1941.

[23] Yoon-Ho Kim, Rong Yu, Sergei Kulik, Yanhua Shih, and Marlan Scully. Delayed Choice Quantum Eraser. *Physical Review Letters*, 84(1):1–5, 2000.

[24] André G S Landulfo, George E a Matsas, and Adriano C. Torres. Influence of detector motion in entanglement measurements with photons. *Physical Review A - Atomic, Molecular, and Optical Physics*, 81(4):8–11, 2010.

[25] Rodney Loudon. *The quantum theory of light*. OUP Oxford, 2000.

[26] Xiao-Song Ma, Johannes Kofler, Angie Qarry, Nuray Tetik, Thomas Scheidl, Rupert Ursin, Sven Ramelow, Thomas Herbst, Lothar Ratschbacher, Alessandro Fedrizzi, et al. Quantum erasure with causally disconnected choice. *Proceedings of the National Academy of Sciences*, 110(4):1221–1226, 2013.

[27] Xiao-song Ma, Stefan Zotter, Johannes Kofler, Rupert Ursin, Thomas Jennewein, Časlav Brukner, and Anton Zeilinger. Experimental delayed-choice entanglement swapping. *Nature Physics*, 8(6):479–484, 2012.

[28] Asher Peres. Delayed choice for entanglement swapping. *Journal of Modern Optics*, 47(2-3):139–143, 2000.

[29] Asher Peres and Dr Terno. Quantum information and relativity theory. *Reviews of Modern Physics*, 76(January):93–123, 2004.

[30] Achim Peters, Keng Yeow Chung, and Steven Chu. Measurement of gravitational acceleration by dropping atoms. *Nature*, 400(6747):849–852, 1999.

[31] Igor Pikovski, Magdalena Zych, Fabio Costa, and Caslav Brukner. Universal decoherence due to gravitational time dilation. *arXiv*, (June):2, 2013.

[32] David Rideout, Thomas Jennewein, Giovanni Amelino-Camelia, Tommaso F Demarie, Brendon L Higgins, Achim Kempf, Adrian Kent, Raymond Laflamme, Xian Ma, Robert B Mann, Eduardo Martín-Martínez, Nicolas C Menicucci, John Moffat, Christoph Simon, Rafael Sorkin, Lee Smolin, and Daniel R Terno. Fundamental quantum optics experiments conceivable with satellitesreaching relativistic distances and velocities. *Classical and Quantum Gravity*, 29(22):224011, 2012.

[33] Thomas Scheidl, Eric Wille, and Rupert Ursin. Quantum optics experiments using the international space station: a proposal. *New Journal of Physics*, 15(4):043008, 2013.

[34] Marian O. Scully, Berthold-Georg Englert, and Herbert Walther. Quantum optical tests of complementarity. *Nature*, 351(6322):111–116, 1991.

[35] Marlan O. Scully and Kai Drühl. Quantum eraser: A proposed photon correlation experiment concerning observation and "delayed choice" in quantum mechanics. *Physical Review A*, 25(4):2208–2213, 1982.

[36] Johannes Skaar, Juan Carlos Garca Escartn, and Harald Landro. Quantum mechanical description of linear optics. *American Journal of Physics*, 72(11):1385, 2004.

[37] André Stefanov, Hugo Zbinden, Nicolas Gisin, and Antoine Suarez. Quantum correlations with spacelike separated beam splitters in motion: experimental test of multisimultaneity. *Physical review letters*, 88(12):120404, 2002.

[38] Giuseppe Vallone, Davide Bacco, Daniele Dequal, Simone Gaiarin, Vincenza Luceri, Giuseppe Bianco, and Paolo Villoresi. Experimental satellite quantum communications. *Physical Review Letters*, 115(4):040502, 2015.

[39] Giuseppe Vallone, Daniele Dequal, Marco Tomasin, Francesco Vedovato, Matteo Schiavon, Vincenza Luceri, Giuseppe Bianco, and Paolo Villoresi. Quantum interference along satellite-ground channels. pages 1–7, 2015.

[40] Reinhard F Werner. Quantum states with einstein-podolsky-rosen correlations admitting a hidden-variable model. *Physical Review A*, 40(8):4277, 1989.

[41] John Archibald Wheeler. Law Without Law. *Quantum Theory and Measurement*, pages 182–213, 1983.

[42] Magdalena Zych, Fabio Costa, Igor Pikovski, and Caslav Brukner. Quantum interferometric visibility as a witness of general relativistic proper time. page 10, 2011.

[43] Magdalena Zych, Fabio Costa, Igor Pikovski, Timothy C Ralph, and Časlav Brukner. General relativistic effects in quantum interference of photons. *Classical and Quantum Gravity*, 29(22):224010, 2012.

’ł“”—íı